NTNU
Innovation and Creativity

Tuneable Diode Laser Absorption Spectroscopy with Optical Fiber

Noise Analysis and Noise Reduction

Dung Do Dang

Master of Science in Electronics
Submission date: July 2006
Supervisor: Astrid Aksnes, IET

Norwegian University of Science and Technology
Department of Electronics and Telecommunications

Problem Description

Tuneable Diode Laser Absorption Spectroscopy with Optical Fiber - Noise Analysis and Noise Reduction

Assignment given: 02. February 2006
Supervisor: Astrid Aksnes, IET

Tuneable Diode Laser Absorption Spectroscopy with Single Mode Fiber - Noise analysis and noise reduction

Author: Dung Do Dang

Supervisor: Astrid Aksnes

Norwegian University of Science and Technology
Faculty of Information Technology, Mathematics
and Electrical Engineering
Department of Electrical and Communication

July 2006

NTNU
Norwegian University of
Science and Technology

Abstract

A prototype of a fiber based absorption spectroscopy instrument is built. A single mode fiber pigtail Distributed Feedback laser (DFB) is used to scan a known NH_3 absorption line near $1512nm$ ($6614cm^{-1}$). $2mm$ diameter InGaAs PIN photodiodes are used to convert the light signal to electrical signals by use of special designed transimpedance amplifiers. Laser modulation, coherent detection at twice the modulation frequency (second harmonic detection), other electronics, and digital signal processing are provided by Norsk Elektrooptikk.

The DFB laser from NEL (NLK1S5EAAA) delivers 10mW fiber output and has maximum output around 30mW at maximum injection current of 200mA. This laser was found to be very quiet at dc operation. However, in wavelength modulation spectroscopy operation it exhibit large modulation noise that was found to stem from the fiber coupling inside the laser module. A detection limit of 6×10^{-5} to 1×10^{-4} in absorbance unit with 0.712m optical path length and an effective measurement bandwidth of 52Hz was achieved by this laser. This is significantly above the detection limit with free air lasers which achieve 3×10^{-6} relative absorbance (0.15ppm NH_3 at room temperature and atmospheric pressure). The acquisition time for each concentration measurement takes 3.2s. Hence, the response time is very fast which is a common property of wavelength modulation spectroscopy.

The modulation noise problem was attacked by an electronic noise cancellation scheme. The idea was that since the noise source is inside the laser module and no external optical component can be used to reduce it. With great linearity and reliability properties of fused biconical taper (FBT) couplers the laser beam is split into two identical beams with nearly equal amount of the same noise. One beam, signal beam, is used to induce second harmonic signals in the gaseous path. The other beam goes directly to an identical photodetector and is used as a reference signal. Two special designed noise canceller circuits were built to remove common signals. Both the circuits, based on current subtraction (not optimized) or voltage subtraction, give comparable results. The modulation noise was reduced by more than 12dB. A detection limit of 5×10^{-6} was achieved with this prototype. Even after transmitting the laser beam through a 3200 meter single mode fiber a signal to noise ratio (relative to 100ppm signal) of 180×. Hence, a sensitivity is 1.1×10^{-5} in absorbance unit was achieved with the basic noise canceller (not optimized). This corresponds to a detection limit of 0.55ppm ammonia (12.5ppm without cancellation). The optimized noise canceller could reduce this by a factor of 3 or more.

The basic noise canceller based on current domain subtraction was investigated in detail and optimized. This new circuit suppressed the intensity modulation signal by more than 70dB. The 2f noise was reduced to approximately 50ppb or 1.1×10^{-6} in absorbance unit with an effective noise bandwidth of 52.3Hz and 1m optical path length. This is a record sensitivity with such simple electronics. The sensitivity of our fiber based prototype is limited by the fluctuating etalon fringing in the signal beam.

Under normal operation the prototype achieves approximately ±20ppb zero point drift in the concentration with an acquisition time of 48s (3.5Hz noise bandwidth). By our knowledge these results are the best available and are competitive with the much more complex frequency modulation spectroscopy technique.

These balanced transimpedance amplifiers also have the ability to measure the absorption spectra directly without modulation. Determining the absorption linewidth and its shape is now a straight forward task. By use of dual beam configuration and noise cancellation thermal effects that caused background fluctuations were greatly suppressed. The laser delivers high intensity light, $\sim 22mW$. The dominating noise is the photocurrent shot noise and the etalon fringing from optical components in the signal path. Remote sensing, in-situ, noninvasive measurements can be performed with this instrument. In some cases it's flexibility, and remote sensing possibility are of great attractiveness for the industry. The sensitivity is also improved by a factor of two with the fiber based tuneable diode laser absorption spectroscopy instrument.

In the end of this thesis we demonstrate the ability to measure multiple absorption lines simultaneously. The number of measurement paths is limited by the laser output power.

Preface

This diploma thesis is a collaboration project between Norsk Elektrooptikk and the Department of Electrical and Communication (IET) of NTNU. Experiments are carried out at the department's lab in Trondheim. I want to thank my supervisor, Astrid Aksnes, for guiding me through this thesis and helping me with english. I will also thank Norsk Elektrooptikk for providing me necessary equipments and Ove Bjorøy for helping me in their lab in Oslo. Without NEO and their support the project could not be possible. I also thank Magnus W. Haakestad for his helpful inputs.

Contents

List of Figures

List of Tables

1 Introduction

In recent years optical gas detectors based on tuneable diode laser absorption spectroscopy (TDLAS) have become more and more important for monitoring gas concentrations. Unlike the traditionally used electro-chemical detectors[32] the optical detectors are small in size, non-intrusive, have low-power consumption, high speed operation (response time to a step change in the gas concentration can be detected in seconds), durability, etc. These flexibility allows them to operate under difficult experimental conditions. Because no part is consumed, the performance degradation is slow and little maintenance is require. Only a few calibrations are needed.

The basic principle of all tuneable diode laser absorption spectroscopy (TDLAS) is to sweep the laser wavelength over a small range and detect the fractional loss. Because gases have unique and narrow absorption lines almost interference free detections are possible. Diode lasers exhibit large intensity noise and make it difficult to detect a small signal riding on top of a large signal. Worse the background also fluctuate and make sensitive detection difficult. To overcome the intensity modulation and background noise the laser is modulated and higher harmonic detections are used [12, 26, 2]. Two techniques have gained great attention and are the subjects for a huge number of publications. They are distinct by their modulation frequency. Modulation frequencies larger than the absorption linewidth are called frequency modulation spectroscopy[1, 43, 5, 9, 30]. This technique has highest sensitivity because of modulating the laser in order of GHz eliminate the laser excess noise and measurements are done at shot noise limit. Sensitivities of 1×10^{-7} to 1×10^{-8} with 1Hz effective noise bandwidth (ENBW) are reported[43, 5, 30, 9]. However this technique requires complex electronics and is high cost.

A sister technique is the more popular wavelength modulation spectroscopy. The principle is the same: modulation of laser wavelength (the wavelength term is used instead of frequency) and phase-lock detection. The modulation frequency is much smaller than the absorption line width. By modulating the laser with frequencies in tens or hundreds of kHz the 1/f noise is negligible. Detection limits of 1×10^{-6} to 7×10^{-7} with 1Hz ENBW are reported[14, 51, 16]. However, in practical applications the sensitivity is limited by background fluctuation and residual etalon fringes from optical windows.

This diploma thesis for the master program at NTNU, Norwegian University of Science and Technology, is a continuation of a student project. In the student project we concentrated on developing a fiber based transmitter unit. The common used free air DFB/VCSEL laser in the transmitter is replaced with a polarization fiber pigtailed DFB laser. The sensitivity was limited to approximately 1×10^{-4} by etalon fringing from the fiber coupling inside the laser module at ENBW=52.3Hz and 0.712m optical length. Hence, theoretically a sensitivity of 0.98×10^{-5} with 1Hz ENBW. Different single mode fiber lengths were tested. Little degradation in performance was achieved with fiber length up to 300m. With 3200m fiber the sensitivity was

reduced to 2.5×10^{-4} (52.3Hz ENBW). In this thesis we concentrate on the receiver side and noise reduction. The goal of this thesis is to investigate and choose fiber based components to achieve as low noise as possible. The goal is to achieve detection sensitivity comparable to NEO's free air lasers: 3×10^{-6} with ENBW=1Hz and 0.712m optical path length.

How to read this document? Chapter 2 deals with the basic theory to give the reader motivation. Chapter 3 deals with the mathematical deviations to arrive at the very important second harmonic signal equation. Some mathematical understanding is required to interpret the results in chapter 7. Chapter 4 goes deeply in each noise sources and we try to give some numerical values to provide some practical feelings. In chapter 5 we analyze two noise cancellation circuits that improved the signal to noise ratio by more than 12dB. Chapter 6 describe the practical setups and provide some key parameters in the LaserGaII software. Due to limitations, detailed descriptions of the temperature controller implemented in this thesis is discussed in appendix E. This temperature controller became a very important tool to identify the temperature effects of the DFB laser.

2 Theory

In this section we try to deal with the fundamentals in optics. This will give the reader relevant backgrounds to understand the topics discussed in this diploma thesis. The main goal of this project is to couple light into a single mode fiber and transmit this laser beam through a measure path to determine the gas concentration. The challenge is to suppress the optical noise added to the system by introducing fiber components to an acceptable level. In this project we use a DFB laser operating at 1511nm that is pigtailed with a polarization maintaining fiber for stable polarization state. Because of the chosen laser we work with NH_3 measurements. However, the results in this project are not only applicable for NH_3 measurements. An another gas can be measured by using an another laser with a different wavelength.

It is recommended to read the student project report [10] before going on with this master thesis. Following we will discuss topics of great importance in wavelength modulation spectroscopy.

2.1 Absorption

This is an interaction between light waves and material. Different material has different absorption characteristics which can be used as fingerprints for that specific material. Earlier several gases on the sun were determine by looking at the spectrum of the sun light. Scientists observed that there were several black lines in a continuous color spectrum. These black lines correspond to the absorption regions of the gases which the sun light were transmitted though. We see colors because the material we are looking at reflect/transmit a wavelength range and absorb the other wavelengths. When we look through a red filter, the wavelength band corresponding to red light (around 600nm-700nm) is transmitted and other wavelengths are absorbed in that filter. Gases have very thin absorption lines that spread over a big wavelength range in the NIR-FIR spectrum. This allows us to choose one of these lines and measure the transmitted light through it for gas detection. We will now investigate this absorption mechanism in gases.

2.1.1 Atomic energy states in gases

Atoms or molecules in gas state have more freedom to move than in solid state. The atoms/molecules can rotate or vibrate and have many different resonant frequencies. Atomic or molecular bonds which can resonantly vibrate or twist in response to infrared wavelengths and thereby absorb such photons[3] are responsible for harmonic signal generation in absorption spectroscopy. Perhaps the most dominant absorbance molecule which absorbs via vibrational transitions is water. In the infrared, the absorption of water is the strongest contributor and therefor responsible for the high absorption in earlier optical fibers operating in the 1550nm region[36, 20, 41].

Gases have many more energy states than semiconductors where atoms are fixed in a regular arrangement in the crystal lattice. The fundamental vibrational modes are in the mid infrared range and the second harmonic components lie in the near

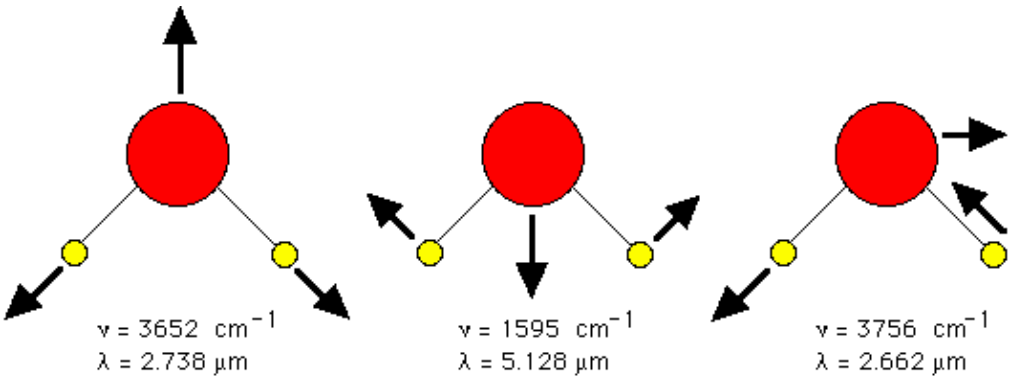

Figure 2.1: In gases the atoms are free to move thus there exist rotational energy modes. The stretching of electrons gives rise to the stretch modes

infrared region where commercial lasers and detectors for fiber communication are available. The absorption line strength decreases with an order of magnitude for each harmonic as discussed in [12, 1]. Figure 2.2 shows the ammonia spectrum. We notice that the absorption strength in 1550nm ($6500cm^{-1}$) is several orders smaller than in the fundamental region at $10\mu m$ ($1000cm^{-1}$). Since no laser at wavelengths in the mid infrared region that can operate at room temperature are available, many techniques have been developed to scan the second harmonics of the vibrational states of the gas atoms. Today quantum cascade lasers operating in the mid-infrared region are commercially available, but they still need extreme cooling and are not capable of operating in continuous wave mode. However, if they become stable and can operate in room temperature they will take over the role of existing communication industry lasers because the absorption strength in the fundamental frequencies are much higher than in the NIR region.

2.1.2 The NH_3 absorption line

In principle an arbitrary absorption line can be measured with wavelength modulation spectroscopy. But in practice detailed research must be done before choosing an absorption line. In industry the gas of interest seldom exists alone and often they are mixed with many other gases. The water vapor has a very broad absorption spectrum[36, 20] and one must carefully choose an absorption line that is separated far enough from other lines to avoid line overlapping and interference. Often it is enough to have a separation a few times of the full width at half maximum (FWHM) of the line of interest. Figure 2.2 shows the ammonia spectrum in the near infrared to the mid infrared region (1420nm to $10\mu m$ or $7000cm^{-1}$) to $1000cm^{-1}$. This line is indicated in figure 2.2. The FWHM of this chosen line is approximately $0.2cm^{-1}$.

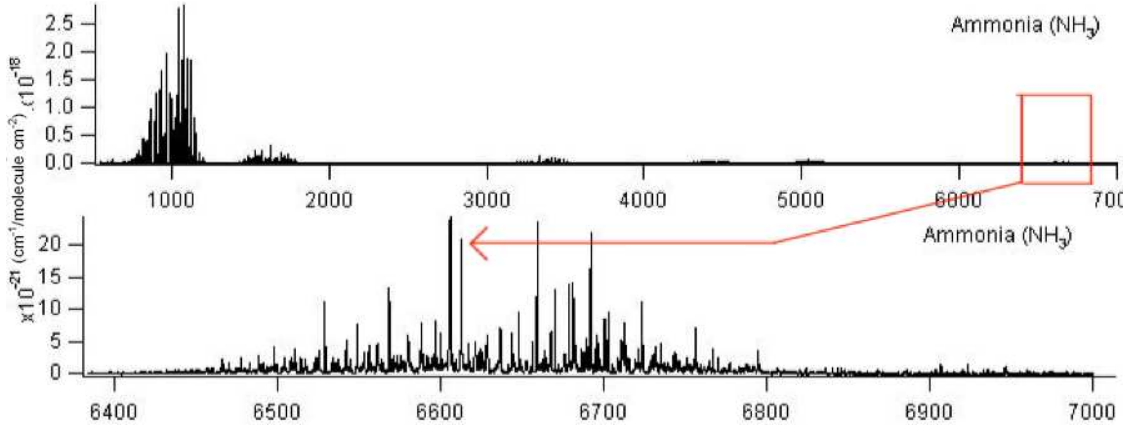

Figure 2.2: Fundamental and overtones of the NH_3 absorption lines. The overtones near $6600cm^{-1}$ are two order of magnitudes weaker than the fundamental lines. This is the drawback with using lasers in the NIR region. Quantum Cascade lasers are the upcoming technology.

2.2 Working principle of the TDLAS

Figure 2.3 illustrates the basic working principle of wavelength modulation spectroscopy (WMS). The wavelength modulated laser beam is transmitted through a gaseous path which generates harmonic components in the optical signal. A photodiode is used to convert the optical signal to photocurrent signal. The very weak photocurrents are amplified up using a transimpedance amplifier. The lock-in amplifier is used to pick out the signal that is oscillating at twice the modulation frequency that is used as a reference signal to the mixer. The mixer shifts the second harmonic signal information down to baseband. A post-filter with appropriate time constant is used to filter out higher harmonic signals. The analog signal is then sampled and converted to digital form. This quantized sample value is fed to a personal computer and an appropriate algorithm is used to calculate the actual gas concentration.

2.2.1 The laser current modulation

The laser current consists of three parts: a DC component, a current ramp component and a high frequency sine wave (ω) component:

$$i_L = i_{DC} + i_{ramp} + i_m \cos(\omega t) \tag{2.1}$$

The DC component is fixed to determine the laser working point (wavelength and intensity). The current ramp used to sweep the wavelength across the absorption line slow (in terms of Hz) compared to the high frequency modulation (in terms of thousands of Hz). The DC component in combination with the laser temperature stabilizes the laser frequency to somewhere close to the absorption line. To do this involves some fine tuning of the temperature and laser current. All TDLAS contain these three components. There exist a vast number of modulation schemes in

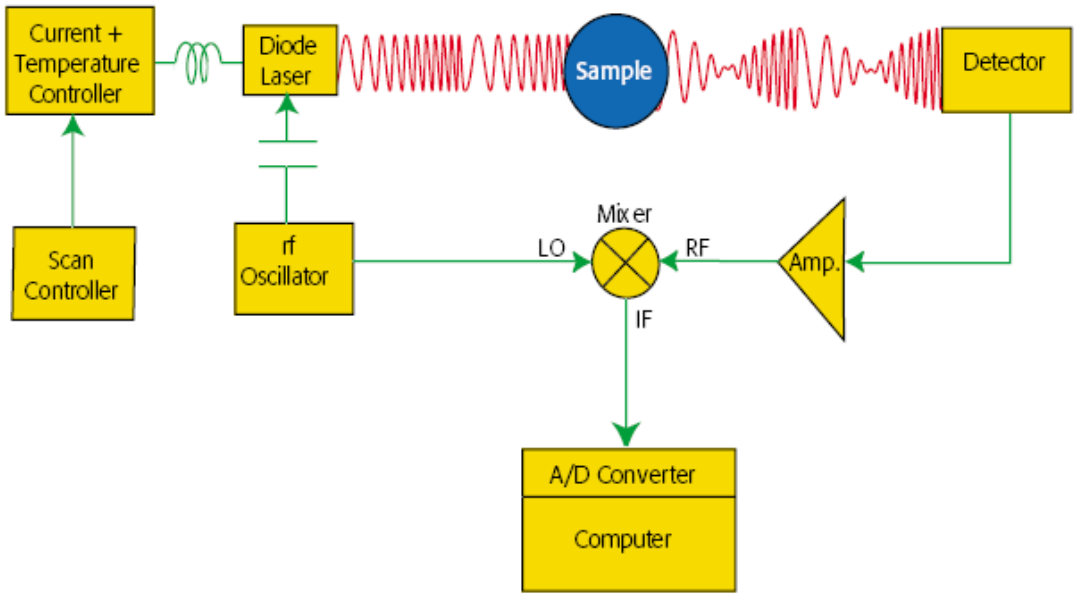

Figure 2.3: Schematic diagram for the WMS working principle. The light from the laser is modulated and sent through the gas cell. In the receiver a PLL is used to amplify the second harmonic component. A computer is used to calculate the actual gas concentration with very good detection limit, in ppm and even in ppb scale. Figure from [1]

the literature. The modulation amplitude is often maximize to get best signal-to-noise ratio. The parameter that vary much is the choice of modulation frequency. Working in low frequency (kHz) regime the technique is called wavelength modulation spectroscopy[12, 37]. Modulation frequency comparable with the absorption linewidth (GHz) is referred to as frequency modulation spectroscopy[37, 43].

2.2.2 Lenses and optical windows

This gas instrument is non-invasive and does not have direct contact with the measured gas. Optical windows are used to prevent the gas to come in contact with the lenses. The collimating lens is use to reduce the divergence of the light beam from the laser facet. In this project we use a single mode fiber and the divergence of such wave guides is quite high. The lens in the receiving unit is used to focus the relative large laser beam (approximately 2cm with our setup) onto a small size optical detector (2mm). Optical facets create etalon fringes[40, 19, 41] that limit the instrument sensitivity. Therefor a minimum number of optical windows are chosen and the optical components are carefully placed/aligned to avoid etalon fringing. These effects are discussed in detailed in section 4.

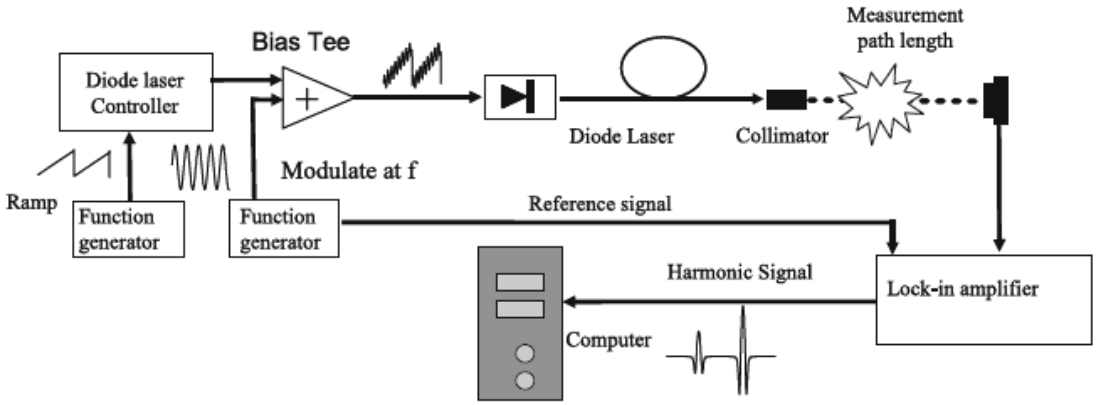

Figure 2.4: Schematic principle of the instrumentation in this thesis paper. The light from the laser is guided to a collimating lens with single mode fibers. After traveling through the gas cell the receiver unit collects the light into a detector. Figure from [48]

2.2.3 Coherent detection of the 2f signal

When the wavelength modulated light beam is transmitted through a gaseous path higher harmonic signals are generated and the detector signal consists of higher frequency components of the modulation signal[26, 12, 8, 32, 37]. It is shown that when taking the Fourier series expansion of the absorption line with the modulation frequency ω as the fundamental frequency, the second harmonic signal amplitude is proportional to the second derivative of the Fourier series coefficients[26, 37, 42]. Shown in [12, 37] the Fourier coefficients are directly related to the n'th derivative of the absorption line.

By introducing a mixer with twice the modulation frequency as an input signal to the mixer, a narrow signal band near the 2ω is shifted to the baseband. This frequency conversion technique is well known in the radio communication literature. For detailed analysis we recommend [38]. After the down conversion a low pass filter removes higher frequencies and the output signal is a slowly varying signal that has the shape of the second derivative of the absorption line. This signal is the 2f signal and is used in the concentration calculation. Many 2f signals are averaged to reduce the stochastic noise. However, etalon fringes can not be reduced with this method.

2.2.4 Practical instrumentation

Wavelength modulation instruments often consist of two parts, one transmitter unit where the beam is launched from and one receiver unit to collect the transmitted light beam onto an optical detector. There are different methods for how this is done.

Instruments for use in the industry pipes also have optical windows to protect the lenses from dust and "dirty" gases. A mounting mechanism to ensure a stable light collection on the detector active surface is important. Some kind of alignment mechanism is also important to maximize the optical signal. The light from a diverging DFB/VCSEL,

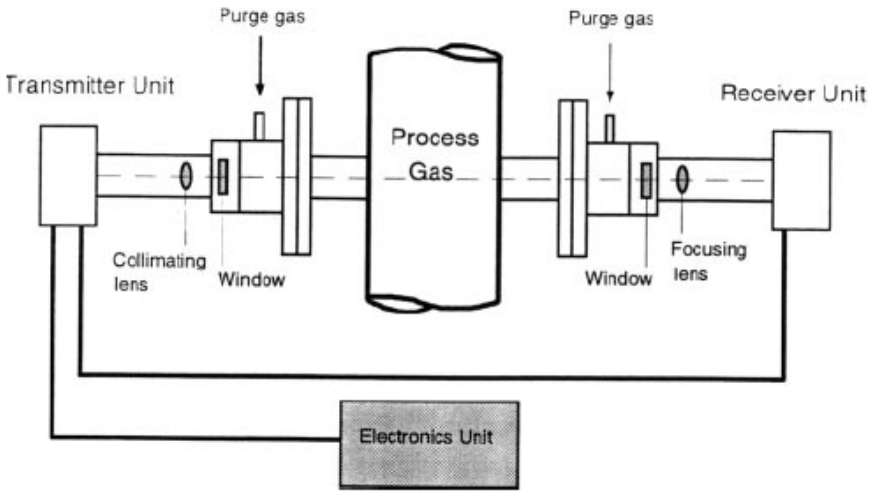

Figure 2.5: A typical setup for gas measurement in the industry.

Distributed Feed Back laser and Vertical Cavity Surface Emitting Laser, is directly collimated by a plano-convex lens inside the transmitter unit. A plano-convex lens in the receiver unit focuses the transmitted light beam onto a PIN detector. The received signal from the detector is amplified and passed to the phase-lock amplifier. This is referred to as coherent detection[13, 7]. The analog second harmonic signal is then sent back to the transmitter unit. The analog to digital conversion circuit converts this signal to digital form. A digital algorithm calculates the gas concentration.

2.3 Electro-optical devices

2.3.1 Lasers

The laser is probably the most critical part in this instrument. A perfect laser only has beam shot noise when detected with a PIN photodiode. Depending on which gas is of interest, the laser wavelength is chosen. Basically only the laser needs to be replaced when other gases are needed to be measured since the detector spectrum response is wide enough to cover many wavelengths where the absorption of different gases exist. Lasers from the optical communication industry are very well suited for gas detection because of the high quality requirements of them from this industry. These lasers are easy to modulate and have low intensity fluctuations under optimal

conditions. Especially VCSEL (Vertical Cavity Surface Emitting Laser) and DFB (Distributed FeedBack) lasers are well suited for wavelength modulation spectroscopy purposes because of their small line width and single mode operation [29, 41]. The detection sensitivity of existing gas detection systems is mainly limited by the laser feedback noise and the residual etalon fringes from optical surfaces in the measured path [26, 37]

2.3.2 Detectors

There are several types of optical detectors available. In this section I will concentrate on two types of detectors which are relevant for gas measurement equipments. The Avalanche photo diode (APD) can provide internal gain which is useful when detecting small signal amplitudes. There are several disadvantages related to these types of detectors, such as high operating voltages, requirement of cooling, and higher noise compared to PIN detectors. We use large area (2mm) InGaAsP PIN (positive-intrinsic-negative) photo diodes. They are cheap and have low response time. Further readings about detectors can be found in e.g. [41, 40, 11]. Because of the limits of this document we only describe the basic working principle needed to understand how the time varying light intensity is converted to time varying electrical signal for signal processing. In a simple manner the detector current can be expressed as

$$i_{ph} = \frac{e\eta P_o}{h\nu} \tag{2.2}$$

where e is the unit charge, η is the light coupling efficiency, P_o is the incident light intensity on the detector active region, h is Planck's constant and ν is the light frequency. Usually the detector current is expressed as a product of the light intensity and the detector responsivity, R_o

$$i_{ph} = \Re_o P_o \tag{2.3}$$

Operating near $1.5\mu m$ the responsivity is close to unity ($\sim 1A/W$). We will make use of this simple expression in the derivation of the second harmonic signal in section 3.4. At high optical power (high transmission) the dominating noise is detector shot noise and at low transmission the thermal noise in the preamplifier becomes dominant. Since we are detecting small signals digging in large signals, small noise properties of detectors are of great importance.

2.3.3 Amplifiers

Low noise operational amplifiers are used to interface the photodiodes. The circuitry is called transimpedance amplifier because it converts the photocurrents to voltages and provide gain. Careful design reduces the noise at the input of the preamplifier, and is very important to maximize the signal-to-noise ratio. Under weak signal conditions the preamplifier dark noise is dominated by the thermal noise of the feedback resistor in the preamplifier. Under normal conditions the photocurrents is in order of mA and the shot noise dominates. Amplifier stages after the mixer and in the direct signal path are less critical since their relative amplification are small.

2.3.4 Electronics

Lasers need low noise current supplies. Detectors need low noise transimpedance amplifiers to convert the small photocurrents to high level voltage outputs. A temperature control circuit provides the laser diode a stable temperature needed to emit a coherent and stable wavelength. The laser current driver modulates the laser with a modulation signal. ADC circuits are needed to convert the analog values to digital form needed by the gas calculation algorithms.

The LaserGasII instrument in this thesis has all this in the main unit. The receiver unit produces the 2ω sine wave and delivers the ω signal to the main unit through a 3m long cable. External communication to a personal computer is provided by the main board. A LCD display shows relevant information is connected to the main unit.

2.4 Optical fibers

Optical step index fibers guide light by total internal reflection[40, 41, 19],TIR, at the core-cladding interface. The refractive index of the core must be higher than in the cladding to satisfy the condition for TIR. Incoming rays with an incident angle smaller than the critical angle, an angle given by $\theta_c = arcsin(n_1/n_2)$, will be partially radiated through the cladding and be lost. A single modus fiber[20] is a fiber designed such that only one mode can be guided, however, two indistinguishable polarization modes exist in the fiber. In this project we will only focus on using single mode fibers to minimize the additive noise. The laser used in this project has a polarization maintaining fiber with an APC connector. The most important parameter for describing a fiber is the normalized frequency V given in [40, 41, 20].

$$V = \frac{2\pi a \cdot \mathrm{NA}}{\lambda} = \frac{2\pi a\sqrt{n_1^2 - n_2^2}}{\lambda} \tag{2.4}$$

where a is the fiber radius, n_1 is the core's refractive index, n_2 is the cladding's refractive index,NA is the numerical aperture and λ is the operating wavelength.

2.4.1 Optical modes

Optical modes are the solution of Maxwell's equations with proper boundary conditions[40]. Further, light propagates in an optical waveguide in the form of modes. In general, the complex envelope of the optical field in the waveguide is a superposition of all the modes supported by that waveguide. The amplitude of each mode depends on the light source used to excite these optical modes. For more details read e.g. [40]. Single mode optical fibers only support one mode. All higher modes are greatly attenuated and will die out after propagating a distance in the fiber. Actually there exist two fundamental modes in the single mode fiber, one mode for each polarization state. In standard single mode fibers the light can easily jump between these modes and gives rise to polarization mode dispersion and limits the transfer rate in communication industry.

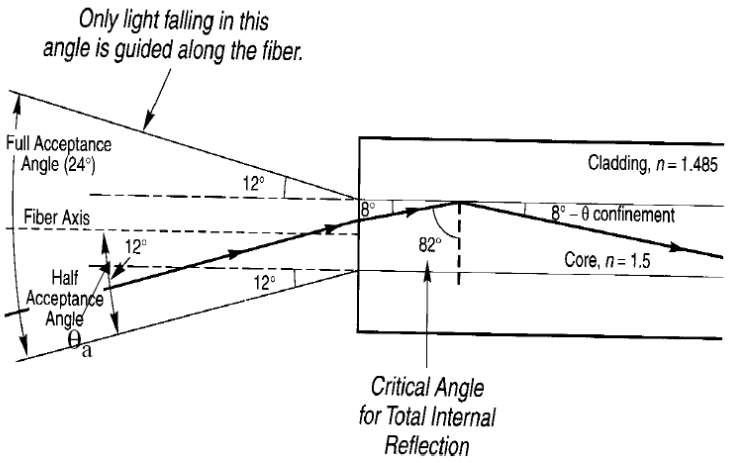

Figure 2.6: Only light rays within the acceptance cone will be guided through the fiber. Others will be lost due to radiative modes. Figure from [36]

Polarization maintaining fibers only support one polarization mode and light can not jump to other modes. The laser used in this thesis has a polarization maintaining fiber mounted to the laser housing and provide excellent polarization state.

2.4.2 Mode field distribution

If we project the laser light coming out from the fiber (SMF) onto a wall we will se a circular beam with highest intensity at centrum and fading intensity outwards. The beam intensity as function of it's radius is described by a Gaussian approximation[20, 40]. This beam will grow in diameter farer away from the fiber end. This is important when choosing collimation lens. A large focal length and small diameter lens is bad since only a fraction of light is collimated and collected. The rest is lost, and lower the signal to noise ratio. The collimated laser beam diameter in our system is approximately 1.6cm.

3 Wavelength modulation spectroscopy

In this section we will go through the working principle of wavelength modulation spectroscopy. To achieve a low detection limit[26, 32, 1] and reliable (small drift) measurement results the laser must be modulated with a modulation frequency, approximately 100kHz in NEO LaserGasII instruments. By doing this and choosing a high enough modulation frequency the flicker noise, 1/f, is reduced. Second harmonic detection by using a phase-lock amplifier gives advantages such as low flicker noise, high detection limit, signal offset caused by the relative intensity modulation[26, 44].

3.1 Beer-Lambert's law

All absorption spectroscopy techniques are based on a very simple formula, Beer-Lambert's law[26, 40]:

$$I(L) = I_0 e^{-Sg(\lambda)NL} \tag{3.1}$$

where S is the absorption line strength, g is the absorption line profile, N is the absorbing species concentration and L is the optical path. L is not necessarily the physical length. In multi path instruments the light beam bounces several times back and forth between two spherical mirrors to increase the travel length of the light beam thus increasing the absorbance. This leads to a higher instrument sensitivity. This formula tells us that when light travels through a path with absorbing species the light intensity will decay exponentially with distance. A more familiar equation is

$$I(L) = I_0 e^{-\alpha(\lambda)L} \tag{3.2}$$

where the $\alpha(\lambda)$ is the absorption coefficient.

3.2 Line profile and broadening effects

Under normal conditions we can approximate the line profile to be Lorentzian shaped[26]. It is well known that the absorption strength ,S, depends on temperature and the integral of line shape function is independent of the line width such that the integral can be normalized to unity.

$$\int_{-\infty}^{\infty} g(\lambda) d\lambda = 1 \tag{3.3}$$

The peak amplitude of the absorption line will decrease and more important the second derivative amplitude of the absorbtion line is significantly reduced thus the second harmonic signal amplitude for a given modulation value $m = \widetilde{m}$ will decrease. It is therefor necessary to increase the modulation index m. This is shown in details later. There are three contributions of the line broadening : natural line broadening, Doppler broadening and collision broadening. In most industrial processes the collision broadening[26, 12] dominates. The resulting line profile still is Lorentzian shaped. In a more careful study of the line width we must include the Doppler broadening which results in a Voigt shaped line profile.

3.3 Derivatives of the absorption line

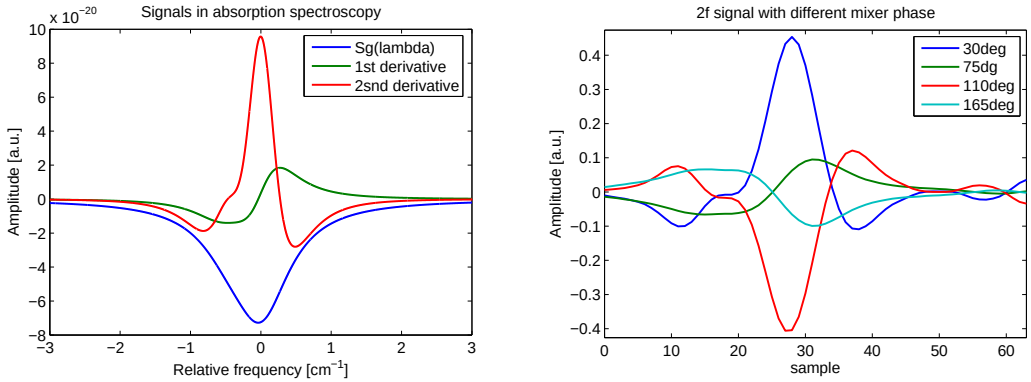

Figure 3.1: Left: Theoretical absorption line and the 1st and 2snd derivatives of equation (3.5). Right: Real 1f and 2f signals acquired with the instrument. acquisition time is 3.2s. Just ignore the phase for now.

The Lorentzian line shape is given by

$$g(\lambda) = \frac{1}{\pi} \frac{0.5\Gamma}{(\lambda - \lambda_0)^2 + (0.5\Gamma)^2} \tag{3.4}$$

where λ_0 is the absorption peak wavelength and Γ is the full width at half maximum (FWHM) of the absorption line profile. It's peak value is $g(\lambda = \lambda_0) = \frac{2}{\pi\Gamma}$.

Lets assume that we have two Lorentzian line shapes with line widths of $\Gamma = 1cm^{-1}$ (real line widths are much smaller) and spaced 0.45Γ from each other and are centered at 1512nm. The line strengths are $S_1 = 20 \times 10^{-21} cm^{-1}/molecule \times cm^{-2}$ and $S_2 = 5 \times 10^{-21} cm^{-1}/molecule \times cm^{-2}$. The absorbance relative to the center wavelength is given by

$$Sg(\lambda) = S_1 \frac{1}{\pi} \frac{0.5\Gamma}{(\lambda - 0)^2 + (0.5\Gamma)^2} + S_2 \frac{1}{\pi} \frac{0.5\Gamma}{(\lambda + 0.45)^2 + (0.5\Gamma)^2} \tag{3.5}$$

Figure 3.1 shows the absorption line (magnified 5×), the first and second derivative of the absorption line. If the lines are spaced several FWHM from each other the first and second derivative signal can extract the them from each other with little interference. We notice that the second derivative has it's maximum value at the absorption line center. In wavelength modulation spectroscopy at ambient pressure the observed 2f signal shape is a combination of the first and second derivative.

3.4 The second harmonic signal (SHS)

3.4.1 General wms theory

Direct absorption is the simplest method for measuring gas concentration. This method scans over a well known absorption line. The line amplitude can be used to find the gas concentration. This method is simple, but suffers from low sensitivity and poor detection limit due to small contrast between light intensity at the absorption peak and outside this peak where the transmission is 1. By modulating the laser and using 2f detection (second harmonic detection) the sensitivity and detection limit is greatly improved. To do this we modulate the laser with a modulation current additional to a ramp current used to move the laser wavelength across the absorption line. Figure

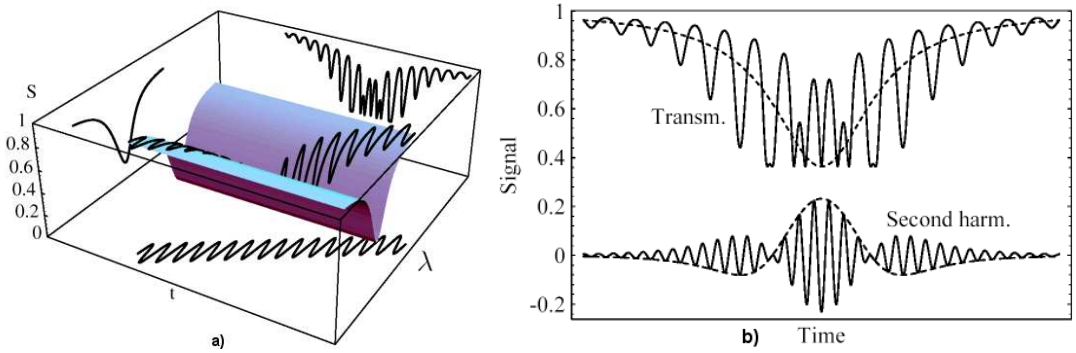

Figure 3.2: a) The laser wavelength is shown in the $\lambda - t$ plane. The absorption line is shown in the $S - \lambda$ plane. b) The detector signal and the second harmonic envelope is shown. Note that the modulation frequency is much higher than that shown in the figure. Figure from [26]

3.2a) shows the modulation used in 2f detection. In the $t - \lambda$ plane we see the laser wavelength as function of time. The ramp amplitude represents the scan range and the oscillation amplitude represents the modulation amplitude. The shaded surface represents the absorption profile. When the laser wavelength is ramped slowly with a high-frequency as shown by the curve in the $t - \lambda$, the detector signal as function of time will be represented by the curve in the $S-t$ plane. Notice that this detector signal consists of higher harmonics and 2f detection just picks out the components oscillating with the twice the frequency. Figure 3.2b) (top) shows the detector signal which can be approximated with equation (3.16). 3.2b) (bottom) shows the demodulated signal after the mixer which can be approximated with equation (3.18). This amplitude is used in the actual gas calculation.

Below we will go through the mathematical steps to find the very important V_{2f} signal. The modulation current consists of three components: a stable DC current, a current ramp and a high frequency modulation current. These three current contributions modulate the laser wavelength. An unwanted residual intensity modulation due to increasing intensity with laser current makes second harmonic detection popular.

The modulation current is given by

$$i(t) = i_0(t) + i_m \cos(\omega t) \tag{3.6}$$

The laser is modulated with a modulation frequency ω and a modulation current amplitude i_m. The current $i_0(t) = i_{dc} + i_{ramp}(t)$ is slowly varying compared to the fast oscillating modulation current. The modulation current injection will cause the laser wavelength to oscillate at the same frequency. The The resulting laser wavelength is given by

$$\lambda(t) = \lambda_0 + (m\gamma)\cos(\omega t - \varphi) = \lambda_0 + \delta\lambda \cos(\omega t - \varphi) \tag{3.7}$$

where m is the modulation index, γ is the half width at half maximum (FWHM/2) of the absorption line and $\delta\lambda$ is the wavelength modulation amplitude . Due to the thermal inertia of the laser chip this wavelength modulation lags behind the laser intensity with a phase φ. At the same time the laser output power is

$$P(t) = P_0 + \mathrm{M} \cdot i_m \cos(\omega t) = P_0 + \delta P \cos(\omega t) \tag{3.8}$$

where P_0 is output power at the wavelength λ_0, and the constant M is the intensity-current ($\frac{\Delta P}{\Delta i}$) slope which can readily be taken from the laser power-current characteristic curve from the datasheet. This quantity depends on the particular laser diode, but does not differ much from sample to sample. We assume the modulation index is small, $m \ll 1$, i.e small i_m. This means that we are moving the laser wavelength in a small region on the absorption line curve. The slow moving laser wavelength λ_0 can be approximated to a constant value. Using Beer-Lambert's law and series expansion of the exponential function the transmission (function of time) through the gas cell is

$$T(t) = e^{-\alpha(\lambda)L} \approx 1 - \alpha(\lambda)L \tag{3.9}$$

Here we neglect the higher terms of the exponential series expansion. Putting the laser wavelength in equation (3.6) into the equation (3.9) we get

$$T(t) \approx 1 - \alpha[\lambda_0 + \delta\lambda \cdot cos(\omega t - \varphi)]L \tag{3.10}$$

Using Taylor expansion of the absorption coefficient we get

$$\alpha(\lambda) = \sum_{k=0}^{\infty} [\delta\lambda \cdot cos(\omega t - \varphi)]^k \cdot \frac{\partial^k \alpha(\lambda_0)}{k! \cdot \partial\lambda^k} \tag{3.11}$$

Putting equation (3.11) into equation (3.10) we get the transmission coefficient

$$T(t) = 1 - \sum_{k=0}^{\infty} [\delta\lambda \cdot cos(\omega t - \varphi)]^k \cdot \frac{\partial^k \alpha(\lambda_0)}{k! \cdot \partial\lambda^k} \cdot L \tag{3.12}$$

The light intensity impinging on the detector is given by the laser intensity multiplied with the transmission coefficient. The detector current is therefor

$$\begin{aligned} I_{detector}(t) &= \eta R_0 P(t) T(t) = \eta R_0 [P_0 + \delta P \cdot \cos(\omega t)] \\ &\times \{1 - \sum_{k=0}^{\infty} [\delta\lambda \cdot cos(\omega t - \varphi)]^k \cdot \frac{\partial^k \alpha(\lambda_0)}{k! \cdot \partial\lambda^k} \cdot L\} \end{aligned} \tag{3.13}$$

where R_0 and η is the photodiode responsivity and the light coupling efficiency into the photodiode respectively. Using $\eta R_0 P_0 = i_{pd0}$ and $\eta R_0 \delta P \cos(\omega t) = \delta i_{pd} \cdot cos(\omega t)$ the current in the photodiode is given by

$$i_{pd}(t) = [i_{pd0} + \delta i_{pd} \cdot \cos(\omega t)] \cdot [1 - \sum_{k=0}^{\infty} [\delta\lambda \cdot cos(\omega t - \varphi)]^k \cdot \frac{\partial^k \alpha(\lambda_0)}{k! \cdot \partial\lambda^k} \cdot L] \tag{3.14}$$

In 2f demodulation only signals oscillating with 2ω contribute to the 2f signal. Multiplying out equation (3.14) and writing only the first few terms yields[1] :

$$\begin{aligned} i_{2f}(t) = -\frac{1}{2} i_{pd0} [(\delta\lambda)^2 \cdot \frac{\partial^2 \alpha(\lambda_0)}{2! \cdot \partial\lambda^2} + (\delta\lambda)^4 \cdot \frac{\partial^4 \alpha(\lambda_0)}{4! \cdot \partial\lambda^4}] cos(2\omega t - 2\varphi) \cdot L \\ -\frac{1}{2} \delta i_{pd} \cdot \delta\lambda \cdot cos(2\omega t - \varphi) \cdot \frac{\partial \alpha(\lambda_0)}{\partial\lambda} \cdot L + ... \end{aligned} \tag{3.15}$$

When using a small modulation ($m \ll 1$), i.e. small i_m, the first derivative contribute little and the i_{2f} is proportional to the second derivative[2] of the absorption line. For higher signal to noise ratio, higher modulation is applied. This gives the well known 2f signal shape derived in section 3.3 for gas under low pressure. When measuring gas at ambient pressure or high temperature the absorption line is broadened which results in a smaller $\frac{\partial \alpha(\lambda_0)}{\partial\lambda}$, making high modulation amplitudes necessary. As indicated in equation (3.15) the δi_{pd} which originates from the residual intensity modulation δP strongly contributes to the signal shape which causes an asymmetry. Since that term is negative the signal shape is pulled down at the end region where the light intensity is higher, as shown in figure 3.3. We notice that the phase of the 2f signal is shifted by 2φ with respect to the modulation signal which is used as a reference input to the mixer. Accordingly a phase term ϕ at the mixer is set to maximize the 2f signal. The mixer output voltage is therefor:

$$V_{mix}(t) = Z_0 G \cdot i_{2f}(t) \times cos(2\omega t - \phi) \tag{3.16}$$

where the Z_0 is the transimpedance gain of the preamplifier (165Ω with NEO's instrument. $1k\Omega$ with our preamplifier design, described in details in section 4 and 5)and the constant G is the amplification factor of the post-amplifier stages after the mixer (G=4831 with our settings). We multiply out this equation and using $i_{2f}(t)$ instead of $i_{pd}(t)$ since we apply second harmonic demodulation.

$$\begin{aligned} V_{mix}(t) = -\frac{1}{2} Z_0 G \times \{ i_{pd0} [(\delta\lambda)^2 \cdot \frac{\partial^2 \alpha(\lambda_0)}{2! \cdot \partial\lambda^2}] cos(2\omega t - 2\varphi) \cdot L \\ +\delta i_{pd} \cdot \delta\lambda \cdot cos(2\omega t - \varphi) \cdot \frac{\partial \alpha(\lambda_0)}{\partial\lambda} \cdot L \} \times cos(2\omega t - \phi) \end{aligned} \tag{3.17}$$

Recall that $cos(2\omega t - \varphi) cos(2\omega t - \phi) = \frac{1}{2}[cos(-\varphi + \phi) + cos(4\omega t - \varphi - \phi)]$. The output voltage from the mixer is low pass filtered such that high frequency components

[1] We neglect DC terms and terms that do not oscillate with 2ω. We used that $cos(\omega t - \varphi) cos(\omega t - \varphi) = \frac{1}{2}[cos(0) + cos(2\omega t - 2\varphi)]$

[2] This is some time called derivative spectroscopy

are removed. However, the time constant can not be too big such that the filter bandwidth is smaller than the bandwidth of the 2f signal. The low pass filter -3dB corner frequency is 6.7kHz. Using the cosine relation and leaving out fast oscillating terms we arrive at

$$V_{2f}(t) = -\frac{1}{2}Z_0 G \times \{\frac{1}{4}(\delta\lambda)^2 \cdot i_{pd0} \cdot cos(-2\varphi + \phi) \cdot \frac{\partial^2 \alpha(\lambda_0)}{\partial \lambda^2} L + \frac{1}{2}\delta i_{pd} \cdot \delta\lambda \cdot cos(-\varphi + \phi) \cdot \frac{\partial \alpha(\lambda_0)}{\partial \lambda} L\} \tag{3.18}$$

where 4ω terms are left out. As indicated earlier a phase term in the mixer can be chosen such that the second derivative signal has maximum value. However, the first derivative (1f) signal depends on this phase term and is not zero for this case. The superposition of two cosine terms with varying amplitude and phase during a current ramp complicates the overall 2f signal shape. Experimentally there is no unambiguous phase ϕ setting in the mixer.

Additionally, if there are any non-linearities in the laser P-i characteristic or the photodiode response R_0 , this will produce a background 2f signal which is in phase with the modulation signal. Experimentally observed a mixer phase ϕ reduces the background 2f signal. However, this will reduce the wanted 2f signal amplitude and a best-compromise must be considered.

For 2f detection the signal amplitude increase with increasing wavelength modulation amplitude m (increasing $\delta\lambda$). However, it start to decrease again after an optimum modulation index. This value is $m_0 = 2.2$ for 2f detection and $m_0 = 2.0$ for 1f detection[42, 26]. It is therefor important to know the laser $\frac{\Delta\delta\lambda}{\Delta i}$ and $\frac{\Delta P}{\Delta i}$ in combination with the phase 2φ to have an optimum demodulation.

3.4.2 Practical implementation of the phase compensation

The practical implementation of the mixer phase is not as an input phase to the mixer. To correct for the phase shift between the intensity modulation and the wavelength modulation a digital generated phase ϕ is added to the laser modulation current. This phase corresponds to the variable phase input to the mixer. When fibers are inserted in the path between the collimator lens and the laser output both the laser intensity and wavelength are delayed by τ in time due to the propagating delay of the light signal. When taking these properties into account the expression for the 2f signal becomes different. The laser modulation current is

$$i(t) = i_0(t) + i_m \cos(\omega t - \phi) \tag{3.19}$$

where ϕ is the variable phase to maximize the 2f signal amplitude, i.e. the input phase of the mixer. The intensity modulation becomes

$$P(t) = P_0(t) + \delta P \cos(\omega t - \varphi_f - \phi) \tag{3.20}$$

where φ_f is the phase caused by the fiber and the wavelength modulation becomes

$$\lambda(t) = \lambda_0(t) + \delta\lambda \cos(\omega t - \varphi_f - \phi - \varphi_\lambda) \tag{3.21}$$

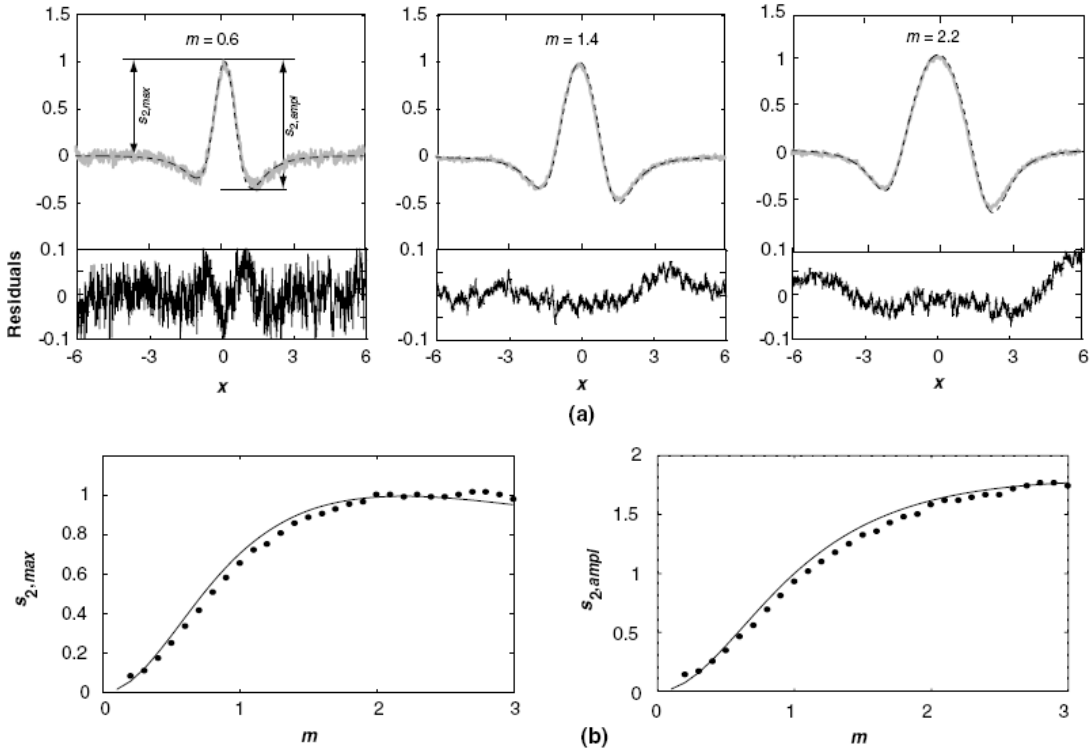

Figure 3.3: Normalized second harmonic signal and residual intensity modulation signal for three values of the modulation index m. Figure from [42]

The local oscillator signal is directly input to the mixer and it becomes

$$V_{LOmix}(t) = cos2\omega t \tag{3.22}$$

Going through the same mathematics as in previous section we arrive at

$$\begin{aligned} V_{2f}(t) = -\frac{1}{2}Z_0G\{\frac{1}{4}(\delta\lambda)^2 \cdot i_{pd0} \cdot cos(-2\varphi_f - 2\phi - 2\varphi_\lambda) \cdot \frac{\partial^2\alpha(\lambda_0)}{\partial\lambda^2}L \\ +\frac{1}{2}\delta i_{pd} \cdot \delta\lambda \cdot cos(-2\varphi_f - 2\phi - \varphi_\lambda) \cdot \frac{\partial\alpha(\lambda_0)}{\partial\lambda}L\} \end{aligned} \tag{3.23}$$

Comparing this equation with equation (3.18) we see that only the phase inside the cosine terms are different. When the 2f signal is maximize by proper mixer input phase, i.e. $\phi = -\varphi_f - \varphi_\lambda$, the 1f signal only contribute with $cos(-\varphi_\lambda)$ of it's maximum amplitude. Ideally this phase lag should be $\pi/2$ and the 1f signal does not contribute to the 2f signal shape when the phase correction is optimized. From equation (3.23) a phase setting in software corresponds to twice the phase setting in case of mixer input phase. Figure **??** show the digital 2f signal for four different phase settings in software: 30, 75, 110 and 165 degrees. The maximum 2f signal amplitude is achieved with 30 degree reference phase in software. By adding 90 degrees in software corresponds to a

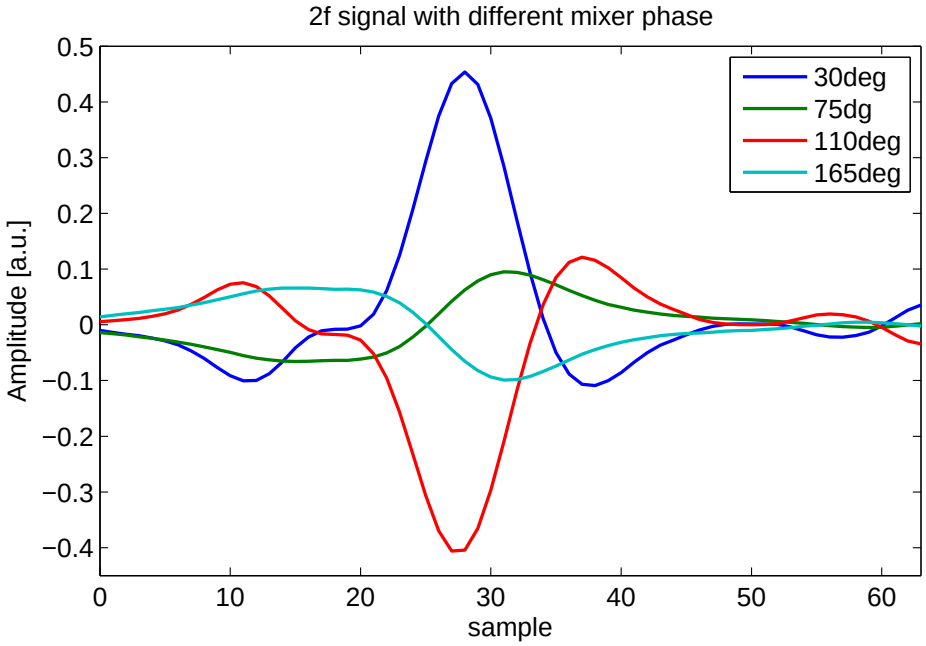

Figure 3.4: Four digital 2f signals from measurements with the 100ppm NH_3 gas cell. Four phase settings in the software with 45 degrees between each phase setting. Hence, 2f, 1f, -2f and -1f are recorded. This shows that the phase setting in software corresponds to twice the phase in detections with a phase as the input to the mixer.

180 phase shift and the 2f signal is inverted. By adding 45 degrees in software the 2f signal is zero and only the 1f signal contribute to the mixer output. Adding another 90 degrees to this signal (165 degrees) inverts the 1f contribution. Recall figure 3.1 for comparison. This line consists of two absorption lines with different line strengths close to each other. The resulting first and second derivative are a superposition of each line independently.

3.5 The impact of the IM-WM phase

Now lets take a closer look at the equation 3.23. In the condition of weak modulation, i.e. small $\delta\lambda$, the observed 2f signal is due to the second derivative of the absorption line. The cosine term has a sum of phase inputs. When modulating the laser diode with a certain modulation frequency and modulation amplitude the wavelength modulation phase lag relative to the intensity modulation phase is fixed, closed to $\pi/2$ [14]. Any phase fluctuation will cause a signal amplitude fluctuation and add noise to the system. The lock-in phase ϕ can change due to noise, and the amplitude of the first term in equation 3.23 can change. Since the concentration is proportional to this amplitude a change in the concentration will occur. It is of great interest to tune this phase difference to zero, because here the amplitude error is minimized for phase fluctuations. This will also maximize the 2f signal as well.

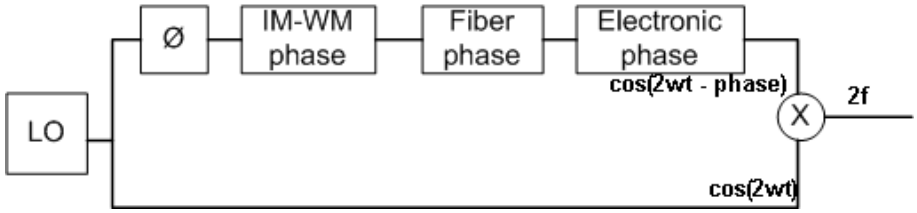

Figure 3.5: Phase components in the demodulation of the 2f signal.

When fibers are used this phase must be optimize for maximin 2f signal. The fiber introduces a phase shift[3]

$$\varphi_f = \tau_{delay} \cdot \omega_m = \frac{n_{eff} L}{c} 2\pi f_m \tag{3.24}$$

where n_{eff} is the effective mode index, L is the fiber length and f_m is the modulation frequency. For example a single mode fiber with $n = 1.48$, $L = 300m$ and a modulation frequency $f_m = 92.75kHz$ would give a phase delay of 49.4 degrees which a software generated phase ϕ must compensate for. If the fiber length is small the phase delay caused by a propagation delay is small and the phase φ_f can be neglected in equation (3.23). Figure 3.5 shows all phase shifts in the demodulation of the 2f signal with our system. A adjustable software generated phase is input to the laser injection signal. The intensity can be assumed to have no phase lags. The laser diode wavelength lags behind the intensity modulation. A fiber propagation delay will add an additional phase to the laser beam intensity (and beam wavelength) as function of time. This signal is converted to a time varying voltage signal. In this conversion the electronic will add a electronic phase. The total phase lag is a sum of all contributors above. The local oscillator signal is directly input to the mixer and will have no phase lag. Maximum 2f signal out of the mixer is achieved if the phase inside the first term in equation (3.23) is zero.

3.6 2f signal bandwidth and filter bandwidth

As mentioned above the low pass filter after the mixer must remove higher frequency components than the 2f signal. However, the filter bandwidth can not be too narrow. If this happens frequency components of the 2f signal will be removed. These are two contradictory requirements. A mathematical work on the 2f signal in equation 3.18 using Fourier techniques and appropriate parameter such as the line shape and the modulation amplitude the signal bandwidth can be determined. The bandwidth of our 2f signal at room temperature and atmospheric pressure can be coarsely estimated in the following manner. The ramp scan has a repetition rate of 80Hz which gives a period time of 12.5ms. Within this period only 2.6ms is used to scan the absorption

[3] A pulse takes a time given by the travel length divided on the pulse velocity. The travel length is the fiber length and the velocity is the vacuum velocity divided on the effective mode refractive index

line. The width of the 2f signal is approximately 15 samples in a 64 sampling window. This is equal to ($2.6ms \times 15/64$) 0.61ms. This value can be directly measured on the 2f signal on the oscilloscope. Using the thumb rule

$$\Delta f = \frac{1}{T} \approx 1.65kHz \tag{3.25}$$

where Δf is the signal bandwidth and T is the pulse width in time domain. However, the bandwidth for the 2f signal shape is more than this. To be on the safe side it is estimated to $2\Delta f = 3.3kHz$.The filter after the mixer must have a bandwidth bigger than this in order to not alter the signal shape. However, at lower pressures the absorption line width is smaller and a smaller modulation amplitude is applied. This results in a narrower 2f signal shape and thus a higher signal bandwidth, Δf.

4 Signal and noise discussions

4.1 Definitions

There are so many ways to define noise. To avoid confusions we use the root mean square amplitude per root hertz as the noise amplitude. We find it convenient to express the noise amplitude normalized to the square root of the detection bandwidth for easy comparison. When talking about the sensitivity we use the minimum detectable signal amplitude which is equal to the rms noise amplitude, i.e. signal-to-noise ratio equal to 1. In absorption spectroscopy it is usual to express the sensitivity in absorbance unit. This is a quantity of how much lost beam light that can be detected. A sensitivity of 1×10^{-6} means that $1nA$ photocurrent change in a $1mA$ steady photocurrent can be detected. Formally it is given by

$$A = \frac{i_n}{i_{pd}} \tag{4.1}$$

where i_n is the noise current and i_{pd} is the steady photocurrent.

Often, sensitivities are also expressed in ppm or ppb units. This means how much concentration change that can be detected. The absorbance unit is general. However, units expressed in ppm are dependent on the absorption strength of the absorption line. Hence, sensitivity expressed in ppm is only meaningful when the line strength is provided. Due to the convenience of each definition we use both in this thesis. Electronic noise is mainly set by the front end electronics. We begin to analyze the electronic noise. Optical noise is discussed at the end of this chapter.

4.2 Sensitive detections

Due to tunability, low cost, cw operation at room temperature and simple control electronics diode lasers are widely used in NIR absorption spectroscopy. DFB lasers have extreme narrow spectral linewidths. Our NLK1S5EAAA DFB diode laser designed for $1.51\mu m$ has a spectral width of 2MHz and 10mW fiber output at 50mA injection current. Despite these advantages, the practical used of diode lasers has been limited by excess noise, sensitivity to optical feedbacks, and sensitivity to injection current fluctuations. Several modulation schemes have been investigated to reduce the noise and improve the sensitivity. Frequency modulation spectroscopy, which is a variant of wavelength modulation spectroscopy, but with higher modulation frequency(GHz), moves the detection bandwidth outside the laser excess noise region. Sensitivities of 1×10^{-7}-1×10^{-8} in absorbance unit have been reported[43, 5, 30, 9]. However, these techniques require complex electronics, are high cost, and are not widely applied for commercial use.

Wavelength modulation spectroscopy uses modulation frequencies substantially smaller (kHz) than the full-width-at-half-maximum (FWHM) of the absorption line. The complexity of the electronics is greatly reduced due to operating in the low RF

region. Engelbrecht[14] used 28kHz modulation frequency and achieved 0.64×10^{-6} sensitivity at 1Hz measurement bandwidth with a DBF fiber pigtaled diode laser and double beam technique. NEO[26] achieves a sensitivity down to 3×10^{-6} with 52.3Hz noise bandwidth with their free air lasers and single beam technique. To obtain a sensitivity like that without a reference beam the instrument apply complex signal processing algorithms. In addition signal averaging is applied to reduce the effective noise bandwidth.

The dominating noises in practical wavelength modulation spectroscopy systems are etalon fringes and laser feedback noise. Etalon noise can be reduced by careful design of the optical system and laser feedback noise can be reduced by use of optical isolators. However, the laser excess noise with noisy lasers can cause problems. Baseband noise suppression to the shot noise limit has been demonstrated by Hobbs[22, 23, 21]. An balance receiver with dual beam measurement can suppress common signals and common noise in the signal beam and the reference beam. The background signal can be reduced by 55-70dB or more. By doing this the laser excess noise is reduced to a level such that the shot noise dominates. Wavelength modulation measurements with sensitivities down to 10^{-8} - 10^{-9} with detection bandwidth of 1Hz is theoretically possible with laser power greater than $1mW$.

4.3 Sensitivity

The system can not detect signals weaker than the noise. The instrument sensitivity is by definition the signal-to-noise ratio SNR = 1 with a detection bandwidth of 1Hz and 1m optical path length. As an example the shot noise of a steady $5mA$ photodetector current is $40pA/\sqrt{Hz}$. This is equal to a line center absorption of 8×10^{-9}. Hence, >0.4ppb NH_3 is detectable ($1ppm = 2 \times 10^{-5}$ at atmospheric pressure and room temperature). In a practical system the sensitivity limit is mainly set by the etalon fringes due to the wavelength scan and laser feedback noise. NEO's instrument has a sensitivity of 0.15ppm with 52.3Hz measurement bandwidth and 1m optical path length.

In a general system the output noise consists of flicker noise or 1/f noise, thermal noise, detector shot noise, laser excess noise, residual amplitude modulation (RAM) noise, background fluctuations and the slowly moving etalon fringes. The expression for the signal-to-noise ratio is given by

$$SNR = \frac{\overline{i_s^2}}{\overline{i_{fl}^2} + \overline{i_{th}^2} + \overline{i_{sn}^2} + \overline{i_{ex}^2} + \overline{i_{RAM}^2} + \overline{i_{et}^2}} \tag{4.2}$$

where the numerator is the signal and the denominator is the square sum of all noise terms stated above(flicker, thermal, shot, excess, residual amplitude modulation and etalon noise). Dependent on operation conditions one of them might dominate. When the laser intensity is weak the thermal noise and op amp noise may dominate because larger feedback resistors are necessary. When the modulation frequency is low the flicker noise may be significant and when the laser intensity is high the detector shot

noise dominates. In many WMS systems based on tunable diode lasers and well designed electronics the etalon noise and the laser feedback noise are the dominating noise problems that limit the instrument sensitivity. Etalon fringes, appear as oscillations in the 2f signal, drift due to temperature fluctuations and mechanical displacements. The fluctuation or drift of the background noise due to nonlinearities in the laser current-power characteristic or the detector power-current response also reduces the sensitivity. The background noise can be reduced by detection at the fourth or sixth harmonics by expense of the signal amplitude[6, 12]. Laser feedback due to backscattered light into the laser cavity change the background noise. In a real system all these noise sources add together and give the observed noise in the 2f signal.

The objective of this chapter is to identify and analyze these noise sources. When all noise sources are identified we try to find methods to eliminate them or reduce them to an acceptable level. In the next chapter we describe two all-electronic noise suppression methods.

4.4 Electronic noise sources

4.4.1 Flicker noise

This noise occurs in all semiconductors at low frequency[47]. This noise amplitude is approximately proportional to 1/f, therefore sometime called 1/f noise. This noise is the predominant noise source for systems operating under 100Hz. In our system, the modulation frequency is near 100kHz and the detection region is around 200kHz, far from this noise region. Hence, we can neglect the contribution of this noise source.

4.4.2 Thermal noise

Thermal noise is due to random motions of current carriers (electrons) in the feedback resistor in the transimpedance preamplifier. This stage converts precious laser photons to photocurrents and is referred as the front end. The thermal noise appears across all resistors in the system. Because of small signal amplitudes at the front end input, the dominating thermal noise source is the feedback resistor in the transimpedance amplifier. This noise is well known and can be easily found in the literature, e.g. [40, 11, 38, 47]. It's spectrum is flat (white noise) and the noise amplitude is dependent on the operating temperature and the detection bandwidth. The rms amplitude is given by

$$i_{th} = \sqrt{\frac{4kTB}{R_f}} \tag{4.3}$$

where i_{th} is the noise current, k is the Boltzmann's constant, T is the temperature in Kelvin, B is the system noise bandwidth and R resistor value. The noise bandwidth is not equal, but related to the filter bandwidth after the mixer. From equation (4.3) the current noise goes up when the resistor value goes down. This resistor determine the transimpedance gain and the bandwidth. Rising it reduce the thermal noise and the

signal to noise ratio goes up (if we for now neglect the op amp input noise). However, the input voltage noise amplification will rise with increasing feedback resistor values and may dominate the total noise. Additionally, rising the feedback resistor too much will saturate the op amp output and reduce the bandwidth. However, it can be safely reduced as long as the shot noise dominates. A 23Ω feedback resistor generates equal amount of thermal noise as 2.2mA photocurrent shot noise ($26.6pA/\sqrt{Hz}$)

When NEO's preamplifier is used the transimpedance gain is set to $R_f = 165\Omega$ which is the minimum gain in order to not exceed the linear region of the mixer. With $22mW$ fiber output power the photocurrent is $18mA$ at the ramp end with two lenses and a detector responsivity close to unity. With our preamplifier designs the feedback resistor is $1k\Omega$ when using the 1x4 fiber coupler to limit the peak output voltage to around 3V ($\pm 5V$ op amp voltage supplies). As a numerical example to illustrate how quiet this noise is at room temperature across a $1k\Omega$ resistor. This current noise is

$$i_{th} = \sqrt{\frac{4 \cdot 1.38 \cdot 10^{-23} \cdot 300}{1000}} \approx 4.07pA/\sqrt{Hz} \tag{4.4}$$

This is equal to a sensitivity of 1.85×10^{-9} with 1Hz measurement bandwidth expressed in absorbance unit with $2.2mA$ photocurrent. The collected photocurrent in the signal photodiode is approximately $2.2mA$ when all optical elements are mounted. The output voltage at the ramp end is approximately $i_s R_f = 2.2V$. Operating at high transmissions (low absorption, little scattering and small signal losses), i.e. high detector current, the thermal noise can be neglected. However, when using multi pass cells where the laser beam bounces many times between the optical mirrors. Each time loosing a fraction of light the detector current can become very small. Hence, more contribution from this noise to the total noise.

4.4.3 Shot noise

Figure 4.1 shows the shot noise[47, 38] in a P-N junction. This noise is generated in the photodiode and all semiconductor devices. It is caused by the discrete nature of charged particles, electrons. The arrival time of the electrons in a photodetector is a Poisson process[40] and each electron carries a charge of $1.6 \times 10^{-19} Coloumb$. The collected current is also a statical process with a mean value. This randomness gives rise to fluctuations in the photodiode current. The variance is defined as the rms noise amplitude and is given by

$$i_{sn} = \sqrt{2e(i_{dark} + i_{ph})B} \tag{4.5}$$

where e is the electron charge, i_{dark} and i_{ph} is the dark current and photocurrent respectively and B is the noise bandwidth. Normally, the shot noise from the dark current can be neglected. The op amp bias current also exhibit shot noise. This noise appear at the input of the transimpedance amplifier and is called input current noise density[17]. BJT devices exhibit large current noise and small voltage noise. When the signal amplitude is low FET devices should be used instead due to the very low bias current thus small input current noise. $13\mu A$ photocurrent noise has the same shot

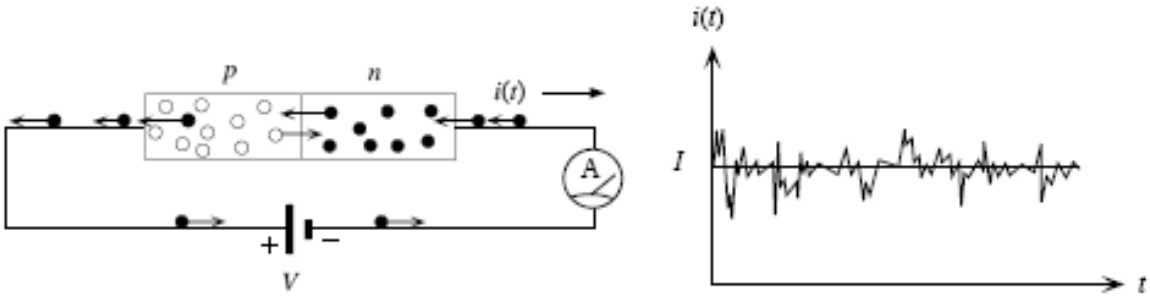

Figure 4.1: A P-N junction generate shot noise. Notice that the noise current and dc current are not in same scale. The noise is much smaller in amplitude. Figure from [41]

noise density as the current input noise density ($2pA/\sqrt{Hz}$) of the ultra low voltage noise AD797 from Analog Devices. With a photocurrent of 2.2mA the rms noise is

$$i_{sn} = \sqrt{2 \cdot 1.6 \cdot 10^{-19} \times 2.2 \cdot 10^{-3}} \approx 26.5pA/\sqrt{Hz} \tag{4.6}$$

which is more than 6 times bigger than the thermal noise and is the fundamental limit in TDLAS systems. This noise is a nature of light rather than an accessible noise source and is the ultimate limit. Hence, an absorbance greater than 1.2×10^{-8} is detectable with a detection bandwidth of 1Hz. Double beam systems, one as a signal beam and one as a reference beam, has a 3dB penalty due to uncorrelated shot noise in the two individual photodetectors. Hence, the shot noise limit is 2.4×10^{-8}

4.4.4 Electronic noise

In all high sensitivity systems the photodiode front end dictates the noise floor because the detected signal so small here. The life between the photodetector and the signal processing electronics is far from glamorous. They are supposed to turn the photocurrents from the detectors into a buffered voltage replica while preserving the signal-to-noise ratio. Nobody notices them until they stop doing their job. The optical system can be as wonderful as it can be and the signal processing electronic can be state of the art. If the front end electronics (preamplifier) is badly designed it can drag the precious photoelectrons deeply into it's own noise. In this section we analyze the noise of the preamplifier. The output noise is not the front end noise alone, but rather a complex combination of many electronic stages before the analog to digital capture process. However, a good preamplifier can make measurements at shot noise limit possible.

Figure 4.2 shows the design of the transimpedance amplifier. The op amp provides the PIN photodetector a virtual ground at the inverting input with very small impedance. Practically no current flows into the input pins and the op amp generates a current of the same amplitude which flows through the feedback resistor and into the summing node of the inverting pin. This satisfy Kirchhoff's current law and a the

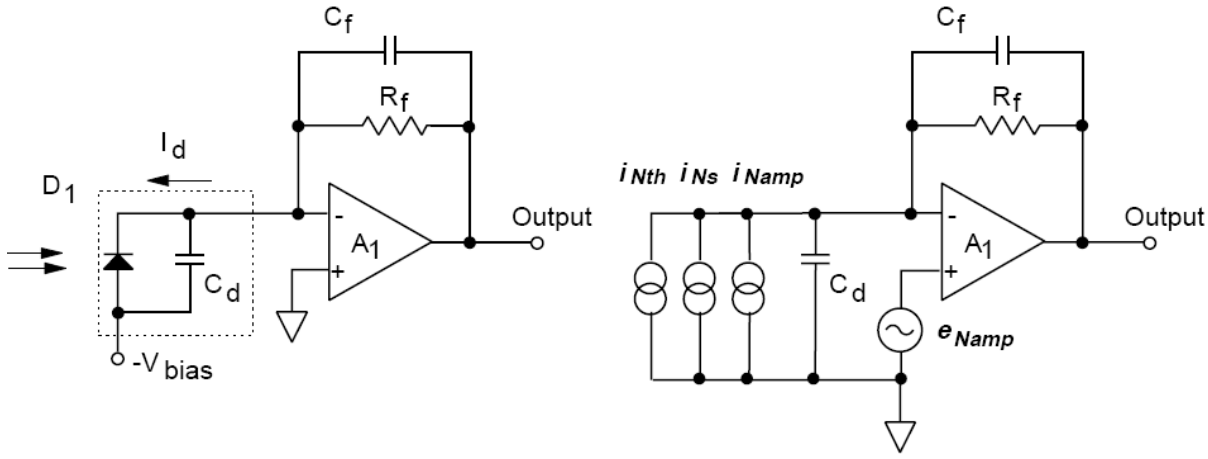

Figure 4.2: The photocurrent generated by InGaAs PIN photodetector is connected to a virtual ground (the inverting pin of the op amp). The same amount current is generated by the op amp and flows through the feedback resistor. The voltage drop across it is a replica of the photocurrent in voltage. Figure from [25]

signal current is translated into a buffered voltage at the output. The conversion gain is simply the magnitude of the feedback impedance (C_f as gain flatness capacitor in parallel with R_f). When using single beam measurement without fiber couplers this impedance is $R_f = 165\Omega$. We use $R_f = 1k\Omega$ for measurements with the 1x4 fiber coupler. Higher gain is used because the fiber output power is less with fiber couplers. In the single beam scheme a peak photodiode current of 18mA at the end of the ramp scan translates to a peak voltage of 2.97V. This is within the dynamic range of the operational amplifier when using $\pm 5V$ power supplies.

The simplified noise model is shown to the right in figure 4.2. As we can see from the figure all noise terms are treated identically, in parallel. Only the shot noise comes from the detector, the resistor thermal noise and op amp current noise is added to the shot noise. In addition the op amp input voltage noise is placed at the non-inverting pin for simple analysis. We can write the current noise for this model as

$$i_n = \sqrt{i_{th}^2 + i_{sn}^2 + i_A^2 + \frac{e_A^2}{R_f^2}} \tag{4.7}$$

where the noise terms inside the square root are thermal noise, detector current shot noise, op amp input current noise and op amp input voltage noise respectively. With no signal beam, for example blocked signal beam, the output noise is electronic noise alone (NEP noise of the detector is negligible in this case). When $i_{sn} = 0$ the remaining components are thermal noise, input current noise and input voltage noise. When the signal amplitude is small a bigger transimpedance gain is necessary, i.e. bigger feedback resistor value. The thermal noise is proportional to $\sqrt{R_f}$ and becomes dominating when it is bigger than the op amp noise. Using equation (4.7) and solving for this

situation we get the relation (remember no photcurrent)

$$4kTR_f > i_A^2 R_f^2 + e_A^2 \tag{4.8}$$

At a given temperature we can find which feedback resistor R_f that value makes thermal noise dominating for a specific op amp (specific i_A and e_A). Table 4.4.4 shows some relevant parameters for different low noise operational amplifiers available.

Op amp	AD797N	LT6233	LF537H	CLC425
Technology	BJT	BJT	JFET	BJT
Current noise	$2pA/\sqrt{Hz}$	$0.73pA/\sqrt{Hz}$	$0.01pA/\sqrt{Hz}$	$1.6pA/\sqrt{Hz}$
Voltage noise	$0.9nV/\sqrt{Hz}$	$1.9nV/\sqrt{Hz}$	$12nV/\sqrt{Hz}$	$1.05nV/\sqrt{Hz}$

Table 4.1: Comparison of noise op amp noise terms terms of different op amps. AD797 and LT6233 are BJT low noise op amps while the LF357H is a JFET op amp which has smaller current noise but bigger voltage noise. CLC425 is a ultra low noise wide bandwidth op amp from Burr Brown (Texas Instruments) with GBWP of 1.9GHz. LF357 has GBWP of 20MHz for comparison.

At room temperature the thermal noise starts dominating at $R_f = 49.5\Omega$ for AD797N. Hence, the dominating noise is the square sum of the op amp input current noise and the input voltage noise. BJT devices have smaller voltage noise, but bigger current noise compared to JFET devices due to a larger bias current. In comparison of different op amps we set the thermal noise and shot noise to zero. Doing this we get

$$i_n = \sqrt{i_A^2 + \frac{e_A^2}{R_f^2}} \tag{4.9}$$

or the voltage noise at the output

$$e_n = i_n R_f = \sqrt{i_A^2 R_f^2 + e_A^2} \tag{4.10}$$

With small feedback resistors (high photocurrent) the input voltage noise dominates and the current noise dominates at big feedback resistors. Input current noise dominates the input voltage noise when $R_f > 450\Omega$ with AD797N, $R_f > 650\Omega$ with CLC425, $R_f > 4.42k\Omega$ with LT6233 $R_f > M\Omega$ with LF357H. Too small feedback resistor values make the input referred thermal noise dominates the electronic noise. 165Ω feedback resistor has a equivalent input referred noise of

$$i_n = \sqrt{(0.78pA)^2 + (\frac{1.9nV}{165\Omega})^2 + (\frac{4kT}{165\Omega})^2} \approx 15.3pA/\sqrt{Hz} \tag{4.11}$$

according to equation (4.7). As we can see the thermal noise and input voltage noise dominate the electronic noise. Our AD797 with $1k\Omega$ feedback resistor has $4.6pA/\sqrt{Hz}$ equivalent input referred current noise. For comparison the photodiode current shot

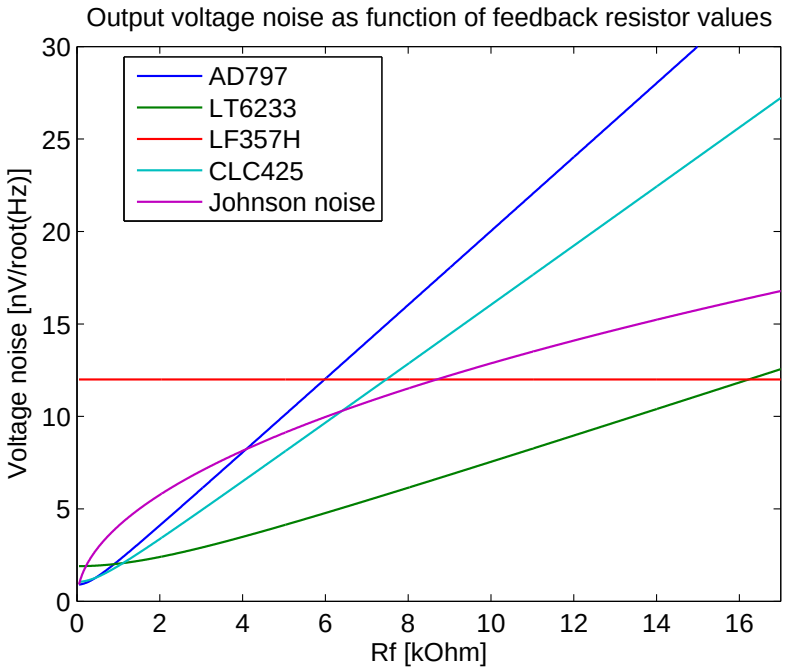

Figure 4.3: The electronic noise as function of feedback resistor values. AD797 and CLC425 is best at low feedback values while the LT6233, used in NEO's preamplifier, is best above 1k. The low cost (LF357H, 10% cost compared to the others, is best when $R_f > 16k$ with an output noise density of $12nV/\sqrt{Hz}$. The thermal noise (Johnson noise) dominates under normal operations

noise is $76pA/\sqrt{Hz}$ (with $i_s = 18mA$). We can therefor safely assume that the shot noise dominates.

Figure 4.3 shows the output voltage noise density given by equation (4.10) as a function of feedback resistor values for four good operational amplifiers. The LF357H is best with $R_f > 16k\Omega$ where the input noise current of LT6233 becomes comparable to the input noise voltage of the JFET LF357. The LT6233 is most quiet from 1k to 16k. The AD797 from Analog Devices which cost many times the LF357H drags the precious photocurrent deeply into it's own current noise already with high R_f values. However, AD797 is best suited for our application since the photocurrent is 4.5-18mA and requires $R_f < 1.2k\Omega$ to keep the output voltage swing less than 3V. If the photocurrents are smaller than 3mA the LT6233 will be best suited. VCSEL lasers have 1/10 output power compared to DFB lasers. When the signal power is below $200\mu W$ one should consider FET op amps to reduce the input current noise contribution. In measurements with much absorption or scattering due to dust (such as in aluminium melting furnaces) little light is collected at the photodetector. In multi-pass (Herriot-cells) gas cells the signal beam is greatly reduced due to many reflection-losses at the mirrors. Hence, larger feedback resistors to increase the transimpedance gain is necessary. The AD797 is a ultra-low-noise device and costs 120NOK from

ELFA/FARNEL[4]. The ultimate example of a pitfall is to blindly trust the "ultra-low-noise" name. Even though it costs only 10NOK the LF357H has many times lower noise than the AD797 when detecting μW signals. In this region the AD797 input current noise is unacceptable.

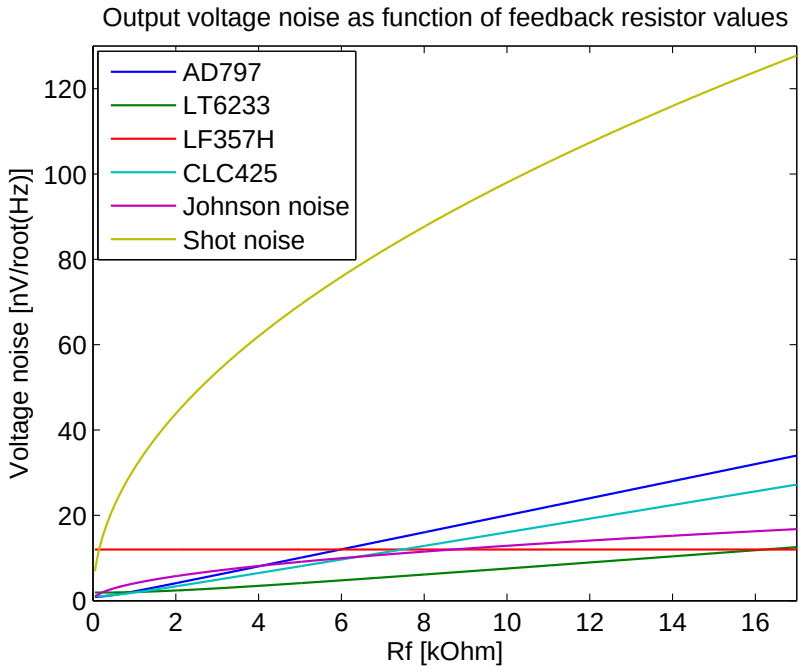

Figure 4.4: Shot noise as function of feedback resistor values is compared with the electronic noise. R_f is chosen such that the maximum output voltage is always 3V.

A plot where the shot noise is compared to the dark noise shown given in figure 4.4. We want a 3Vpp output signal and the feedback resistor is set to meet this requirement. The rms shot noise at this criteria is given by

$$e_{sn} = R_f \cdot i_{sn} = R_f \cdot \sqrt{\frac{3V}{R_f} \cdot 2 \cdot 1.6 \cdot 10^{-19}} = \sqrt{R_f} \cdot \sqrt{3 \cdot 2 \cdot 1.6 \cdot 10^{-19}} V/\sqrt{Hz} \quad (4.12)$$

This noise is plotted with the electronic noise for comparison. Notice that for each feedback resistor value the peak output voltage (at the end of the ramp scan) is 3V. Hence, an increasing R_f means decreasing signal current. This means that the SNR goes down when the signal current goes down. The SNR as function of signal current is given by

$$SNR = \frac{i_s}{i_{sn}} = \frac{i_s}{\sqrt{2ei_s}} = \sqrt{\frac{i_s}{2e}} \quad (4.13)$$

[4]www.elfa.se/no or www.farnell.no

Thus, a larger detector current by increasing the laser power improves the signal-to-noise ratio.

4.5 Analog Digital Conversion noise

The final 2f signal output is converted to a digital signal representation by the ADC. In this process the ADC itself contributes to a noise given approximately by[24]

$$e_{adc} = \text{ADU}/\sqrt{12} \tag{4.14}$$

where ADU is the Analog to Digital Unit ($V_{max}/2^n$ with n-bits amplitude representation). A 5V dynamic range and using 12 bits representation this noise is 0.35mV. It is important to ensure that this noise is not the dominating one. Our ADC noise is approximately 1.5mV. The shot noise contribution was measured to around 60-100mV. However, when using averaging the effective noise goes down and the shot noise also goes down (inverse proportional to the root of the bandwidth).

4.6 Detection bandwidth and noise bandwidth

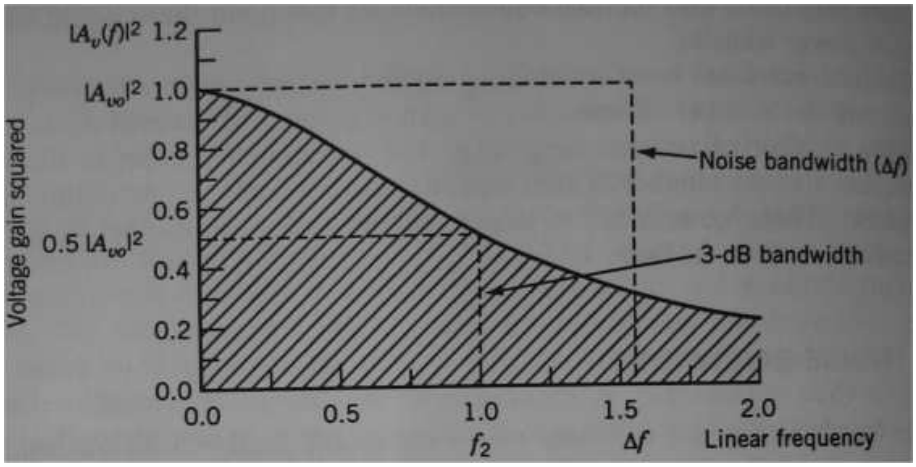

Figure 4.5: Filter and noise bandwidth. Figure from [35]

In section 3.6 we discussed about the bandwidth requirements for the post-filter after the phase-lock-amplifier. This bandwidth must be big enough to let through the 2f signal, and in the same time small enough to suppress higher harmonic signals. The post filter has a transfer function $H(f)$ and a 3dB corner f_{3dB}. Signals outside the 3dB are attenuated and thereby limits the noise bandwidth. The detection bandwidth is set by this transfer function bandwidth. The frequency response can be measured by using a signal generator to generate an input signal at different frequencies. The output amplitude divide on the input amplitude gives the amplitude response $H(f_1)$ at frequency f_1. The bandwidth can be found to where the amplitude response has

been reduced to 0.707 of it maximum value. The noise bandwidth is related to this detection bandwidth but is not the same. The noise bandwidth is defined as the area under the power transfer function divide on the maximum transfer function value[35]. Mathematically it is

$$B_n = \frac{1}{G_0}\int_0^\infty G(f)df \tag{4.15}$$

where G_0 is the maximum value and $G(f)$ gain at the frequency f. Usually $G_0 = 1$ (normalized transfer functions) and is left out. In electrical circuits the output is in voltage/current. The power function is then the square of the transfer function $H(f)$. Using $H_0 = 1$ as the maximum value, the analog noise bandwidth is given by

$$B_n = \int_0^\infty |H(f)|^2 df \tag{4.16}$$

The noise amplitude is proportional to the square root of this bandwidth. Since the noise bandwidth is related to the area under the frequency response curve it's area should be minimized. A filter with faster roll off after the -3dB frequency gives smaller noise bandwidth. Hence, the detection bandwidth should be minimized to reduce the noise bandwidth. Linnerud[31] has measured the noise bandwidth for our system and estimated it to be $13.4kHz$.

The signal bandwidth depends on the modulation scheme and physical parameters. The wavelength scan takes approximately $2.7s$ (dependent on software parameters). Within this ramp sweep we have the 2f signal shape. This shape was roughly estimated to be $3.2kHz$ in section 3.6. However, at lower pressures larger filter bandwidths are necessary to let through a narrower 2f signal shape. The signal bandwidth must always smaller than the detection bandwidth!

4.6.1 Effective noise bandwidth and acquisition time

When using averaging the effective noise bandwidth is reduced by 1 over number of scans. In one second the ramp scan sweeps 80 times across the absorption line. Each sweep the ADC takes 64 samples of the 2f signal. The instrument averages 256 samples before calculating the gas concentration, thus reducing the noise bandwidth by a factor of $\sqrt{256} = 16$. A concentration calculation takes approximately (256/80=) 3.2 seconds.

4.7 Optical noise sources

4.7.1 Relative intensity noise/laser excess noise

Laser excess noise is referred to noise above the shot noise. Diode laser excess noise comes from a statistical process in the gain medium. Backscattered light affects the coherence light amplification in the gain medium and thus causes variations in the laser intensity[40]. This happens when the light escaping the laser facet is reflected back from the fiber end. This light is transmitted into the laser cavity and stimulates

new photons that are not in phase with the photons in the resonant modes. The fiber end is placed a distance from the laser facet thus making a Fabry-Perot cavity with short cavity length. An isolator can be inserted right after the PM fiber to reduce back reflections and thus reduce this noise. However, the feedback noise from the cavity between the laser facet and the fiber facet inside the laser module can not be reduced. RIN noise can be measured using a PIN photodetector and low noise preamplifier in combination with a spectrum analyzer to record the spectral noise density. This noise decreases with increasing modulation frequency. Frequency modulation spectroscopy uses high RF frequency to escape this noise and shot noise limit sensitivity is obtained. RIN is expressed as

$$RIN(dB) = 10log(\frac{<\Delta P>}{P_0})^2 = 20log(\frac{<\Delta P>}{P_0}) \tag{4.17}$$

where P_0 is the average laser power. Relative intensity noise is due to random fluctuations in the laser intensity. Good lasers have RIN less than $-140dB/Hz$. To illustrate this noise we look at an example: If our laser is operating at an average output of $P_0 = 22mW$, the noise amplitude is $\Delta P = 2.2nW/\sqrt{Hz}$ according to equation (4.17). With a linear responsivity R_0 the noise current on the photodiode can be written as:

$$\Delta i_{pd} = \eta R_0 \Delta P \tag{4.18}$$

If we assume a coupling efficiency $\eta = 85\%$ (loss in collimation lens, focusing lens and beam waste) and $R_0 = 0.95$ at $1512nm$, this gives us a RIN noise of $i_n = 1.78nA/\sqrt{Hz}$. However, we notice a worse noise with our DFB laser when operating in single beam mode. We measured this noise by turning off the ramp scan, thus the laser frequency is fixed. In addition the modulation signal is also turned off. The laser beam is therefor a steady dc beam and the recorded 2f signal is a sum of the laser noise and the electronic noise. Since the electronic noise is much smaller ($15.3pA/\sqrt{Hz}$ as calculated earlier) we can safely assume that all the noise stems from the laser excess noise. Figure **??** shows the 2f signal captured with these instrument settings. The excess noise is 40 times lower than the noise in normal mode (with scan and modulation). The excess noise amplitude is 1.53×10^{-6} in absorbance unit or 0.06ppm NH_3 at ambient pressure and temperature with 1m optical path length. This result is $43.8dB$ above shot noise. What cause this penalty is a complex combination, but we suspect back reflections from the fiber coupling and the non-ideal behavior of the laser diode temperature controller. This topic is discussed further in chapter 7.

4.7.2 Etalon noise

This is the dominating noise source in our optical system. The noise is caused by non-uniform transmission characteristics of the laser light through optical components. Glass windows work like weak mirrors with a reflectance given by

$$R = |r|^2 = (\frac{n_g - 1}{n_g + 1})^2 \tag{4.19}$$

where n_g is the refractive index of the glass window. If we now consider two such windows placed with a distance L from each other filled with air. The transmittance is given by[19]

$$T = 1 - R = \frac{1}{1 + Fsin^2(\delta/2)} \tag{4.20}$$

where the coefficient of finesse $F = \frac{4R}{(1-R)^2}$ and $\delta/2 = \frac{2\pi}{\lambda} nLcos(\theta)$. For transmission normal to the glass interface $\theta = 0$ and n=1 for air. Figure 4.7.2 shows the transmittance for different values of F, thus R. For air-glass interfaces $F \approx 0.2$ and the

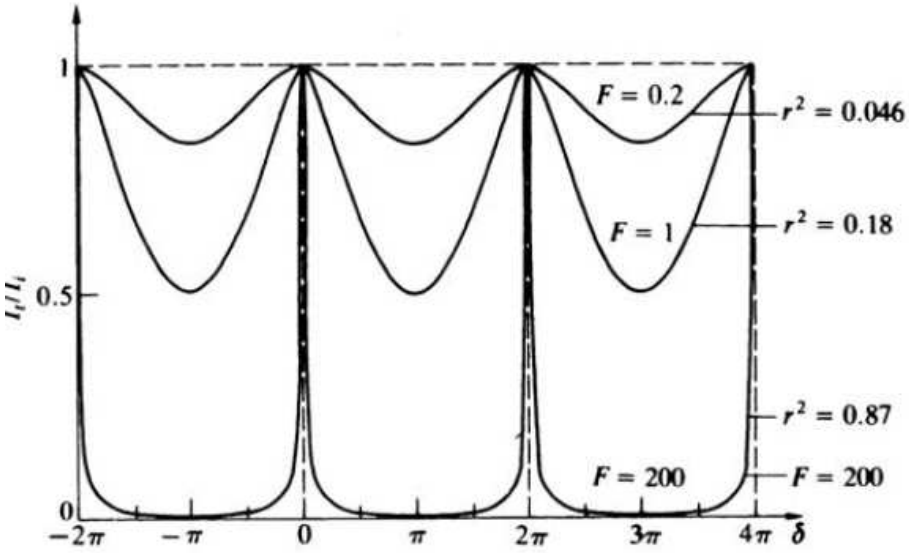

Figure 4.6: Transmission for three values off. The period depends on the spacing between optical interfaces. The width depends on the optical reflectance. Figure from [19]

transmission as function of δ is shown in the figure. The total transmission coefficient is a cascade product of all transmission coefficients, i.e. $T = T_1 \times T_2 \times ... \times T_n$. If we consider our laser beam is transmitted through this system, the light intensity on the detector is simply the laser intensity multiplied with the transmittance, i.e. $I_{det} = T \cdot I_{laser}$. When the modulated laser wavelength is slowly ramped over the transmission minima higher order harmonic signals are generated. The amplitude and shape of this etalon signal depends on the spacing distance between the optical interfaces and their refractive indices. Short distances result in slowly varying oscillations and far spaced optical windows give fast oscillation signals. As an example glass windows 3cm from each other give 5 oscillation minimas/maximas within a ramp scan. The amplitude is approximately 10^{-3} expressed in absorbance unit (can bee seen from figure 4.7). This signal is superimposed on the second harmonic signal generated by the gas absorption line and alter it's shape. Unfortunately, very small optical path length (in magnitude of the light wavelength) changes in this transmission system can cause the oscillations to "run". In the time domain these oscillations move relative to

the 2f signal shape and alter it amplitude and shape. This phenomena is common in all TDLAS systems. Careful optical design reduces this problem. By installing piezo elements on the critical glass surfaces and inputs RF signals oscillating with a high frequency makes these oscillations "run" fast compared to the ramp scan. Averaging many many ramp scans suppress the this etalon noise. The detector can not differentiate which signal comes from the absorption line and which is the unwanted signal component from the Fabry-Perot. This unwanted signal is regarded as noise in our system. However, in some cases the 2f is useful, such as determining the wavelength ramp, the wavelength modulation coefficient[14], the intensity-wavelength lag phase φ. The free spectral range, FSR, is given by

$$FSR = \frac{\lambda^2}{2nL} \tag{4.21}$$

where λ is the laser wavelength. In IR spectroscopy it is common to use the wavenumber, $\frac{1}{\lambda}$. The FSR is $\frac{1}{2nL}$ in wavenumber. For air-glass interferometers the transmission minimas can be treated like absorption lines spaced FSR from each other. The width of these transmission minimas is approximately half of the free spectral range, as readily seen from figure 4.7.2. Free spectral ranges close to the FWHM of the absorption line profile is detrimental in absorption spectroscopy. These etalons will generate 2f signals of significant amplitudes and destroy the clean second derivative shape of the gas absorption line. It is difficult to remove these oscillations with analog or digital signal processing. Etalon fringes must be avoided when designing optical systems. FWHM of the chosen NH_3 absorption line at atmospheric pressure is approximately $0.2cm^{-1}$ and optical surfaces spaced with $L \approx 2 - 4cm$ must therefor be avoided. An ultimate example of how destructive this is for absorption spectroscopy is shown in figure 4.7. These figures are taken from the oscilloscope when the instrument uses our

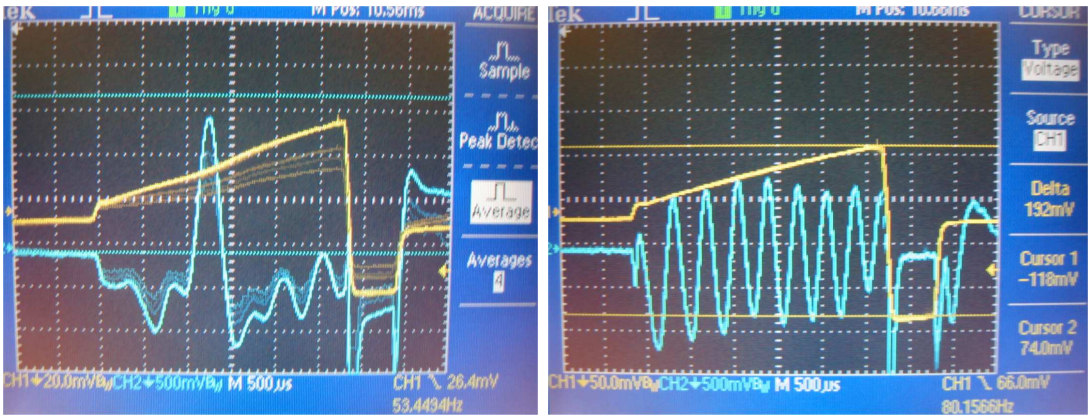

Figure 4.7: Etalon noise with the focusing lens 4cm from the detector window. The strong contribution of the etalon fringes destroys the 2f signal shape. Notice the small dip in the direct signal due to the absorption line. Measured with our own noise suppresser with dual beam technique

own preamplifier design and dual beam measurement. Here the 3.1cm focal length is

placed approximately 4cm from the detector to de-focus the beam. That lens was fast replaced with a 10cm focal length to avoid these effects. Usually we observed much smaller FSR because of the long distance between optical components. Usually optical windows are wedged to avoid multiple reflections. There are also much bigger FSR due to thin optical windows and lenses. These noises are more difficult to eliminate, but fortunately for big FSR compared to the wavelength modulation, i.e. $\delta\lambda \ll$ FWHM, the $\frac{\partial^2 T(\lambda)}{\partial \lambda^2}$ (second derivative of the transmission) is small and contributes little to the measured 2f signal.

4.8 Noise sources in optical fibers

4.8.1 Phase fluctuation

If the second derivative of the absorption spectrum at the actual wavelength range (near 1512nm) where the NH_3 absorption line occupy is of considerable magnitude a background signal from the second derivative of the transmission will be added to the output. In section 3.4 we discussed about the phase φ_{fiber} which is a phase lag in the intensity signal due to a longer optical path. This phase depends on three parameters: modulation frequency, effective mode index and the physical length of the fiber as indicated in equation 3.24. We assume that the modulation frequency and the physical length of the fiber are stable and fixed. In industry applications the fiber will be exposed to temperature changes. When the temperature changes the mode refractive index will change. This change leads to a change in the phase φ_{fiber} according to

$$\Delta\varphi_{fiber} = \frac{2\pi f L}{c} \cdot \Delta n_{eff} \tag{4.22}$$

where Δn_{eff} is the refractive index change due to an temperature change. When the fiber length is long and the frequency is high the instrument is more sensitive to the temperature effects. A small refractive index change in short fiber lengths gives small effects on the phase. However, for fiber lengths of several kilometers the phase change $\Delta\varphi_{fiber}$ becomes significant as can be calculated approximately by use of equation (3.24). To compensate for the phase error we need the refractive index slope $\Delta n/\Delta T$ and the fiber temperature. Having control on the fiber temperature profile is is difficult to realize.

5 Noise suppression

The sensitivity limits of laser based instrumentation is often set by laser excess noise and spurious signals of one or another kind. The excess noise[22, 21, 51] from the laser beam stems from the laser driver current fluctuations, the laser feedback noise, temperature fluctuation in the laser diode due to non-ideal temperature control, mode hopping, etc... Optical systems have very wide temporal bandwidth and linearity[22]. Hence, the signal to noise ratio is constant throughout the entire measurement path. No relative change in amplitude or phase occur on the laser beam. The noise intensity is therefor proportional to the DC[5] level. Lets say that our laser beam consists of a DC signal (used to tune the laser wavelength), a modulation signal (used to modulate the laser wavelength) and a noise term (all unwanted signals) given by

$$P = P_{DC} + P_{mod} + P_{noise} \tag{5.1}$$

where P is the laser beam power or intensity. If we split this laser beam into two beams all the components above split equally.

$$P_s = \alpha(P_{DC} + P_{mod} + P_{noise}) \tag{5.2}$$

$$P_r = (1-\alpha)(P_{DC} + P_{mod} + P_{noise}) \tag{5.3}$$

where P_r and P_s are the reference and the signal beam intensity respectively. α is the splitting amount and ranges from 0 to 1. If we let the signal beam go through a gas cell harmonic signals are added to the signal beam. At the same time, since the optical system temporal bandwidth is very wide all components above are attenuated equally due to loss in optical interfaces, scattering and absorption. Figure 5.1 illustrates this principle. These two beams hit two identical photodetectors and a automatic gain circuit adjusts the DC level of the two beams to the same level. Hence, after the summation the DC signal and common signals are cancelled. Ideally we only have left harmonic signals generated by the absorption line. As seen earlier in equation (3.14) from section 3.4 the signal to the mixer is given by

$$i_{pd}(t) = [i_{pd0} + \delta i_{pd} \cdot \cos(\omega t)] \cdot [1 - \sum_{k=0}^{\infty} [\delta\lambda \cdot cos(\omega t - \varphi)]^k \cdot \frac{\partial^k \alpha(\lambda_0)}{k! \cdot \partial\lambda^k} \cdot L] \tag{5.4}$$

Noisy lasers can easily have a noise spectral density 50dB above the shot noise floor. We showed that our laser exhibits approximately 40dB above the shot noise level. If we can cancel this excess noise, measurements at the shot noise limit are possible. Amplitude noise cancellation has been available for some while. Nuss[15] et. al. demonstrated 50dB reduction of the amplitude noise. The control system takes a sample from the laser beam and adjusts the injection current such that the noise is suppressed. This is a forwarding regulator system. A different method ("Noise Eater")

[5]By DC level we mean the slowly varying signal compare to the modulation signal. In this paper the DC level is the sawtooth signal, and has a repetition frequency of 80Hz, in our modulation scheme. In case of a steady laser beam the DC level is a constant.

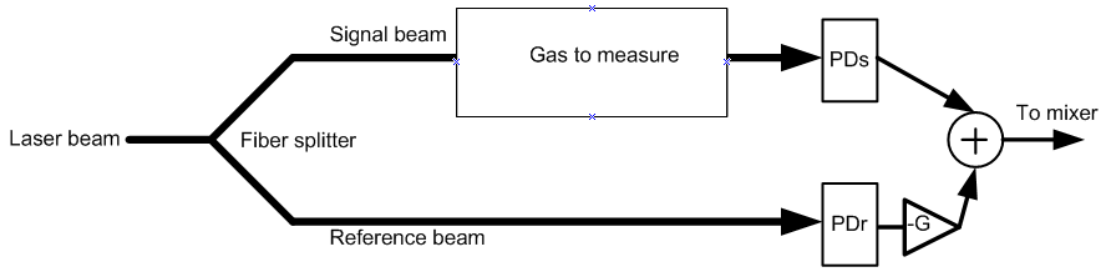

Figure 5.1: The laser beam is split into two beams, one goes through the gas cell and harmonic signals are added to this beam, the other goes outside the gas cell and no additional signal is added. The negative gain G inverts the reference beam. Summation removes common signals in the two beams and ideally the input to the mixer is free of laser excess noise.

is to use an external Electro-Absorption modulator to suppress the noise. The stable intensity is traded by a reduced beam intensity. They are useful but not capable to approach the shot noise because of their weak sample beams and poor bandwidths. A low noise laser beam is required for pumping lasers since it is driving the system. However, in second harmonic absorption spectroscopy we only require a stable and low noise photodetector current. This enables us to use wide bandwidth electronics and low noise components (transistors and operational amplifiers) to suppress the photodetector current noise. The noise canceling technique was first investigated by Hobbs[22] in 1991. Hobbs used two reverse bias photodiodes and two bipolar transistors to form a current divider. A feedback loop outside the signal path continuously monitors the dc level at the transimpedance amplifier output and a servo integrating amplifier, working as the feedback, balances the current splitting ratio of the two transistors such that the dc level at the summing node of the transimpedance amplifier is zero all the time. Since the noise is proportional to the dc level, it is cancelled with the current ramp.

The other configuration is based on the photovoltaic mode of the photodetector. The design presented by Zhu[51] et al. uses a light dependent resistor (LDR) and a light emitting diode (LED) to adjust the dc level of the detector current. Unlike Hobbs' design this uses zero biased PIN detectors for best linearity, at the expense of a reduced bandwidth due to a larger internal capacitor inside the photodiode. This configuration also eliminates the dark current thus removing the offset. When high speed is required a bias voltage across the photodiode will enlarge the depletion region and thus reduce the parasite capacitor. However, the bandwidth requirement is not a problem with existing photodiodes. Large area ($> 1mm$) can reach several MHz and we detect at 200kHz. More importantly, the linearity of the photodiode must be good to reduce the background noise which stems from the nonlinearity of the the photodiode response when using large modulation amplitudes. The laser background noise also increases with larger modulation depths, but is not accessible in the receiving

end of the system. However, a good designed noise suppresser will suppress this noise and lower the noise floor.

5.1 Why use dual beam technique?

The signal to noise ratio increases with increasing photodetector current as indicated by equation 4.13, SNR $= \sqrt{\frac{i_s}{2e}}$. By using dual beam techniques the available laser power must be split into two beams. In addition the reference beam must be stronger than the signal beam, and the signal beam is therefor reduced by a factor larger than 2. This will decrease the signal to noise ratio by a factor of $\sqrt{2}$ or more. However, the dominating noise in many laser systems is not the shot noise. Dual beam detection can reduce coherent noise that is common in both the signal and the reference beam. The signal to noise ratio can be increased many times, as we will see in section 7. Additional, the unwanted intensity modulation signal can be removed to relax the mixer requirements. We successfully reduced the intensity modulation signal by more than 70dB. One more bonus is the ability to measure the absorption spectrum directly. This spectrum can be acquired from the log output or the linear output with the cosine modulation signal turned off.

5.2 Voltage domain subtraction

Figure 5.2 shows the schematic diagram of the electronic based noise canceller. The design consist of two operational op amps operating in transimpedance[39, 24] mode. The photodetector is zero biased with a virtual ground provided by the op amp. The high open loop gain generates a current flowing back through R_f to null out the voltage swing across the photodiode, hence zero biasing it. In this mode the amplifier input impedance is very small and all currents flows through R_f to the output. The photocurrents from the reference photodiode PDr and the signal photodiode PDs are converted into voltages at the outputs of each transimpedance amplifier. The AD797 was chosen because of its high gain bandwidth product (450MHz) and ultra low voltage noise ($0.9nV/\sqrt{Hz}$). Operating in high light level the feedback resistor is small thus the op amp current noise ($2pA/\sqrt{Hz}$) is of less concern. Large are photodiodes have large shunt capacitance which can greatly amplify the input voltage noise of the op amp. It's input voltage noise is also very little and is very suited for this application. The output voltages from these two preamplifiers are connected to the positive input of a summing op amp. A summing op amp gives an output voltage proportional to a weighted sum of the input voltages. Ideally the dc[6] summation current at the input of U2 is zero and all common signals are effectively canceled. The servo integrating feedback circuit controls the output resistance of the opto-isolator thus providing a scaling factor between the signal and reference voltage. The opto-isolator consists of a LED and a photoresistor in which it's resistance is controlled by the light intensity

[6]The dc component is the current ramp, 80Hz, and power drifts and are slowly varying signals compared to the 2f signal oscillating at 187.5kHz

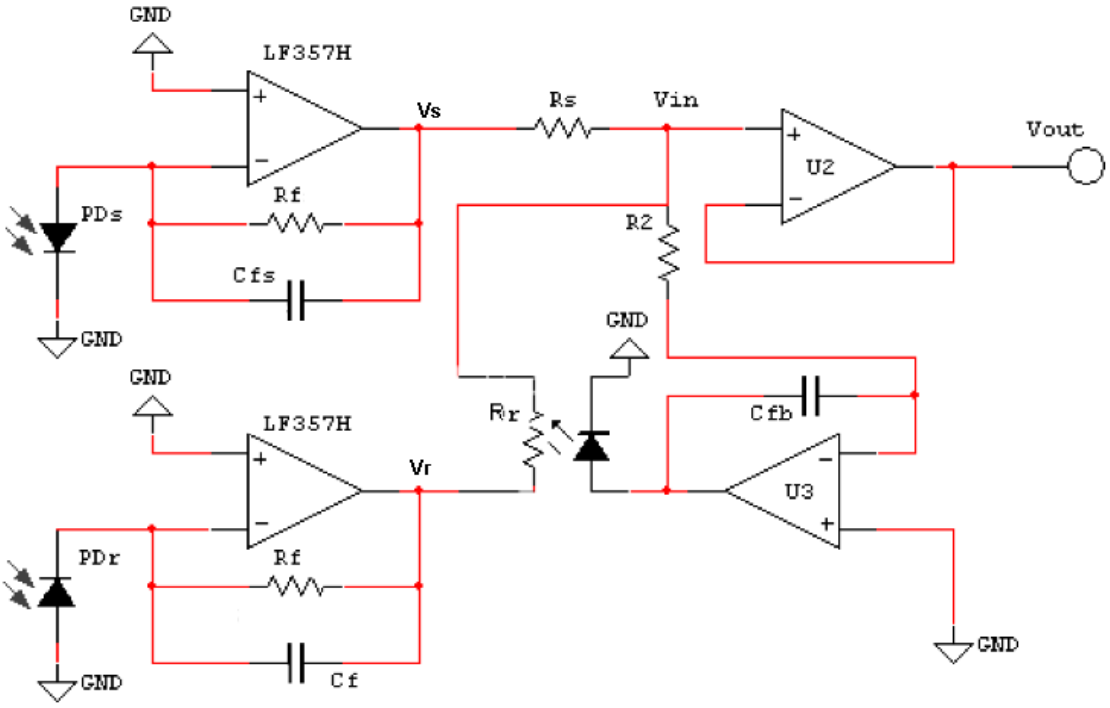

Figure 5.2: Schematic diagram of the noise canceller working voltage domain. Reference and signal output are subtracted at the input pin of the voltage follower. U3 output controls the light level thus R_r such that the dc output is always zero

falling on it. To investigate this circuit in detail we go through the mathematical steps and finally calculate the noise at the output terminal $Vout$.

The most fundamental equation which is applied to all op amps is the relation between the output voltage and the two input voltages given by

$$V_{out} = A_{ol}(V^+ - V^-) \tag{5.5}$$

where V^+ is the voltage at the positive input, V^- is the voltage at the negative input and A_{ol} is the open loop gain (i.e. with no feedback) which is usually extremely large (20×10^6 at dc for AD797, but decreases as 1/f). Due to the extreme open loop gain a slight voltage difference between the two input ports gives a saturated output voltage at the operational amplifier output. This seems quite meaningless. Well, this true, thus almost all op amps circuits are used with feedback (in some special circuits the large open loop gain is employed to give a two state output, i.e. threshold comparator). A negative feedback is achieved by connecting a resistor between the output pin and the inverted input pin. Hence a current can flow from the output back to the negative pin to force the voltage difference between the two pins to be equal. That's why all feedback applications we can assume that the two input pins always have the same

voltage potential. This and assuming to current flowing into the input pins greatly simplifies the calculations. These assumptions are valid because of the high input resistance and high open loop gain.

The positive input of the op amp in figure 5.2 is grounded and $V^+ = 0$. A negative feedback (R_{fs} and C_{fs}) forces the negative input to have the same voltage as the positive input, thus $V^- = V^+ = 0$. The photocurrent flowing into the negative input can not flow into the op amp due to a large input impedance and must be equalized by the feedback loop consisting of a 1k in parallel with the bandwidth limiting capacitor of 80pF. Applying Kirchhoff's current law to the negative input we get

$$i_s + i_{fb} = i_s + \frac{(V^- + V_o)}{R_f} = i_s + \frac{(V_o)}{R_f} = 0 \tag{5.6}$$

where i_s is the photocurrent, i_{fb} is the feedback current set up by the op amp to cancel the photocurrent and V_o is the transimpedance amplifier output voltage. The output voltage of the op amp is simply the feedback current multiplied with the feedback resistor. Rearranging the above equation and solve for the output voltage we arrive at

$$V_o = -i_s R_f \tag{5.7}$$

where i_s and R_f are the photocurrent and the feedback resistor respectively. Thus the output voltage at the op amps is the photocurrent multiplied with the feedback resistor. An input current is converted to a voltage at the output with a conversion gain equal to the feedback impedance(C_f and R_f). Notice that the reference photodiode is reversed with respect to the signal photodiode. This is done to achieve a negative reference current, in order to cancel the dc component and common noise. A differential amplifier can be used if the reference photodiode is not reverse connected. The signal output and the reference output are connected to a voltage follower. To find the voltage at the positive input pin we apply Kirchhoff's current law at the input pin. It states that the sum of currents flowing into this pin equal to zero.

$$\frac{V_s - V_{in}}{Rs} + \frac{V_r - V_{in}}{Rr} = 0 \tag{5.8}$$

V^- is connected to the output thus we have negative feedback. The high open loop gain forces the two input pins to have the same voltage potential. Hence, $V_{out} = V^+ = V_{in}$. Rearranging equation (5.8)and solving for V_{out} we arrive at

$$V_{out} = V_{in} = \frac{V_s R_r}{R_s + R_r} + \frac{V_r R_s}{R_s + R_r} \tag{5.9}$$

where R_r, R_s, V_s and V_r are shown in figure 5.2. Thus the output is a weighted sum of the input voltages. Recall that the reference photodiode is reversely connected and the V_r has a opposite sign compared to the signal voltage V_s. If we consider $i_r = -2 \times i_s$, the reference output voltage is also twice large. The circuit adjusts itself such that $Rr = 2 \times R_s$ and the subtracter output is zero. In a perfect subtracter the phase

added by the transimpedance circuits are equal and all coherent signals are removed. The only signals that appear at the output are the harmonic components generated by the absorption line in the gas sample. But in practice there are deviations in component values thus give nonidentical phase response. Hence the suppression is not perfect. Because of drifts in the signal beam intensity due to more gas, scattering at dirty glass surfaces or other effects an auto gain circuit is necessary to guaranty good laser noise cancelation. This feedback signal is provided by the integrating amplifier. Xu and Larsen [49] used an another approach for balancing the beams. In their circuits the integrator is left out and good balancing relies on precise control of the reference beam diameter with an opaque aperture. In industrial applications this method comes short, because of the intensity drift. Their circuits eliminate a noise source, but calibrations must be done often. Under the development of this noise canceller we used a fixed resistor instead of the photoresistor. The beam intensities were adjusted by alignment such that the ramp is cancelled. Only few minutes were necessary to create an imbalance with our simple lab setup.

In the implementation of the auto gain circuit an integrating configuration of the op amp is employed. A capacitor is used as a feedback element. The current through this capacitor is now the feedback current and is given by the fundamental current equation for a capacitor

$$i_c = C_{fb} \cdot \frac{dV_c}{dt} \tag{5.10}$$

Again using Kirchhoff's current law at the inverted input pin and using equation 5.10. Recall $i_{in} = V_{in}/R_{in}$ we achieve a expression for the output voltage of the integrating op amp

$$V_{servo}(t) = -\frac{1}{R_{in}C_{fb}} \int_{-\infty}^{t} V_{in}(t')dt' \tag{5.11}$$

This circuit is actually a low pass filter. Slowly varying signals such as the ramp appears at the output. The output voltage determine the light level of the LED and thus the value of R_r. This balance nulls out the current ramp and the circuit is at equilibrium. Fast oscillation signals such as the second harmonic oscillations will not pass through this filter and not contribute to the output voltage. Zhu chose the feedback resistor to be 1M and the feedback capacitor to be 100nF to achieve a auto-gain bandwidth of approximately 100Hz. The auto-gain bandwidth is ultimately determined by the input resistor and the feedback capacitor as long as the response of opto-isolator allows it. The rise time for the opto-isolator is 2.5ms, but has a considerably longer fall time of 500ms.

The output voltages of the integrating op amp is used to control the current into the LED inside the opto-isolator. When there is an negative voltage at the summing node[7] this voltage difference is integrated and the output is rising. Simultaneously the light level of the LED is rising. The light level reaches a point where the photoresistor

[7]The implementation of this noise canceler requires a stronger reference signal in order to give a positive output voltage at the integrating op amp to adjust the LED light level.

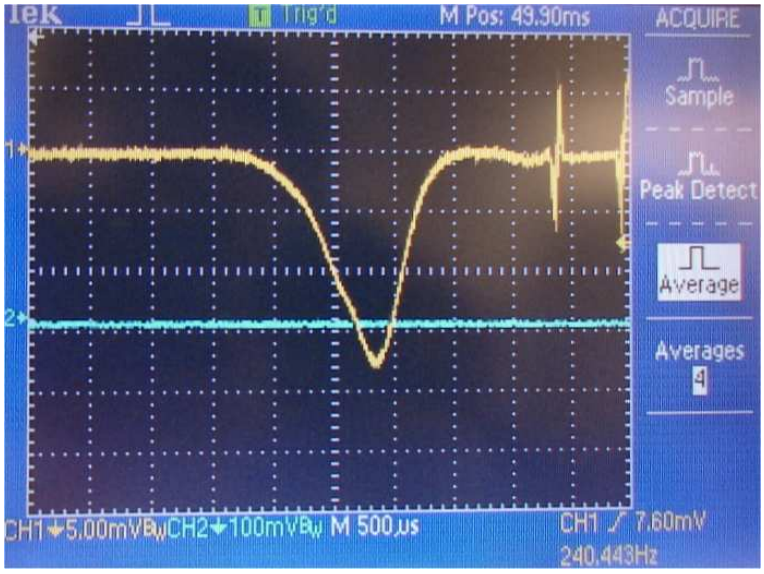

Figure 5.3: One scan with the noise subtracter. The ramp is cancelled and the small absorbtion signal is revealed. The absorbance is 2×10^{-3}

value provides a balanced sum at the summation node. At this point the input voltage is zero and no further increase of the output resistance and the photodiode resistance value is clamped and the laser noise canceler circuit provides a balance signal at the output.

5.3 Noise subtracter performance

5.3.1 Frequency response

The frequency response of the photodiode connected to a simple load resistor is dependent on the shunt capacitance and the load resistor. The 3dB corner is given by

$$f_{RC} = \frac{1}{2\pi C_d R} \tag{5.12}$$

where C_d is the shunt capacitance of the photodiode and R is the load resistor. We have assume that the photodiode capacitance is much larger than parasite capacitance from the input pin and stray capacitance. Hence the total input capacitance is $C_in \approx C_d$. Using feedback resistor $R_f = 1000\Omega$ will convert the photocurrents in order of mA to Volts. The photodiodes (PD2000W) has a shunt capacitance of 627pF and 588pF. Hence a 3dB corner at 250kHz is too close to the detection bandwidth of 13.4kHz centered at 187.5kHz. The frequency response must be flat at the detection bandwidth to avoid distortion to the 2f signal shape. Using a transimpedance amplifier this 3dB corner is raised in frequency thus wider bandwidth. Transimpedance amplifies has

virtual input impedance given by

$$Z_{in}(j\omega) = \frac{V_{in}}{i_s} = \frac{V_{out}/A_{ol}(j\omega)}{V_{out}/R_f} = \frac{R_f}{A_{ol}(j\omega)} \tag{5.13}$$

The detector sees a reduced load resistance and the 3dB corner is raised in frequency. The enhanced bandwidth is given by[25, 17] (a different notation is used in [27])

$$f_{cl} \approx \sqrt{f_c \times f_{RC}} = \sqrt{\frac{f_c}{2\pi C_d R_f}} \tag{5.14}$$

where f_c is the unity gain crossover frequency of the op amps open loop frequency response (gain bandwidth product: GBP) and R_f is the feedback resistor. The LF357H has GBP=20MHz thus moves the f_{cl} to 2.2MHz. AD797 has GBP=450MHz and would raise this frequency to 10.6MHz. One of the fastest op amps available is the AD657 has GBP=1.9GHz and would raise the 3dB corner to 21.8MHz. The bandwidth improvement can be further improved by reducing the shunt capacitance. The large shunt capacitance will hogs most of the photocurrents at higher frequencies since it appears parallel to the current source. Reverse biasing the photodiode with 2-5V the C_d is reduce to approximately 200pF. A 4.0MHz bandwidth and $1k\Omega$ gain is achieved by use of the LF357H, more than sufficient for our 187.5kHz detection frequency.

Beside of limiting the bandwidth the shunt capacitance also makes the circuit unstable and amplify the op amp intrinsic input voltage noise. Careful analysis of the feedback loop reveals a feedback factor (As Msc from NTNU we use a different notation compared to [17])

$$\beta(j\omega) = \frac{Z_i}{Z_f + Z_i} = \frac{1 + j\omega C_f R_f}{1 + j\omega R_f (C_f + C_d)} \tag{5.15}$$

where $Z_i = 1/sC_d$ and $Z_f = 1/sC_f||R_f$. This function tells how much the feedback signal shows up at the input pin and is a transfer function from the output to the input. If the feedback capacitor is zero the photodiode introduce a pole in the feedback transfer function. Poles in feedback transfer functions creates a phase lag and cause instabilities. The ideal output response to an input current is modified to

$$V_{out} = \frac{i_d R_f}{1 + 1/A_{ol}\beta} \tag{5.16}$$

where A_{ol} is the open loop gain. At low frequencies $A_{ol}\beta \gg 1$ and the response is ideal. At higher frequencies the pole caused by C_d attenuates the feedback signal and more requirements is put on the open loop gain. Inserting a feedback capacitor will create a zero in the transfer function. A zero puts a phase lead thus compensates for the phase lag from the pole. In signal amplitude point of view the feedback impedance becomes smaller with rising frequency and compensates for a feedback attenuation created by the low pass filter($C_f = 0$ in equation 5.15). The feedback resistance and the photodiode shunt capacitor forms a low pass filter with negative phase at the

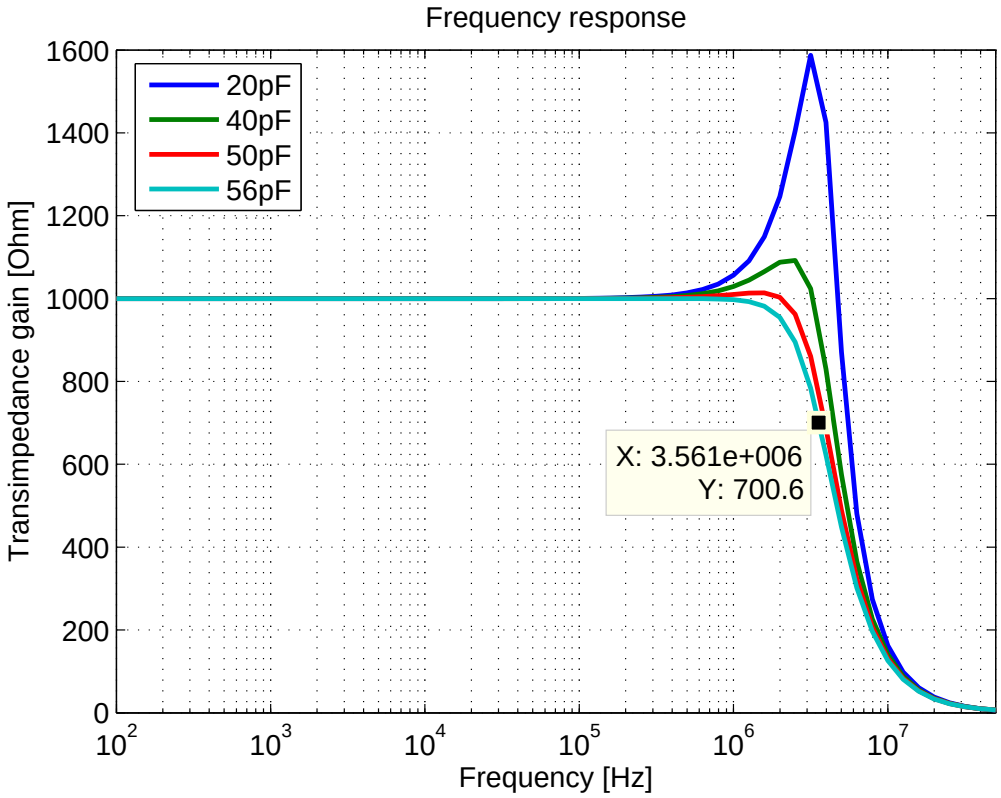

Figure 5.4: SPICE simulation of the frequency response. $C_d = 200pF$, $R_f = 1k\Omega$, $C_f = 20, 40, 50, 56pF$, $R_{shunt} = 12.1M\Omega$. Linear-log plot is used to emphasize the peaks in the frequency response

feedback loop. Negative phase in the feedback loop lowering the phase margin (a term from cybernetics and control techniques). The value of this capacitor is given by[17, **?**]

$$C_f \geq \frac{1}{2\pi R_f}\sqrt{\frac{2\pi C_d R_f}{GBP}} = \sqrt{\frac{C_d}{GBP \times 2\pi R_f}} \tag{5.17}$$

Putting known quantities into this equation we get $C_f \geq 56pF$. Introducing this bandwidth limiting capacitor as it also is called the bandwidth is reduced a bit, but it makes the circuit stable. Going too fast by setting a smaller capacitor than this value makes a peak in the frequency response just at the 3dB corner. Ringings or oscillations can occur if not enough capacitive feedback is inserted.

Using bigger feedback capacitors the bandwidth is limited. Figure 5.4 shows a SPICE[8] simulation of a transimpedance design using LF357H. The gain bandwidth product is 20MHz and the shunt capacitance is $C_d = 200pF$. Four values of C_f is

[8] A demo version can be downloaded from http://www.penzar.com/

simulated. The bandwidth is reduced from 4MHz to 3.6MHz by use of the capacitive feedback, but the frequency response is flat in the entire bandwidth.

5.3.2 Input voltage gain peaking

The non inverting noise gain peak in the frequency response cause by the photodiode shunt capacitor can be a serious limit, since the op amp input noise amplitude starts rising where the peak occur. The non inverting gain response is

$$G_+(j\omega) = 1 + \frac{Z_f}{Z_i} = \frac{1 + j\omega R_f(C_d + C_f)}{1 + j\omega C_f R_f} \tag{5.18}$$

where $Z_f = R_f||1/sC_f$ and $Z_i = 1/sC_d$. This gain amplifies the op amp intrinsic input voltage noise (AD797=$0.9nV/\sqrt{Hz}$ and LF357H=$12.0nV/\sqrt{Hz}$). Without C_f to reduce the feedback impedance this gain becomes larger with increasing frequency due to decreasing Z_i. With the noise subtracter component values ($R = 1k\Omega$, $C_d = 627pF$,$C_f = 100pF$) the gain is only $G_+(200kHz) \approx 1.12$ and the op amp input voltage noise amplification is negligible.

5.3.3 Signal and noise analysis

We define

$$K \equiv \frac{i_r}{i_s} = \frac{R_r}{R_s} = \frac{V_r}{V_s} \tag{5.19}$$

R_r will be adjusted such that the noise canceller output is zero (equation 5.9). At this condition $KR_s = R_r$ and common signals are zero. The harmonic signals at the transimpedance amplifier output, V_s, will see a voltage divider network between R_s and R_r. We use the principle of superposition and analyze what the harmonic signals see. These signals see the same potential at the reference amplifier output, V_r, as for ground (0V) since the photocurrents at these frequencies are zero. Hence zero output voltage for these signals at the reference output. The input pin of the buffer amplifier will see a voltage drop across R_r and puts it to it's output. Hence

$$V_{out} = \frac{V_s R_r}{R_r + R_s} \tag{5.20}$$

where V_{out} is the noise canceller output. We divide this equation by R_s both in the numerator and denominator and insert equation (5.19). The output becomes

$$V_{out} = \frac{V_s K}{K + 1} \tag{5.21}$$

The output voltage becomes V_s when K becomes large, i.e. strong reference beam. This can be explained in a more intuitive way: V_s sees a voltage divider network between R_r and R_s. At the point of view of the second harmonic signal, the potential at V_r is zero. The input pin sees $R_r/(R_r + R_s)$ of the signal output voltage. If $i_r = i_s$ the output only see half amplitude of the signal. Hence, the reference beam should be

stronger than the signal beam. The noise from the signal transimpedance amplifier becomes

$$e_{si} = \frac{e_s R_r}{R_r + R_s} = \frac{e_s K}{K+1} \tag{5.22}$$

at the input pin and the reference transimpedance amplifier noise becomes

$$e_{ri} = \frac{e_r R_s}{R_r + R_s} = \frac{e_r 1/K}{1/K+1} = \frac{e_r}{1+K} \tag{5.23}$$

The total noise at the buffer input is the rms sum of the noise from the signal amplifier and the reference amplifier. Using equation (5.22) and (5.23) the voltage noise at the buffer input is

$$e_{tot} = \sqrt{e_{si}^2 + e_{ri}^2} = \sqrt{\frac{e_s^2 K^2}{(K+1)^2} + \frac{e_r^2}{(K+1)^2}} \tag{5.24}$$

The noise from each transimpedance amplifier consist of input current noise, input voltage noise, thermal noise and photocurrent shot noise. This noise is given by

$$e_s = \sqrt{i_A^2 R_f^2 + e_A^2 + 4kTR_f + 2ei_s R_f^2} \tag{5.25}$$

and

$$e_r = \sqrt{i_A^2 R_f^2 + e_A^2 + 4kTR_f + 2ei_r R_f^2} \tag{5.26}$$

where i_s and i_r are the signal photocurrent and reference photocurrent respectively. Under normal conditions the shot noise dominates. Signal and reference shot noise becomes $e_{sn} = \sqrt{2ei_s R_f^2}$ and $e_{rn} = \sqrt{2ei_r R_f^2}$. Recall that we have $i_r = Ki_s$. Using this and inserting equation (5.25) and (5.26) into equation (5.24) the total noise contributions from both channels become

$$e_{tot} = \sqrt{\frac{2ei_s R_f^2 K^2}{(K+1)^2} + \frac{2ei_s R_f^2 K}{(K+1)^2}} = \sqrt{2ei_s R_f^2 \cdot \frac{K}{(K+1)}} \tag{5.27}$$

Using equation (5.21) and (5.27) the signal to noise ratio at the output is given by

$$\text{SNR} = \frac{V_{out}}{e_{tot}} = \frac{\frac{V_s K}{K+1}}{\sqrt{2ei_s R_f^2 \cdot \frac{K}{K+1}}} = \frac{i_s R_f}{\sqrt{2ei_s} R_f} \sqrt{\frac{K}{K+1}} = \sqrt{\frac{i_s}{2e}} \sqrt{\frac{K}{K+1}} \tag{5.28}$$

If we make the reference beam much stronger, $K \gg 1$, the output signal to noise ratio is approaching the shot noise limit of the signal beam alone. This is similar to the ignored contribution from a strong local oscillator in heterodyne detection[34]. Figure 5.5 shows the signal to noise ratio relative to the shot noise level. In our experiments the reference beam is approximately twice as strong as the signal beam. Hence, from the graph, the theoretical signal-to-noise ratio is $-20log(0.8165) = 1.8dB$ below the signal to shot noise level of the signal beam.

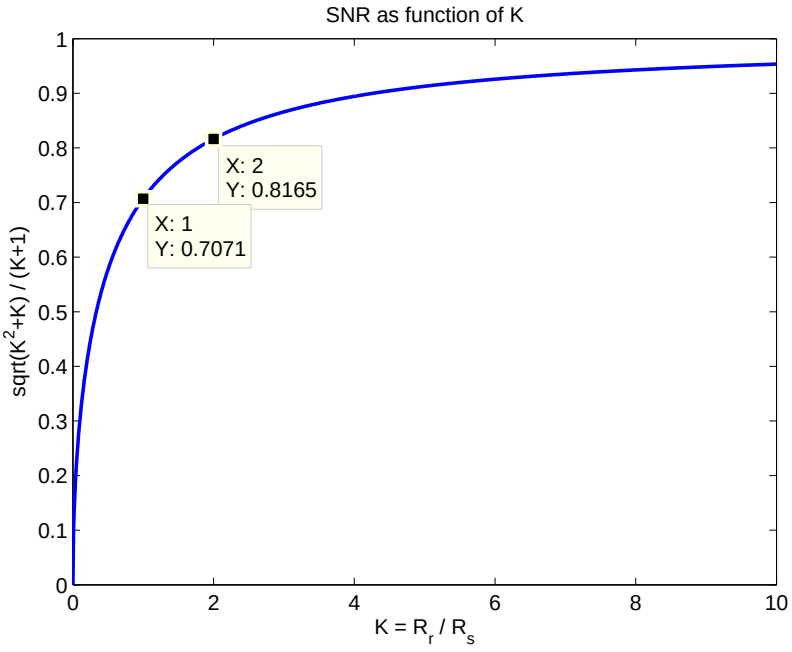

Figure 5.5: Signal to noise ratio relative to shot noise level as function of $K = R_r/R_s$

5.4 Current domain subtraction

The circuit is based on the design of Hobbs[22] and has the potential for lower noise. This circuit consist of two reverse biased photodiodes in the photoconductive mode. In this mode there is some dark current, but the speed is higher. The PNP transistor Q1 is used to block the current flow into the junction capacitor of the signal photodiode. NPN transistors Q2 and Q3 forms a current divider. The optical alignment is adjusted in a such way than the reference current is always higher than the signal current. Thus part of the reference current will flow through Q2 and the rest will flow through Q3. By properly controlling the differential base-emitter voltage $\Delta V_{BE} = V_{BEQ2} - V_{BEQ2}$ the current through Q3 is exact equal to the signal current through Q1. The summation current at the junction node is therefor zero according to Kirchhoff's current law. Since no current flows into the inverted node no feedback current will be generated by the transimpedance amplifier U1. The DC output voltage is therefor zero and common signals are effectively canceled. Assuming an imbalance occur in the system by a change in the DC levels between PDs and PDr the DC output of U1 is non-zero. The servo integrating amplifier U2 functioning as a feedback will integrate this error and set a new voltage over the Q3's base-emitter junction. In this way the circuit auto adjust itself such that the DC current at the summing node is zero. The performance of this circuit can be expected to be better since only one op amp is used and BJT transistors are quieter than the best op amps. The bandwidth is also higher in this configuration because the signal subtraction is done directly in the current domain before current

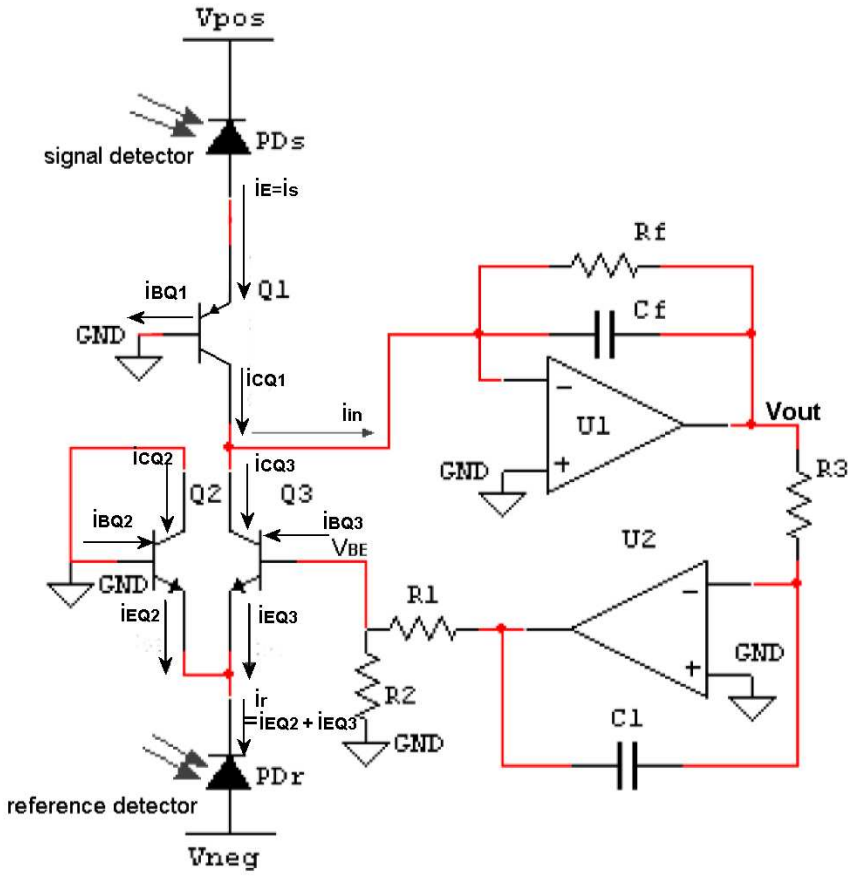

Figure 5.6: schematic diagram of the noise canceler working current domain. The currents photocurrents are subtracted directly before converting to voltages. Notice that the photodiodes are biased which gives a dark current offset

to voltage conversion which is limited by the gain-bandwidth product of the op amp. The bandwidth of cancelation is determined by the amplification bandwidth f_T of the transistor. We use 2N3904 NPN transistor pair with a $f_T = 300MHz$. The cancelation bandwidth is independent of the feedback loop, however, high enough feedback bandwidth gives better cancelation of the DC level fluctuate during the ramp scan, e.g. non-identical detector responses. The feedback bandwidth is proportional to the product of the input resistor and the feedback capacitor of the servo op amp. Hobbs and Haller demonstrated shot noise limited detections with their circuits. However, the electronics must be modified to fit into NEO's instrument. The direct signal used to normalize the second harmonic signal turned out to be troublesome. To get the direct signal we add a small resistor, 10Ω, in series with the photodiode and use a difference amplifier. The final circuit design is shown in figure 5.7.

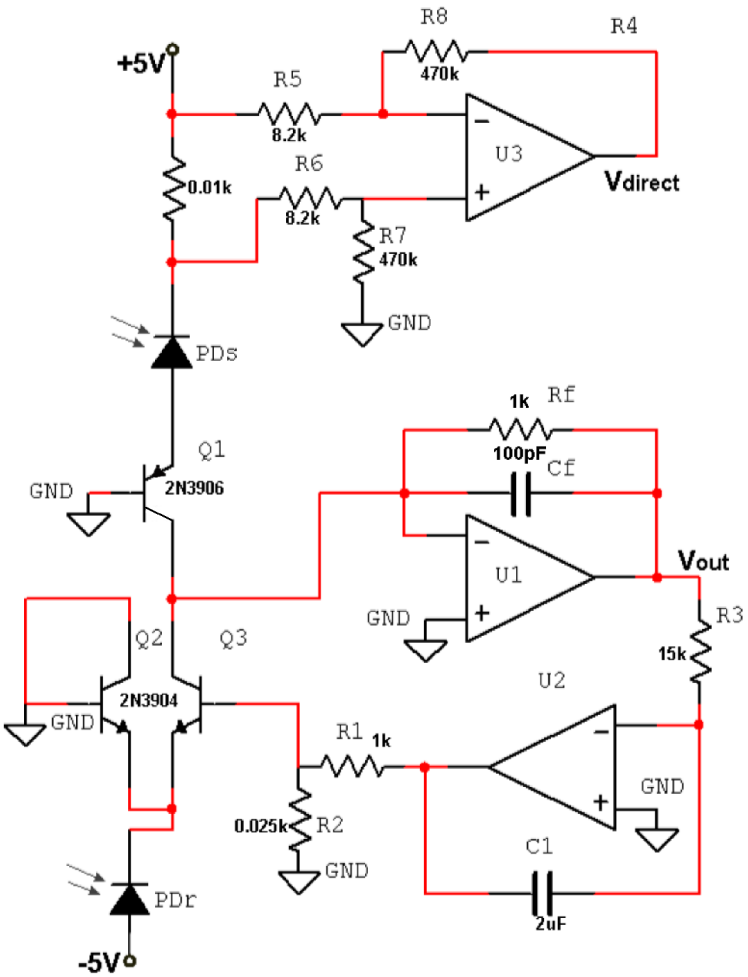

Figure 5.7: Final circuit design. The voltage drop across the 10Ω resistor in series with the signal photodetector is amplified by a differential amplifier circuit to provide a direct signal.

5.5 Noise canceller performance

5.5.1 Circuit analysis

BJT transistors follow Ebers-Moll equations[45, 24]. The collector currents of Q2 and Q3 are approximately given by

$$i_{cQ2} = I_0[\exp(\frac{qV_{BEQ2}}{kT}) - 1] \approx I_0 \exp(\frac{qV_{BEQ2}}{kT}) \tag{5.29}$$

and

$$i_{cQ3} = I_0[\exp(\frac{qV_{BEQ3}}{kT}) - 1] \approx I_0 \exp(\frac{qV_{BEQ3}}{kT}) \tag{5.30}$$

where I_0 is the intrinsic leakage current of the semiconductor and is very small, q is the electron charge, k is the Boltzmann constant, T is the temperature, and V_{BEQ3} is

the base-emitter junction voltage. Hence, the ratio of the current through Q2 and Q3 is given by

$$\frac{i_{cQ3}}{i_{cQ2}} = \exp(\frac{q\Delta V_{BQ3}}{kT}) = \exp(\frac{qV_{BQ3}}{kT}) \tag{5.31}$$

since the $V_{BEQ2} = 0$. The base voltage of transistor Q3 is determined by the servo amplifier output and the voltage division network formed by R_1 and R_2.

$$V_{BQ3} = V_{U2}\frac{R_2}{R_1 + R_2} \tag{5.32}$$

where the servo amplifier output is given by equation (5.11). Hence the base voltage of Q3 is given by

$$V_{BQ3} = -\frac{R_2}{R_1 + R_2} \cdot \frac{1}{R_3 C_1} \int_{-\infty}^{t} V_{out}(t')dt' \tag{5.33}$$

The pnp transistor Q1 prevents the $627pF$ photodetector shunt capacitance to load the summing junction at the negative input of the op amp. The op amp U1 sees a base-collector capacitance which is much smaller than the photodiode shunt capacitance. This is precious when the feedback resistor has to be increased due to low transmission. The photodetector current flows into the emitter lead of Q1. The current that flows into the base lead is given by i_c/h_{fe}. The collector current is therefore given by

$$i_c = i_E - i_B = i_E - \frac{i_c}{h_{fe}} = i_s - \frac{i_c}{h_{fe}} = \frac{i_s h_{fe}}{h_{fe} + 1} \tag{5.34}$$

where i_s is the signal photocurrent. We see that when the current gain is large all the signal photocurrent flows into the summing node. A super beta transistor should be used. The 2N3906 transistor from Fairchild Semiconductor has a dc current gain of $h_{fe} \geq 70$ @$i_c = 1mA$. Two transistors can be connected to form a darlington transistor with a current gain of h_{fe}^2. The signal voltage at the preamplifier output is given by the photocurrent flowing out of the collector lead multiplied by the feedback resistor of the op amp U1. Hence, the output signal voltage is given by

$$V_{out} = \frac{i_s h_{fe}}{h_{fe} + 1} \cdot R_f \tag{5.35}$$

where R_f is the feedback resistor of the transimpedance amplifier U1. Comparing this equation with the voltage domain noise canceller output given by equation (5.21), we see a clear advantage. If h_{fe} is sufficiently large, all the signal photocurrent appears at the output. The noise subtracter (voltage subtraction) never puts all of the signal photocurrent at the output, unless the reference signal is very large. This is because of the voltage division network.

Figure 5.8 shows a Fast Fourier Transform of the noise canceller linear output. Blue trace shows the frequency spectrum of the output with the reference beam blocked. The dominating signal is the intensity modulation signal at 93.75kHz. In tuneable diode laser absorption spectroscopy (TDLAS) wavelength modulation is achieved by

injecting a modulation current into the diode laser. At the same time the intensity is modulated. Higher harmonic detection eliminates the intensity modulation. When the reference beam is unblocked the intensity modulation signal is reduce by approximately 45dB. The optimized version of this noise canceller can reduce this intensity by more than 70dB, as we will see in chapter 7.

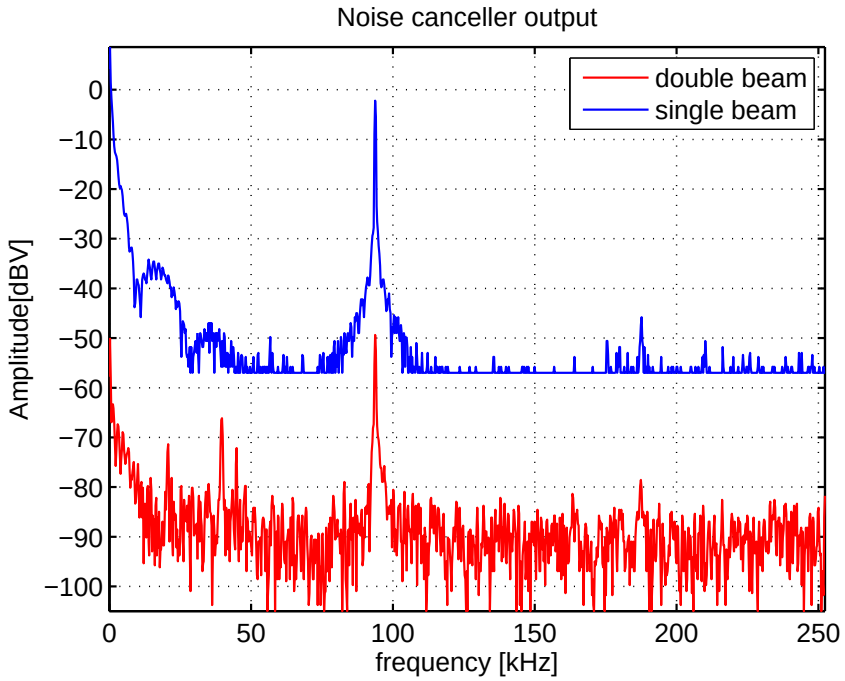

Figure 5.8: FFT spectrum of the noise canceller output. The intensity modulation signal is suppressed by approximately 45dB.

5.5.2 Frequency response

The frequency response of the transimpedance amplifier U1 differ from earlier calculations because of the cascode configuration formed by Q1. The photodiode sees the 10Ω resistor in series with the emitter resistance R_E. According to the Ebers-Moll model the emitter resistance given by[25]

$$R_E = \frac{kT}{qi_c} \tag{5.36}$$

where $kT/q = 25mV$ at room temperature. If we assume a collector current of $1.5mA$ (signal photocurrent) the emitter resistance becomes approximately 16.7Ω. If we assume that the reversed biased photodiode shunt capacitance is $200pF$ the RC corner frequency is $30MHz$. However the bandwidth limiting feedback capacitor C_f will limit the 3dB corner frequency to approximately $1.6MHz$. The shunt capacitance is

now isolated from the inverting input of the op amp. The feedback resistor can be raised to increase the signal to noise ratio. However, increasing the feedback resistor to much can cause harmonic distortion or output saturation.

The feedback frequency response can be calculated by taking Laplace transform of the servo amplifier output voltage given by equation (5.33). Hence, the frequency dependence of the base-emitter voltage is given by

$$V_{BQ3}(s = j\omega) = L\{V_{BQ3}(t)\} = -\frac{R_2 V_{out}}{R_1 + R_2} \cdot \frac{1}{j\omega C_1 R_3} \tag{5.37}$$

where we have used that $L\{\int V dt = 1/s\}$. This shows that the feedback 3dB corner is given by $1/(2\pi R_3 C_1)$. The 3dB corner frequency of the feedback loop with component values in figure 5.6 is 5.3Hz. It's job is to balance the dc level such that common signals cancel out. Low feedback bandwidths are necessary when direct absorption spectrum is acquired from the linear output. Higher feedback bandwidths give better common signal cancellation. When the log output is used the feedback bandwidth must be larger than the signal bandwidth!

5.5.3 Noise model

The front end noise expressed in voltage per root Hertz is given by

$$e_n = R_f \sqrt{i_A^2 + \frac{e_A^2}{R_f^2} + 2e(i_s + i_r) + \frac{4kT}{R_f^2} + i_{Q1}^2 + i_{Q1}^3} \tag{5.38}$$

Where the first term is the amplifier current noise, the second term is amplifier voltage noise, the third term is shot noise, the fourth term is the Johnson noise, and the last two terms are noise from the pnp and the npn transistors respectively. With 1.5mA signal beam photocurrent and room temperature the shot noise term dominates. The noise contributions from the transistors can also be neglected when the shot noise dominates. Using $i_s \approx i_r$ (good balancing) and incorporating gain in later stages the noise before ADC can be expressed as

$$V_n = R_f \sqrt{4ei_s} \sqrt{B} G \tag{5.39}$$

where R_f is the feedback resistor, e is the electron charge, i_s is the photocurrent, B is the noise (the area under the signal bandwidth) bandwidth and G is the gain in later stages. A numerical application gives a rms noise equal to 8.7mVrms with $i_s = 1.5mA$, $G = 2408$, $B = 13.4kHz$ and $R_f = 1k\Omega$. The minimum noise with dual beam is 3dB above the shot noise of the signal photocurrent alone. Hobbs[23] showed that placing many diodes in series with the photodetector the output noise approaches the shot noise of the signal photocurrent.

6 Instrumentation

6.1 Instrument setup

In this section we describe the instrumental setup for measurements. Most of these experiments are carried out at the laser lab at Department of Electronics and Telecommunications. The transmitter unit is controlled by the LaserGasII mainboard. The receiver unit and the main electronics are connected by a shielded signal cable. The RS232 interface is connected to a laptop using a standard RS232 cable. Figure 6.1 shows the experimental setup for this project. The laser is mounted on a heating sink (not shown in the figure). The laser has 1.5m polarization maintaining fiber mounted to the laser module. The other end has a FC/APC connector. The laser beam from this end is placed approximately 7-8cm from a collimation lens from Melles Griot . The FC/APC connection adaptor is mounted on a moveable setup to adjust the distance from the fiber end to the lens. The most frequently used lens is LPX143, but other lenses are tested as well. In free air instruments the light coming out from the laser facet is directly collimated by a lens. In dual beam measurements the fiber output is coupled into a fiber splitter (1x4 and 2x2 were tested). Two output beams are used, one as a signal beam and one as a reference beam. A test fiber is placed between the PM fiber and the collimation lens.

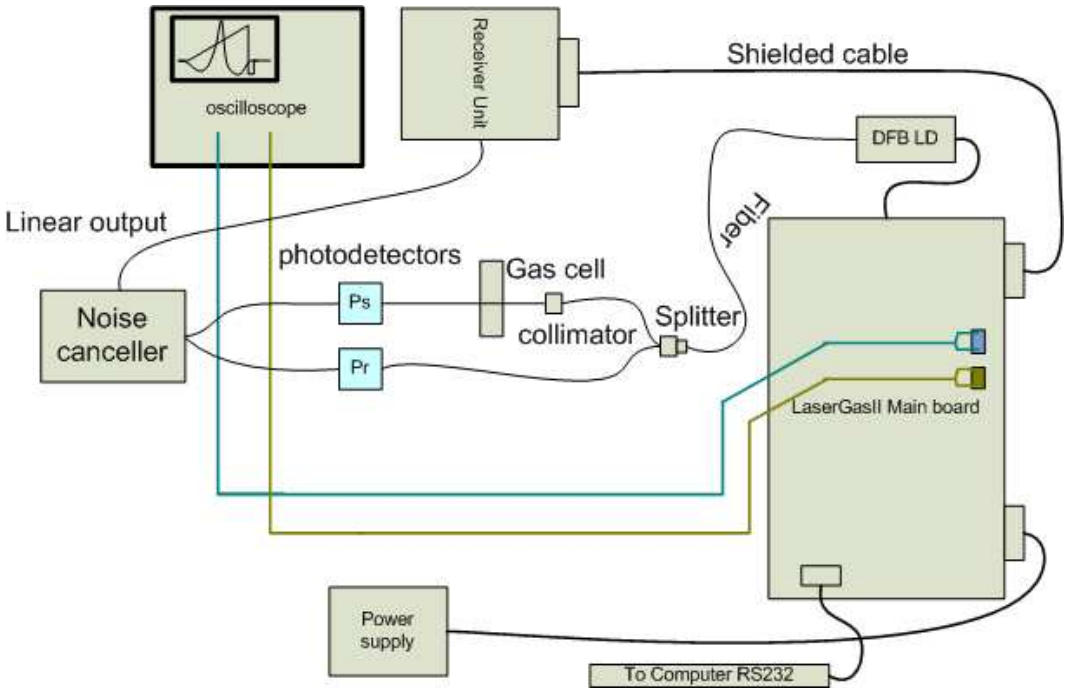

Figure 6.1: Schematic setup of the wavelength modulation spectroscopy scheme. When using single beam measurements either NEO's preamplifier is used or the reference beam is blocked.

6.2 Software settings

Some important software settings to control the laser modulation are listed in table 6.1.

Laser model	NKL1S5EAAA 1512nm
DC value	75
Current ramp value	3x1851
Modulation value	2.992V
Laser temperature	1.4614V
Reference signal phase	35 degrees

Table 6.1: Some software parameters

6.3 Collimation

The laser light from the fiber end is collimated by a 76mm focal length plano-convex lens from Melles Griot (LPX143). The beam waist is set close to middle of the measurement path. No collimation is applied to the reference beam to avoid unnecessary etalon fringing. The beam diameter escaping the collimation lens is measured to approximately 1.63cm.

6.4 Focusing

We are more free to choose a lens to focus the signal beam onto the photodetector active area. The collimation lens is limited by the divergence of the light beam coming from the fiber end. If choosing a lens with too large focal length the beam will overfill this lens, and only a fraction of light is collimated. We choose a lens with a focal length of 10cm to increase the oscillation frequency in the 2f etalon signal. Faster oscillations are easier to remove by analog and digital filtering. Both lenses (collimate and focus) are not AR-coated. Etalon effect would be reduced if AR-coated lenses are used.

6.5 Beam splitting

The fiber output intensity is 22mW at the end of the ramp scan. The fiber splitters from Diamond were used to split the signal and noise to two or more channels for noise cancellation. The 2x2 fiber splitter puts 50% of the laser intensity on each output. The 1x4 fiber splitter puts 25% of the input intensity on each output. In multiple gas detection three outputs of the 1x4 splitter were used. A typical single beam measurement setup is shown in figure 6.2.

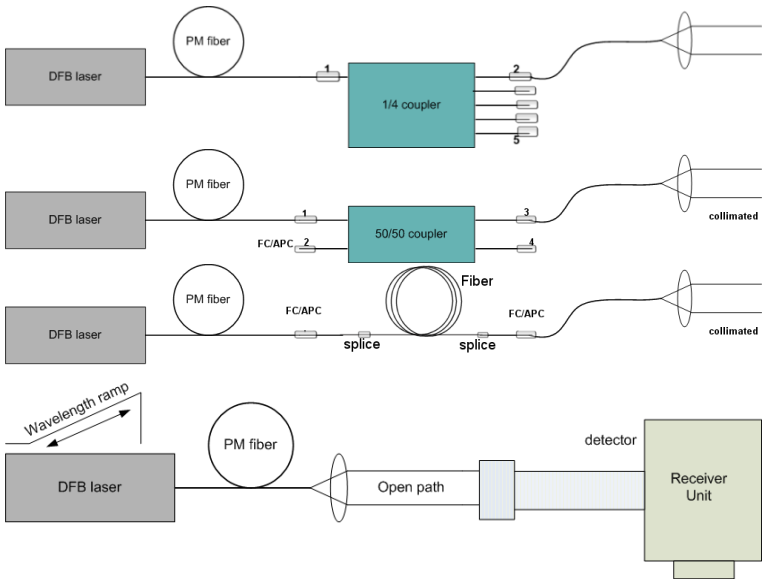

Figure 6.2: Typical setup when using single beam measurement. In double beam measurements one of the three available ports are used as the reference channel. No significant cancellation strength difference between the output ports.

6.6 Laser modulation

The laser temperature is set close to room temperature. The dc injection current is set to 51mA. This tunes the laser frequency to approximately $6613.2cm^{-1}$ ($1512.131nm$). The current is fed to the laser through a coax cable for minimum noise. The laser is connected to a guitar-form-card connected to the mainboard using a flat-cable. A current ramp of 31.6mA is superimposed on the dc current. This sweeps the laser frequency $0.77cm^{-1}$, enough to cover the NH_3 absorption line of interest. Next to this line there is a weak line from H_2O. The modulation amplitude is set to $14.61mA$. With the transimpedance gain settings this gives a modulation signal of 600mV peak to peak to the input of the mixer. This amplitude is kept inside the linear region of the mixer. Figure 6.6 shows the modulation scheme for this laser.

Measurements in this section were done with a 12.1Ω resistor instead of the laser diode. The instrument is powered up and we measure the voltage drop across the resistor. The currents were determined using Ohms law.

6.7 Switch settings

The receiver unit has four switches, three for each amplifier and one for the detector biasing. First the photocurrent is converted into a voltage representation in the transimpedance preamplifier, also referred to the front end. Switch settings determine the feedback resistor value. The second switch determine the second harmonic signal amplification. The switch for direct signal amplifies a low pass filtered version of

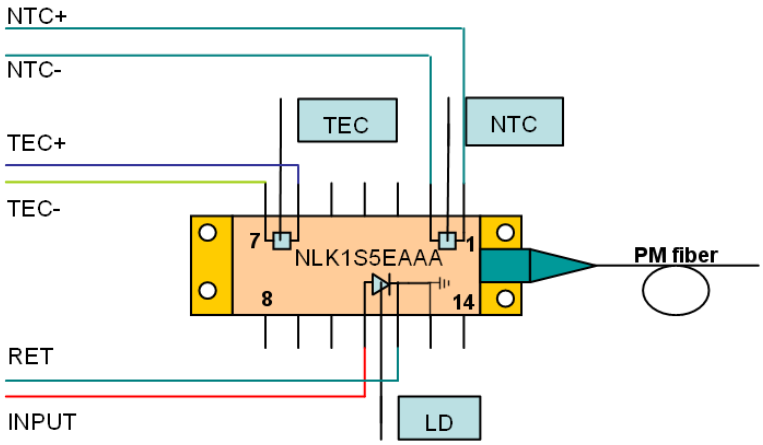

Figure 6.3: The laser diode, NTC and cooler element is connected to the interface board.

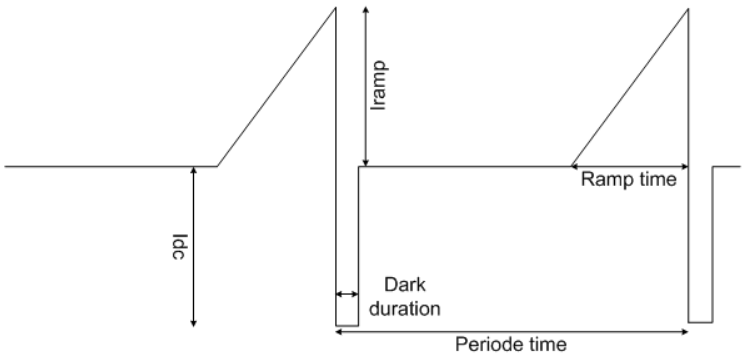

Figure 6.4: Modulation of current to the laser

Dark duration	$500\mu s$
Period time	$12.5ms$
Ramp time	$2.68ms$
I_{dc}	$51.23mA$
I_{ramp}	$31.6mA$
$I_{modulation}$	$14.61mA$
Modulation frequency	92.75kHz
Ramp scan frequency	80Hz

Table 6.2: Modulation currents. The laser injection current is the sum of the three contributions.

the transimpedance output. This signal provides the software a representation of the transmission and is used in normalization of the 2f signal.

Switch settings for the preamplifier are given in the tables below.This results in current-voltage conversion gain of 165×. SW1-8 is usually on for detector background compensation.

SW1-1	SW1-2	SW1-3	SW1-4	SW1-5	SW1-6	SW1-7	SW1-8
ON	ON	ON	ON	ON	ON	ON	ON

Table 6.3: Switches for the preamplifier, SW1-1,..,8. This give a feedback resistor value of 165Ω. Switch 8 is normally on.

The reverse bias voltage for NEO's photodiode is 4.8V and is set by the switch settings given in table 6.4

SW2-1	SW2-2	SW2-3	SW2-4
OFF	OFF	ON	OFF

Table 6.4: Switch settings to give 4.8V reverse biasing voltage.

The second harmonic signal after the mixer is amplified 133× to become approximately 3.24V at the ADC input.

SW3-1	SW3-2	SW3-3	SW3-4
ON	ON	OFF	ON

Table 6.5: Switches for the second harmonic amplifier, G=133.

The settings in table 6.6 results in an amplification factor G=5.5 for the direct signal. The output voltage is approximately 12V at the ramp end.

SW4-1	SW4-2	SW4-3	SW4-4
ON	OFF	OFF	OFF

Table 6.6: Switches for the direct signal amplifier, G=5.5.

6.8 Electro magnetic noise shielding

We experienced external noise sources that affect the measured results. The short term (less than 2 hours) stability is quite good as reported in the project report. However, the long term (days) stability were poor, and occur in every measurement taken. Somehow the noise from each measurement did not have any correlations.

The relative fluctuation in the measured concentration were some times as high as 15-20%. We decided to build a laser box to reduce the effect of external noise on the laser modulation. This box is made of aluminium. The laser is strategically placed inside this box and the fiber is fastened to prevent signal distortion when the fiber is pulled. A significant change in the signal shape was observed when a moderate force was applied to the fiber close to the pigtail connection. This box prevented noise, and protects the fiber against mechanical strain resulting in signal distortion as well.

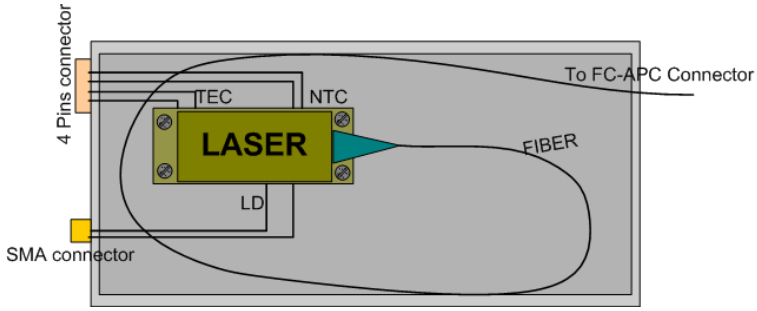

Figure 6.5: Schematic of the laser box to prevent noise and protect the fiber against pulling force.

6.9 Noise cancellation

The noise cancel designs that were developed and built were tested. Both (current domain subtraction and voltage domain subtraction) circuits were tested with the same pair of photodiodes for comparison. The noise canceller connection to the receiver board is schematically shown in figure 6.6.

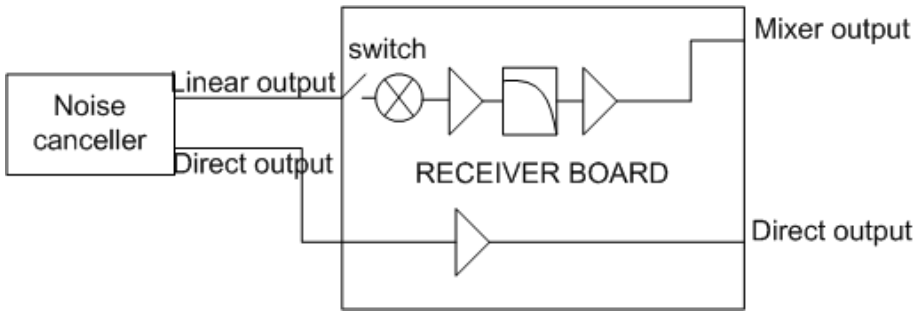

Figure 6.6: Schematic connection of the noise canceller electronics to the receiver board. Direct signal and the linear output is transferred over short twisted pair cables.

7 Results and discussion

The thesis task description is to couple light into optical fibers and do measurements to give a comparison with existing free air lasers. The goal is to achieve results that approach the sensitivities existing instruments can perform. During our work, we have identified most of the noise sources. Several attempts were done to minimize these noises. We met several practical issues that were not identified in the theory. After hours or even weeks of trouble shooting we obtained surprising results.

We have built a simple temperature controller based on an AVR microcontroller from Atmel (detailed description is given in appendix E). The temperature effects of the laser were ultimately discovered with this tool, etalon fringes due to multiple reflections in optical surfaces, drift because of temperature fluctuations and mechanical instabilities. The free spectral range (determining the 2f fringe shape) is practically stable because of small changes in the optical path lengths between the optical surfaces The free spectral range is determined by the refractive index and the optical path length between two reflective optical interfaces. However, the phase of these oscillations in the 2f signal fluctuate very much. An optical path length change of $\lambda/2$ gives a phase change of 180 degrees. Because of linear addition of these oscillations in the 2f signal, the 2f shape can be distorted when measuring small concentrations. In comparison the FSR needs changes on the orders of millimeters to be observable.

Electro magnetic interference from power supplies, fans or other facilities were observed to cause problems for our sensitive measurements. To reduce these problems we mounted all electronics inside metal boxes and used coax cables to transfer analog signals, such as the laser modulation signal. The actions above reduced these interferences to an acceptable level when using single beam measurements. However, they become observable when using the noise reduction circuits that were analyzed and designed in this thesis. We were forced to move to an another location to avoid these effects. In industry applications we can not do this. However, a real product will be mounted inside metal boxes and all electronics will be shielded from these external perturbations.

When using single beam configuration we observed very large second harmonic noise with high detector photocurrents. The 2f signal was saturated at the end of the ramp scan. These harmonic distortions was found to stem from the preamplifier electronics and the mixer. When the signal level is approaching the output limit the harmonic distortion in the op amp starts to rise. At large modulation intensity amplitudes the mixer starts to show nonlinear effects. Both this must be avoided!

In this section we mainly focus on the noise amplitudes. Stability in concentration when measuring the 100ppm gas cell is also important. It is obviously meaningless to have an instrument with a very high sensitivity most of the time, but randomly exhibit noise peaks in small time periods. When talking about the noise level, we distinguish between three noise types. The noise at the mixer output when no modulation signal is

present(dc laser injection current) is labeled as beam noise. This noise was measured by turning off the modulation signals in the LaserGasII software. The modulation noise is the mixer output noise when both ramp scan and modulation signal is turned on. This noise is the dominating noise. Electronic noise is the mixer output noise when both the signal beam and the reference beam are blocked. This noise was very sensitive to electro magnetic radiations from the clean room and fans at the department of electronic and telecommunications's laser lab (A409). After reducing all wire lengths and moving to a new location, this noise was reduced.

7.1 NH_3 spectrum

What does the selected NH_3 spectrum around $1512nm$ look like? To give an answer to this question we utilize the ability of removing intensity modulation by use of the balanced detector. The noise canceller is actually a balanced detector. It removes common signals and can almost completely remove the slow ramp signal. Hence, the slowly varying intensity modulation caused by the laser injection current ramp is removed. The time constant of the servo amplifier which adjusts the current splitting ratio must be adjusted slow enough to not pass the absorption signal ($> 0.2s$ is sufficient). We turn off the modulation signal and use the ramp to scan the spectrum. Initially, we adjust the detectors such that the intensity ramp is removed. This is done automatically by the noise canceller if the reference beam is stronger than the signal beam. A large signal to noise ratio is required to record the spectrum. To do this we wet a piece of paper dipped into a household ammonia solution ("Salmiakk") and seal it in a transparent plastic bag. The concentration inside this bag is quite high and the optical path length can be easily adjusted to achieve a good absorbtion spectrum. Figure 7.1 shows the noise canceller output (top) and the phase-lock-amplifier output (bottom). We use GPIB and Labview to acquire and save the oscillator signal onto a file on the hard drive for signal processing. Matlab is use to process and present the spectrum. The noise canceller output is a replica of the laser intensity when the wavelength is swept through the spectrum. We see three dips. The first one is the NH_3 absorption line used to generate harmonic signals. The next two lines are substantially smaller and are H_2O lines. It is quite difficult to distinguish the last two lines from each other. The lock-in-amplifier output shows the second harmonic signal under the same scan range. This signal is achieved by turning on the modulation signal and measure at the mixer output. Without modulation no harmonics are generated and the output will be zero. The modulation current is $14.6mA$ which results in a wavelength modulation well smaller than the gas linewidth (see figure 7.37). Here the wavelength modulation spectroscopy really shows it's strength. Weak absorption lines hiding behind a big absorption line are extracted and shown clearly. The second harmonic signal is actually proportional to the double derivative of the spectrum with respect to wavelength. Wavelength modulation spectroscopy is some times also called derivative spectroscopy because of this property.

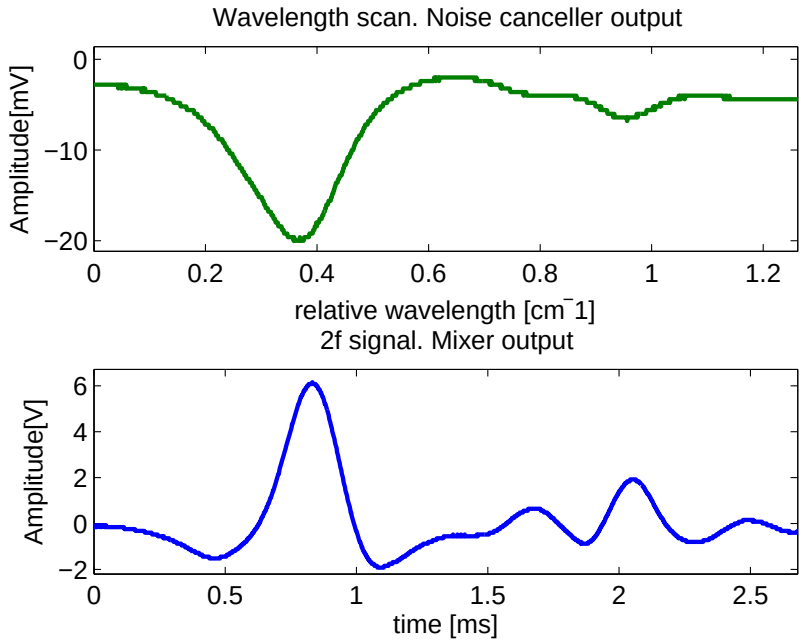

Figure 7.1: Top) direct absorption scan of the ammonia spectrum. Bottom) second harmonic signal when wavelength modulating the same spectrum

7.2 Etalon fringing

The noise canceller can remove laser excess noise, background signal or etalon fringes that are common on both beams. The digital signal processing algorithm effectively removes fast oscillations due to far spaced optical interfaces such as between the signal photodiode window and the focusing lens ($\approx 10cm$). Slow oscillations due to short distance between optical interfaces are also removed. However, if not applying digital signal processing they are of significant amplitude and worsen the detection limit. Figure 7.2 shows a part of an etalon fringe created between the active medium surface and the photodiode window. We observed that this contribution in the 2f signal looks like a dc offset. To investigate the source of this offset we turned off the laser modulation signal and looked at the noise canceller output. With this approach we ensure that this signal does not come from the modulation effects. The distance is 0.127cm (0.05 inches, given in the datasheet). This would give a distance of approximately $4cm^{-1}$ between two fringe tops with air in the gap. The laser ramp current was extended to approximately 52mA. This would extend the laser wavelength scan to approximately $1.26cm^{-1}$ covering more of this fringe. Within this fringe we can see a small dip. This dip comes from the H_2O line to the right of the NH_3 line. By tilting the photodiode we can change the phase of the etalon fringe. The bottom graph shows the noise canceller output with this arrangement. It was difficult to remove this fringe by tilting the photodiode. Engelbrecht[14] removed the reference photodiodes's glass

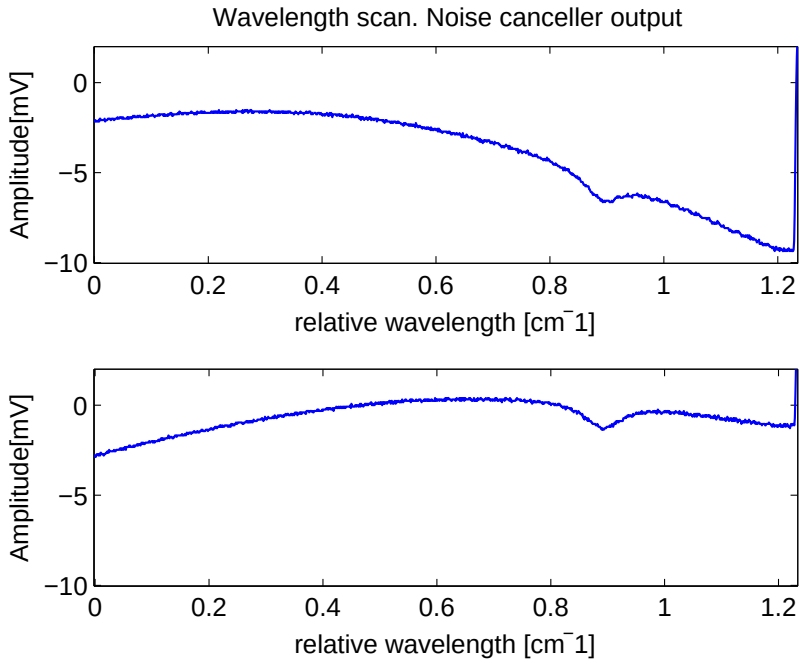

Figure 7.2: $1.26cm^{-1}$ wavelength scan with the 100ppm gas cell removed. The small dip comes from a H_2O line in the air. This line would be cancelled if the optical path length in the reference and signal path is the same.

window to avoid this etalon. Since this noise is not a problem in our measurements (because of the digital signal processing) this window is kept to avoid contaminations on the active area.

The more serious etalon fringes come from optical surfaces spaced 2-5cm from each other. Figure 7.3 shows a comparison between the etalon noise from a 3cm focal length lens (top) and a 10cm focal length lens (bottom). The FSR from 4cm air cavity (to defocus the laser beam) between the detector window and the focus lens gives oscillations in the 2f signal that are difficult to suppress by analog or digital filtering. It is difficult to achieve very steep amplitude response with analog filters. Digital filters are relatively easy to implement and can have very sharp frequency responses. The rapid oscillations in the bottom graph are effectively removed by digital filtering. In contradiction to the oscillation in the top graph which has many frequency components in common with the 2f signal from the gas absorption line. Therefore it can not be fully suppressed. In order to avoid these effects the system designer must know these effects and carefully design the optical system to avoid this.

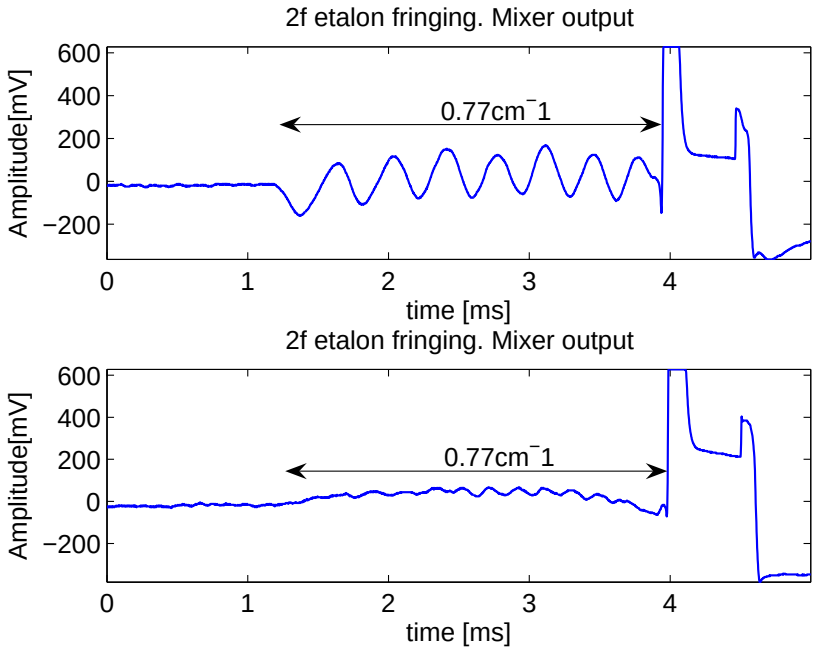

Figure 7.3: Serious etalon oscillations from the 2.5cm focal length lens used to focus the light into the signal photodiode. The peak to peak etalon noise amplitude corresponds to a 1.33×10^{-4} absorbance

7.3 Line broadening and concentration

In the theoretical description of the absorption lines we showed that the line strength is dependent on the gas temperature and pressure. To investigate how much influence the temperature and pressure has on the concentration the 100ppm gas cell set in the optical path. Different temperatures are manually set in the LaserGasII software and the concentration values for each temperature are logged. The pressure is kept constant when the temperature is changed. To investigate the pressure effects we set the temperature to a fixed value and change the pressure values in the software. Figure 7.4 shows the concentration as function of pressure (a) and temperature (b). The concentration is actually inverse proportional to the pressure.

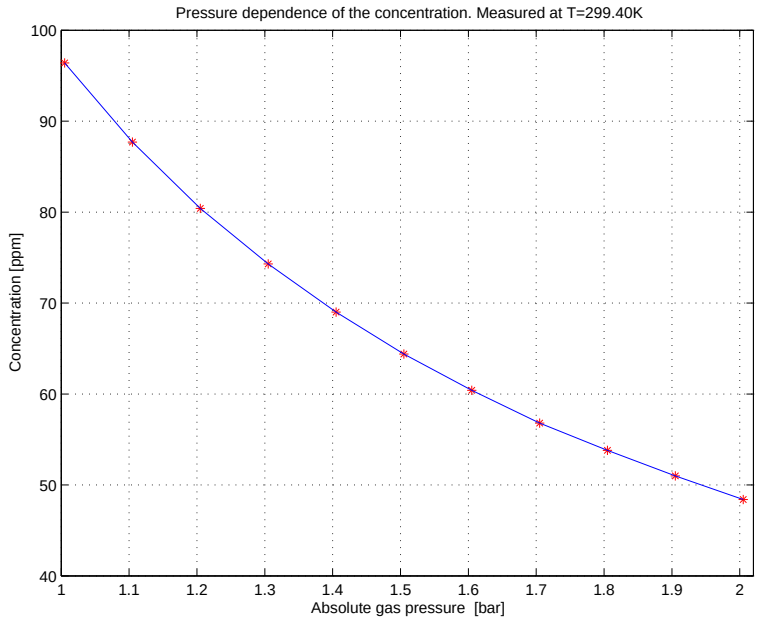

(a)

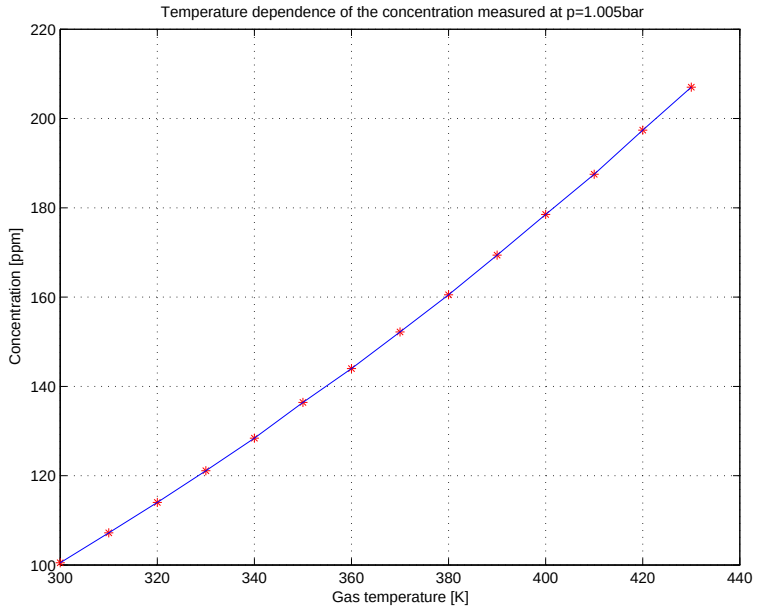

(b)

Figure 7.4: Concentration as function of pressure and temperature. The concentration values are calculated by the LaserGasII software with different input values of temperatures and pressures.

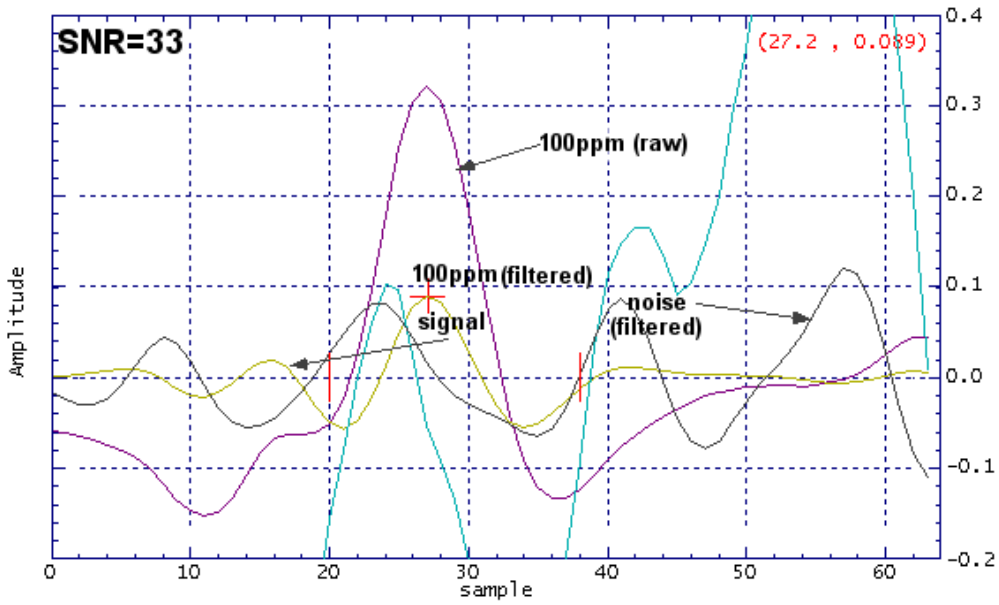

Figure 7.5: Signal and noise with the standard preamplifier. A signal-to-noise ratio of 33 times gives a detection limit of 3ppm.

7.4 Residual noise

In the discussion of signal to noise ratios we always use the noise amplitude relative to the 100ppm signal. Before we measure the noise, the 100ppm signal amplitude is recorded for comparison. This 100ppm line amplitude is dependent on software parameters and the gain settings for the direct signal and the second harmonic signal. In this thesis we define the signal to noise ratio as

$$\text{SNR} = \frac{S_{100ppm}}{N} \tag{7.1}$$

where N is the noise amplitude and S_{100ppm} is the 100ppm 2f signal amplitude.

The prototype described in the project report[10] used the standard preamplifier with a feedback resistor set to 165Ω. With this feedback resistor the thermal noise current is $10pA/\sqrt{Hz}$ which is much more than the op amp input noise current. However, due to a high power laser beam the shot noise is 7.5 times more than this. The 22mW laser beam is collimated by using a plano-convex lens from Melles Griot with a focal length of 7.6cm. This beam goes through a 100ppm gas cell and the lens inside the receiver unit focuses the beam onto a 4.8V reverse biased InGaAs photodiode. The modulation signal at the detector is approximately 600mV, within the linear range of the mixer. The gain stages after the mixer are 133 and 31.4 respectively. The direct signal gain was adjusted to give 100% transmission (12V peak direct signal). With these configurations the 2f signal amplitude was 3.24V. Figure 7.5 shows the captured second harmonic signal. 256 normalized scans are averaged to

represent this signal. The amplitudes shown in the figure are digital values which are related to the analog 2f signal. A line amplitude of 9×10^{-2} in software corresponds to 3.2V in the analog signal at the mixer output. However, the relation is dependent on the software parameters, and the gain adjustments of the second harmonic signal amplifiers and the direct signal amplifier.

For each scan the ADC electronics sample the analog 2f signal 64 times. The amplitude of the raw 2f signal represents the 2f amplitude at the mixer output divided by the ramp amplitude. 256 scans are averaged to represent the 2f signal (purple graph). This signal is used as the input signal to the digital signal processing. Matched filtering is done by digital filtering of the raw 2f signal with a known filter to remove fast and slow oscillations in the 2f signal. After matched filtering the dc offset and fast oscillations in the 2f signal are removed. This (yellow graph) signal peak (0.089) is used to calculate the gas concentration. The signal processing algorithm also calculates the linewidth based on the digital 2f signal. Both this and the line amplitude affects the concentration if they fluctuate due to noise. By removing the gas cell the residual noise was determined. We use the plot function provided by the LaserGasII software to compare the signal and noise. The noise is then scaled to 33:1 to have the same magnitude as the signal. Thus a signal-to-noise ratio of 33× gives a detection limit of 3ppm. As a comparison NH_3 detectors from NEO using free air lasers achieve 0.15ppm, 20 times better sensitivity.

7.5 Stability

7.5.1 Standard components and measurement stability

Figure 7.6 shows a plot of the measurement with the 100ppm cell over time. The fluctuation in the plot comes from temperature effects from the fiber coupling and external electronic noise from the electromagnetic interferences. The fans from the clean room significantly contribute to the electronic noise. To remove this influence we mount critical components inside metal boxes.

7.5.2 Stability with laser module mounting inside a metal box

The goal of this experiment is to investigate the external electromagnetic noise effects on the concentration. The metal box shields out the electromagnetic waves thus reducing the noise currents induced in the cable carrying the current from the motherboard to the laser diode. In addition, we now use a coax cable for better noise immunity. Figure 7.7 shows a plot of the measurement with the 100ppm gas cell. As we can see in this plot, the concentration fluctuation is reduced. Now the noise is dominated by the etalon effects from the fiber coupling inside the laser module. This etalon noise is very sensitive to temperature.

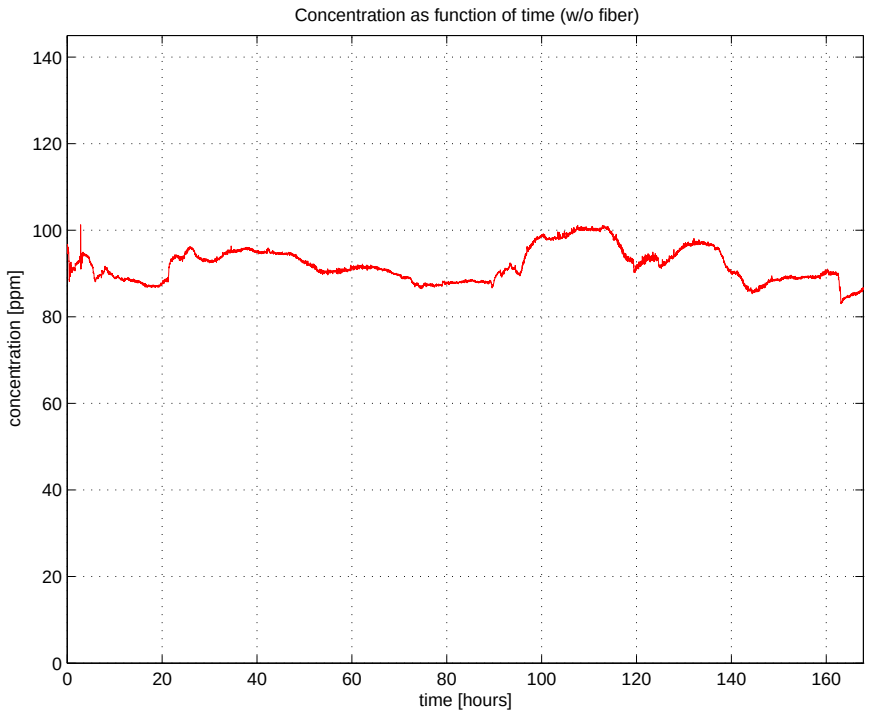

Figure 7.6: Concentration measurement of the 100ppm gas cell with the standard electronics.

7.5.3 Stability with controlled laser housing temperature

Under our experiments we observed that the DFB laser module is very sensitive for external temperatures. To avoid this problem we decided to build a temperature controller described in the appendix. The laser module housing temperature is set to $30.5C$ in software and the room temperature is $24 - 25C$. The actual temperature inside the metal box where the laser module is mounted is approximately $30.2C$. An external temperature sensor is mounted in proximity to the gas cell for gas temperature logging. The instrument is set to use a fixed gas temperature of $299.40K$ and a fixed pressure of $1.005bar$. All optical windows are tilted with small angles to avoid etalon fringes. Figure 7.8 shows the concentration log for the temperature stabilized laser module. The blue plot is the temperature inside the metal box, thus the laser housing temperature. The green plot show the gas temperature. At the first glance this plot still seems to have some concentration fluctuation. If we consider the gas temperature fluctuation is almost $1.5C$ which corresponds to $1.13ppm$ and a pressure swing of $16mbar$ which corresponds to $1.4ppm$. Thus a total contributions of $2.55ppm$ due to the fixed temperature and fixed pressure setup. The concentration fluctuation in the plot is $3.8ppm$. The etalon noise is therefore responsible for $1.25ppm$ fluctuation. Notice that the residual noise amplitude is approximately 3-5ppm. As long as this noise is stable we only have an offset in the concentration. However, etalon noise is

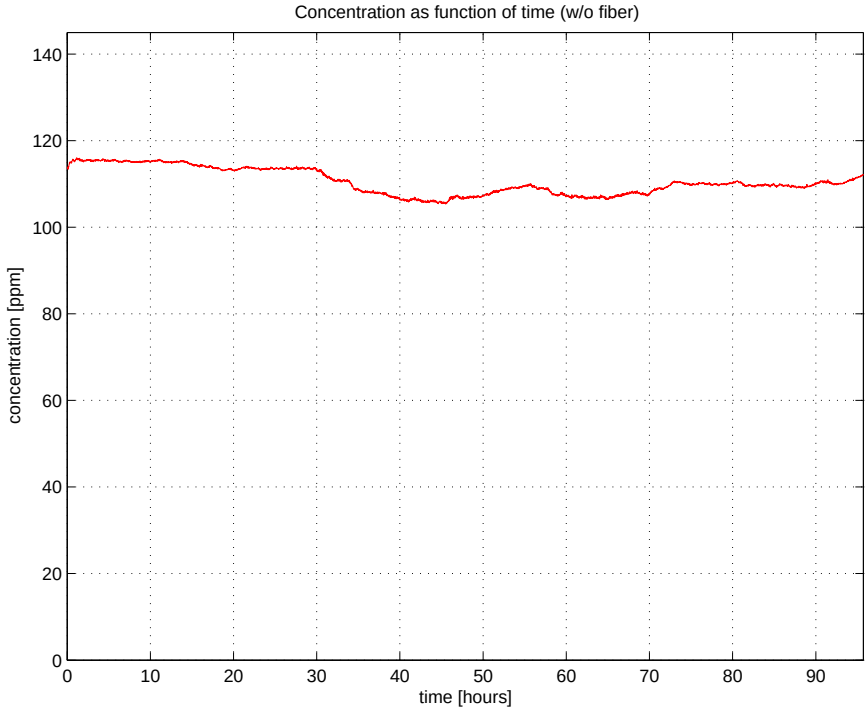

Figure 7.7: Concentration measurement of the 100ppm gas cell. The laser is mounted inside a metal box to reduce electromagnetic noise. The fluctuation in the plot comes from etalon effects from the fiber coupling.

seldom stable. The fluctuation of the etalon contributes to 1.25ppm fluctuation in the concentration as function of time.

An indirect verification of that the temperature and pressure affects the concentration can be seen in the plot. The initial concentration starts at $98.43ppm$, the line width starts at 0.7629 (software value) and the signal amplitude starts at 0.098. The signal amplitude gradually grows while the line width coherently decays. This continues until $t = 21$ hours and then the signal amplitude starts decreasing. At the same time the line width is rising. This correlation can be explained following. In chapter 3 we mentioned two broadening effects: Doppler broadening and collision broadening. Equation 3.3 states that when the line becomes broader the absorption peak will decrease. Equation 3.18 shows the dependence of the absorption line on the 2f signal. As the line becomes broaden due to higher pressure or a rise in temperature the second derivative of the absorption line will become smaller. Since all other parameters such as modulation amplitude, optical power and the phase are constant the 2f signal amplitude will decrease, in great agreement with the experimental observation.

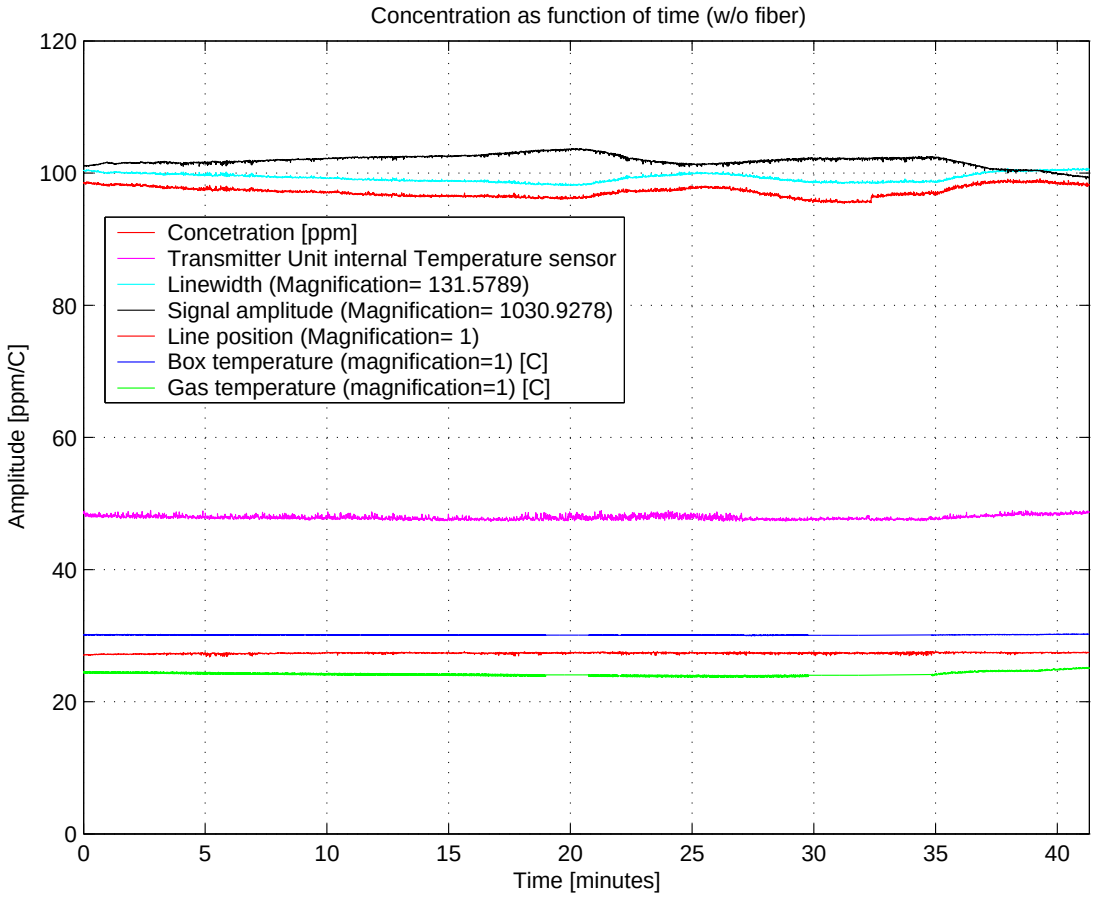

Figure 7.8: The room temperature fluctuation is just above 1C and the pressure fluctuation is just above 16mbar. These two contributions is equal to approximately 2ppm in the concentration value. Notice the very stable laser box temperature and the line position.

7.6 Temperature effects

7.6.1 Temperature effects on the laser

Figure 7.9a) shows the transmission as function of time. The transmission is logged using LaserGasII software. Figure 7.9b) shows the laser housing temperature as function of time. The temperature sensor (LM35CZ) is mounted on top of the laser module. The laser module is mounted inside a metal box. The laser housing temperature is approximately the temperature inside the metal box. The temperature inside the box is logged with the JAVA program written under this project (more details about this is given in the appendix). The JAVA program gets the averaged (32 samples from the Atmega16 microconroller) temperature values over the RS322 interface (serial port). The heating elements (two 47Ω resistors in parallel) are mo-

unted on the outside wall of the box to avoid electromagnetic noise from the pulse width modulation to disturb the laser modulation. The laser have been switched on for long time so it's transient effects can be neglected. The laser housing temperature is roughly 3C above the ambient temperature due to heat generated by the laser diode and the peltier element inside the laser housing. The temperature is suddenly set to 40C from the computer. The JAVA program sends this value to the microcontroller and the heating elements are turned on. After 20 minutes the temperature reaches a maximum value approximately 39.1C. An error of 0.9C is due to a property of the proportional regulator without an integrator. Integrators in regulators integrate up the error and ideally remove it completely.

As can be seen in the plots the transmission is very sensitive to the laser housing temperature. The transmission increases with increasing temperature. When the temperature is flat the transmission is essentially flat. After approximately 28 minutes we set the reference temperature to 0C and the heating elements is turned off. The transmission starts decreasing immediately. The slope ($\frac{dP}{dt}$) is smaller this time due to a smaller temperature-time slope ($\frac{dT}{dt}$). Notice that the temperature lags behind the transmission. After 30 minutes the transmission falls back to 53.05% but the temperature reaches the value that corresponds to this transmission 5 minutes later. This is because of the temperature sensor (LM35Z) has some mass and there is a small air gap between the temperature sensor and the laser module. Due to a small temperature difference between the laser module/air and the sensor longer time is required to transfer heat away from the sensor. Hence, it cools down slower than the laser housing. The information we harvest from this experiment is quite interesting. There are two important effects which are described below.

7.6.2 Thermal expansion leads to smaller coupling

When the temperature rises materials will expand. Due to different temperature coefficients of the laser housing (aluminium) and the fiber support cylinder (stainless steel), they will expand with different amounts. Aluminium has a expansion coefficient of $24\times10^{-6}K^{-1}$ and stainless steel has a smaller expansion coefficient of $13\times10^{-6}K^{-1}$. The relation between temperature, expansion and the expansion coefficient is given by[50]

$$\Delta L = \alpha L \Delta T \tag{7.2}$$

where ΔL is the additional length, α is the expansion coefficient and ΔT is the additional temperature. The fiber supporter has a thickness close to $1mm$ and using a $\Delta T \approx 12C$ the ΔL can be estimated to

$$\Delta L_{\Delta} = 11 \cdot 10^{-6} \cdot 10^{-3} \cdot 12 = 0.132\mu m \tag{7.3}$$

where ΔL_{Δ} is the expansion difference between the laser housing and the fiber supporter. This difference will displace the fiber axis in the transversal direction (and other directions as well). The beam coming out of the DFB laser will now experience that the fiber has moved and a different amount of laser light is coupled into the fiber. An

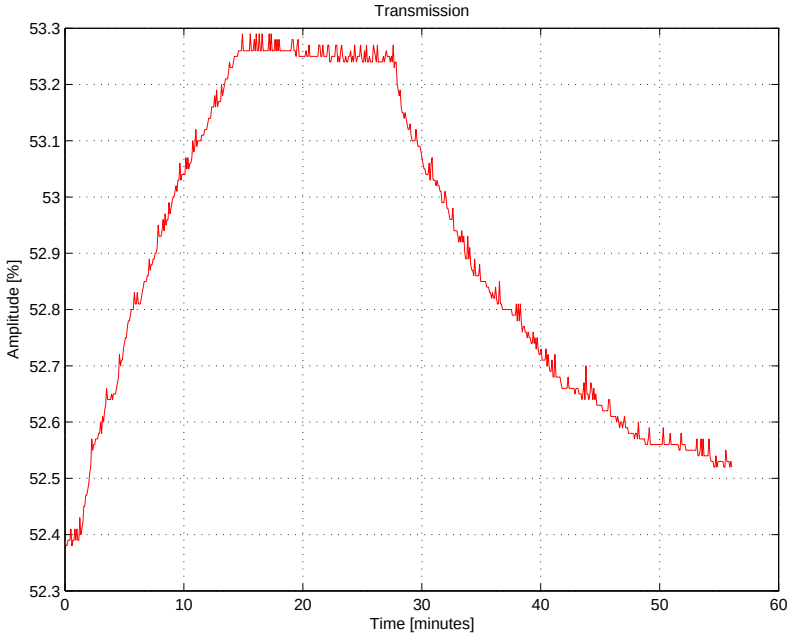

(a)

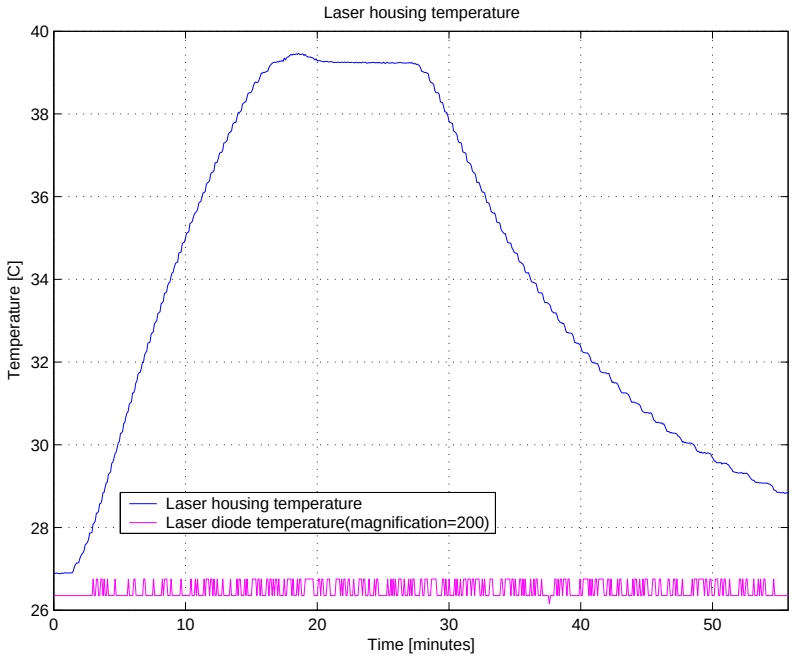

(b)

Figure 7.9: Coupling efficiency and housing temperature. a) transmission as function of time. b) Laser housing and laser diode temperature as function of time. The thermistor voltage is essentially constant. Hence, constant laser diode temperature with external perturbations.

increasing in the intensity with increasing temperature shows that the coupling efficiency is not optimum at 27C: it increases with temperature. Assuming two identical fibers and using Gauss beam approximation the expression for the coupling efficiency is given by[18]

$$\frac{P}{P_0} = \exp(-[\frac{u}{\omega}]^2) \tag{7.4}$$

where ω is the approximated mode field diameter[33] and u is the transversal displacement relative to the fiber coupler. With a maximum transmission of 53.25% and a minimum transmission of 52.4% the relative intensity loss for 12C change is therefor

$$Loss(dB) = 10log(\frac{52.4}{53.25}) \approx 0.07dB \tag{7.5}$$

This is indeed a very small loss and will be ignored in the communication industry. Taking 10 base log on both sides of equation 7.4 and inserting $\frac{P}{P_0} = \frac{52.4}{53.25}$ and solving for the transversal displacement u we get $u \approx 0.127\omega$. The mode field diameter in the polarization fiber is slightly smaller compared to standard step index single mode fibers (SMF). When $\omega \approx 6\mu m$ is used a displacement of $0.76\mu m$ will reduce the intensity with 0.07dB. Thus this displacement is approximately 6 times greater than the thermal expanded length estimated earlier. Actually the mode field diameter of the DFB laser beam is not the same as for the polarization maintaining fiber and there are also longitudinal and angle misalignment that will contribute to the reduced power (or increase in this case). A stable power loss does not affect the signal 2f amplitude. We believe this is not the source of the fluctuation in the 2f signal amplitude. What causes the fluctuation in the 2f signal?

7.6.3 Change in the facet angle leads to change in feedback noise

Since the force acting on the cylinder (fiber supporter) is not uniformly distributed from all directions the displacement is therefor not uniform. This leads to a fiber bending which will change the fiber angle relative to the fiber axis. A angle misalignment will reduce the coupling efficiency and less power is couple into the fiber. Thus a fraction of the uncoupled power is reflected back into the laser cavity. This reflected light has the same wavelength spectrum and will trigger electrons to jump down to a lower energy level and give of photons in phase with the back-reflected light. These photons are not coherent with the majority of the photons inside the cavity and are considered as noise. This leads to an increasing laser feedback noise and will affect the 2f signal amplitude. This is one of the two sources that give rise to the concentration fluctuation. The last effect is not because of the laser itself but the temperature controller and will be discussed below.

7.6.4 Spatial nonuniform distribution of the 2f noise

Figure 7.10 shows the 2f noise with several aperture sizes. The laser beam is blocked with a adjustable aperture. Note that the etalon noise is so large that the nonuniform

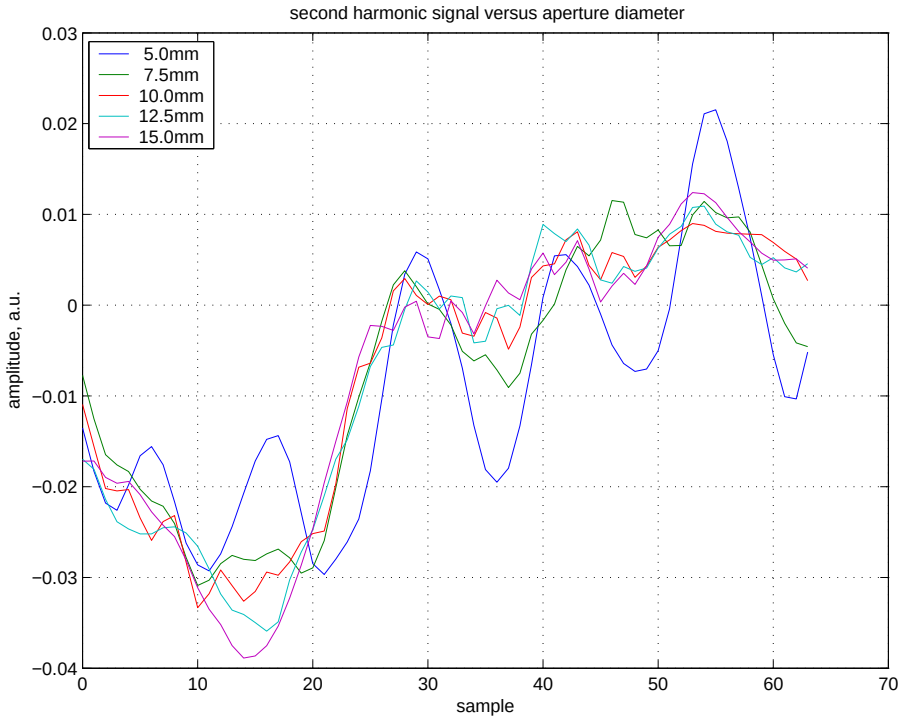

Figure 7.10: The noise distribution is nonuniform. Different amount of noise is coupled in if the fiber axis is displaced caused by temperature effects.

distribution is not clearly shown. This is of importance when we optimize the noise canceller.

7.6.5 Fluctuation in line position leads to fluctuation in the measured line width

The rise in laser housing temperature will force the laser temperature controller to change the peltier current. Ideally this change in the peltier current is just enough to cancel the external perturbations. More heat must be pumped away from the laser diode to compensate for the extra heat flow from the hot side to the cold side due to an increase $T_{hot} - T_{cold}$. The results of an non-ideal temperature controller is a fluctuation in the LD temperature. Additionally, the laser diode is not linear over the full range of the current scan. This nonlinearity will give a fluctuation in the measured line width. Since this value is an important parameter in the concentration calculation the concentration also fluctuate. If the absorption line moves the 2f signal amplitude will change. The concentration dependence on the laser housing temperature is shown in figure 7.11.

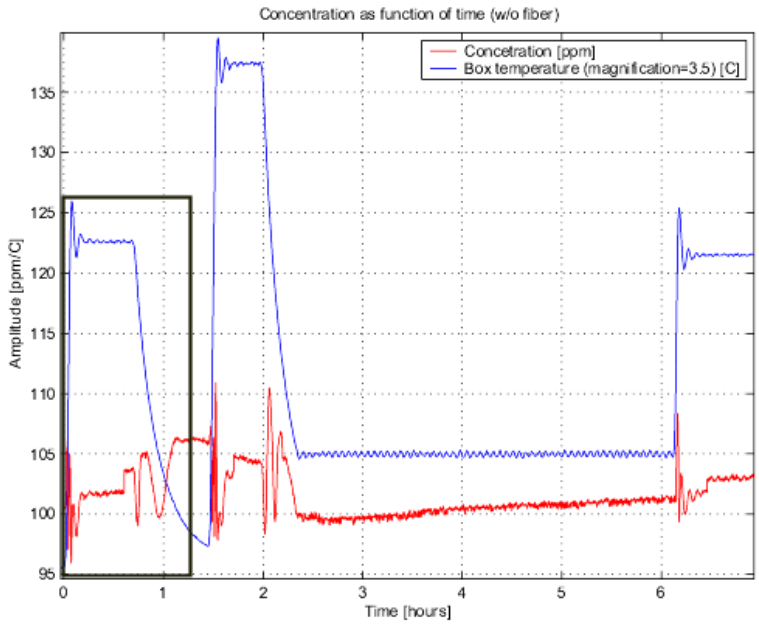

(a)

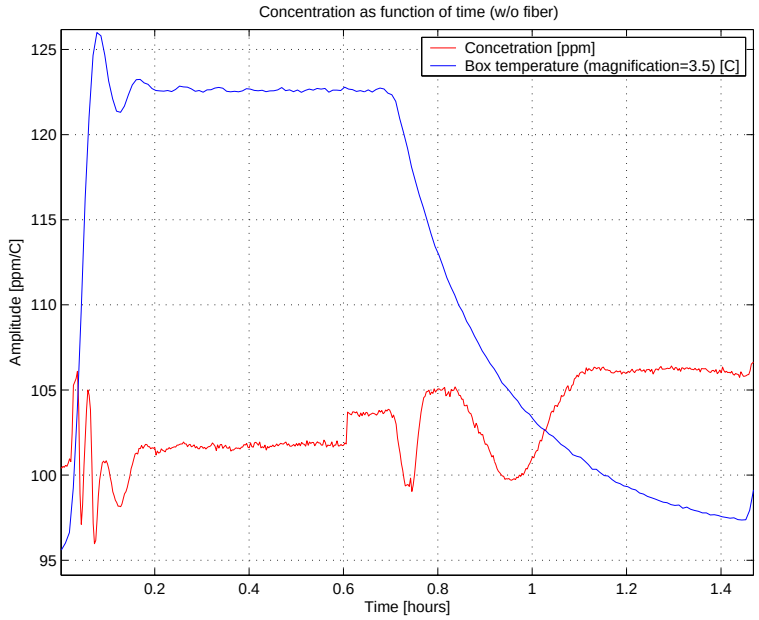

(b)

Figure 7.11: Concentration and temperature plot. a) concentration response to temperature steps inside the metal box thus the laser housing temperature. b) A portion of the response is showed.

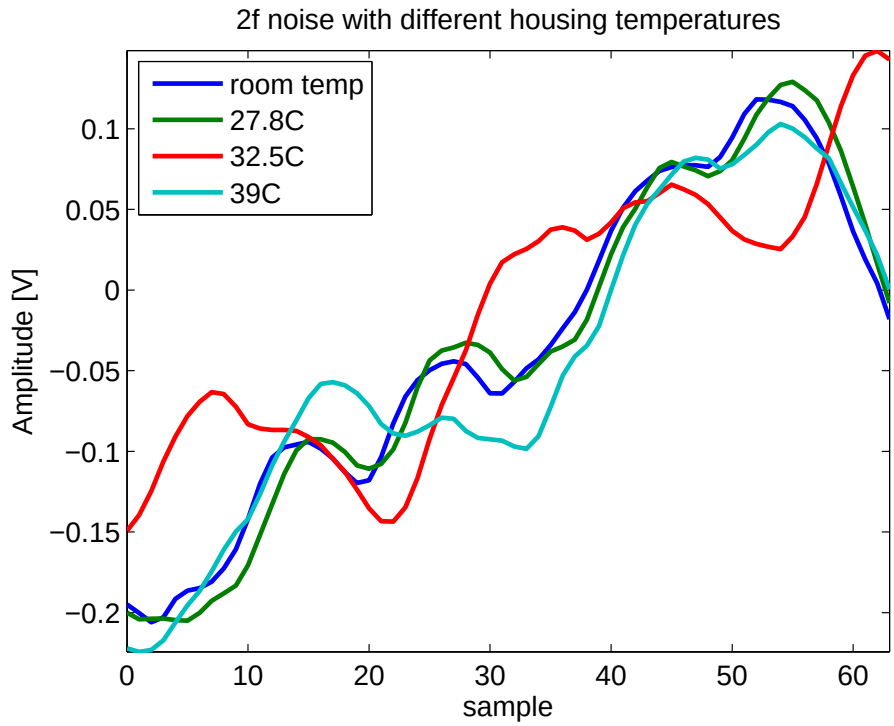

Figure 7.12: 2f noise with different housing temperatures. We see a drift in the noise shape when the laser housing temperature is changed.

7.6.6 2f noise versus housing temperature

As discussed above both the 2f noise amplitude and 2f noise shape changes with the laser housing temperature. To investigate how the 2f noise changes with changing room temperature we control the housing temperature and record the 2f noise. Figure 7.12 shows the 2f noise for four different laser housing temperatures. The noise shape and amplitude changes rapidly with temperature and is never stable under the temperature ramp. Four acquisitions represents the noise for four different temperatures. Since the noise is linearly added to the 2f signal the resulting signal shape fluctuates. The line amplitude and the linewidth is affected by the noise shape. The noise shape is rapidly changing as function of time, seconds. Since the linewidth is calculated from the 2f signal shape the line width also fluctuates. This makes it very difficult to obtain reliable results with single beam measurements under fast varying temperature environments. However, in real applications the temperature fluctuation is slow and the concentration is less affected. The fluctuations tends to slow down when the temperature is stabilized. This can be seen in figure 7.11.

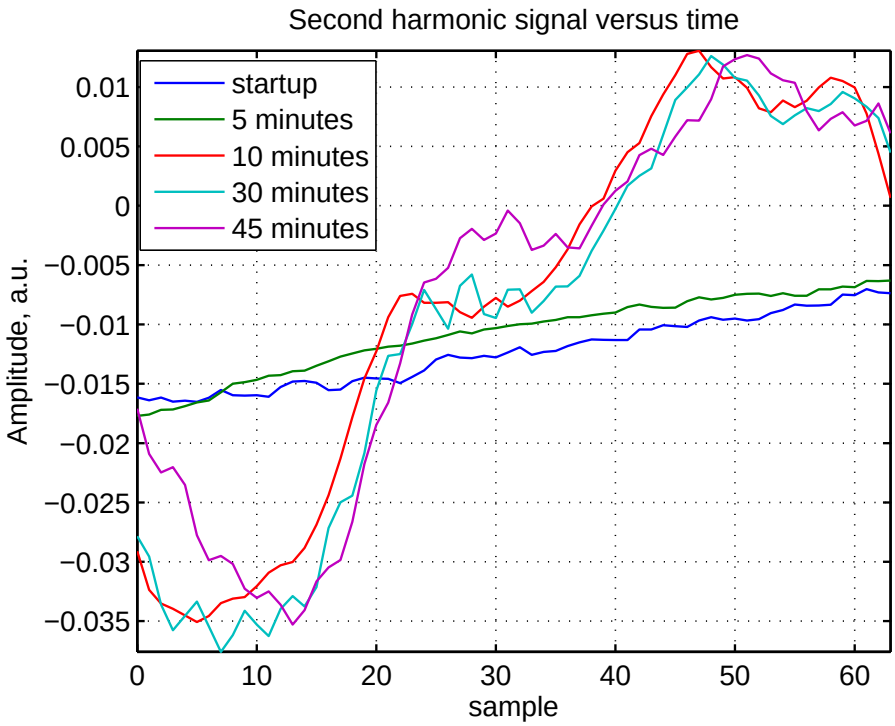

Figure 7.13: Noise versus time after startup. Drift in the 2f noise due to temperature change limits the instrument sensitivity

7.6.7 Transient noise and stabilization time

Above we have seen that the temperature effect on the laser housing significantly change the 2f noise. One more evidence that support this theory is the change in 2f signal shape and amplitude after laser startup. Figure 7.13 shows the noise as function of time after laser startup. In can be clearly seen that after 5 minutes the noise is lowest. After 10 minutes the noise changes little and becomes stable after 30 minutes. Before startup the laser housing has ambient temperature. Because of the operating temperature of the laser diode chip is slightly below ambient temperature the peltier starts pumping heat to the metal housing. The peltier it self generates some heat and after 30 minutes equilibrium is reached. The stable housing temperature is experimentally observed to be 27-28C while room temperature is approximately 23C. This has similar effects as discussed above. The time constant is larger now. Hence, the noise drift is not as dramatic as the 27C to 40C step within 10 minutes.

7.7 Noise and background signal suppression

Problems with fiber noise, temperature effects of the laser, and laser power supply noise pickup motivate us to implement the dual beam system. The following results are achieved with the current domain subtraction circuit.

Our preamplifier designs have approximately the same noise floor compared to the standard preamplifier since the feedback resistor used here is small, $R_f = 1k\Omega$. With larger feedback resistors the input current noise of the AD797 starts to dominates (discussed in section 4). The following measurements are done by connecting the noise canceller output to a digital oscilloscope (Tektronix TDS2022). Labview software and GP-IB are used to acquire measured data from the oscilloscope. Figure 7.14a) shows the noise canceller output (current domain subtraction). When the reference beam is blocked the circuit operates as a normal transimpedance amplifier. Blue graph shows the 800mVpp modulation signal and the ramp signal (3.4V peak). This signal is so large that a small absorption signal will be swamped. Red graph shows the same output when the reference beam is unblocked. The modulation signal is reduced by approximately 30 times, thus resulting in a modulation amplitude of only 22mVpp. When the reference beam is unblocked the servo amplifier adjusts the current division ratio of the NPN transistor pair such that the dc output is zero. Ideally the modulation signal also is zero far from the absorption line center. Near the absorption line center first, second and higher harmonics are generated in the signal beam, but not in the reference beam. Hence, they can not be removed. We would see a signal oscillating at the modulation frequency with an envelope given by the first derivative of the absorption line. The second harmonic oscillations are an order of magnitude smaller and is not easy to observe.

However, we do not see this effect here because the balancing is not perfect. There are three possibilities. 1) A phase mismatch between the signal current and the reference current. This prevents perfect cancellation. The phase shift between these two signals must be 180 degrees for perfect cancellation. This condition is achieved by circuit design. The optical path difference between the reference beam and the signal beam is approximately 1m (from the fiber end to the photodetector). The phase shift would be $5.75mrad$ for the modulation signal and $11.5mrad$ for the 2f signal. This contribution is small and can be neglected in most calculations. However, a phase shift caused by the electronics in the signal and reference photocurrent path can cause problems. 2) Spatial nonuniform response and difference in the photodetector response (difference in the signal and reference photodiode response). This makes the $\delta = \frac{i_{ac}}{i_{dc}}$ to be different in the signal and the reference photocurrent. Since the feedback loop uses the i_{dc} for balancing we have an amplitude error in the i_{ac} current and non perfect cancellation. 3) In real transistors the small signal and large signal current is not the same ($h_{FE} \neq h_{fe}$) and the ac signal splits differently in the npn transistor pair. This gives an ac amplitude error even though the dc level is exactly zero. These effects are discussed more in the optimization of the current domain noise canceller.

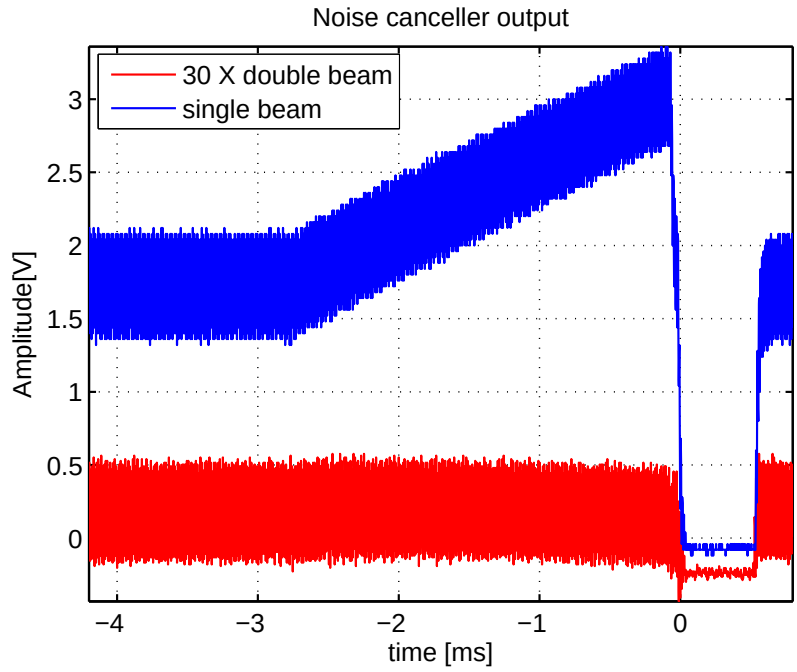

(a)

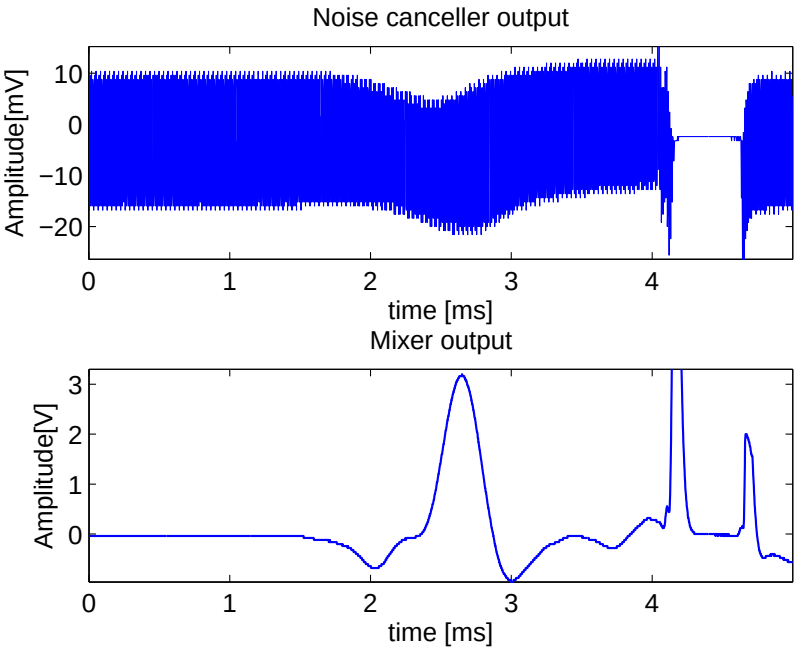

(b)

Figure 7.14: a) Noise canceller output with the gas cell removed. 30dB suppression of the modulation signal and almost zero ramp signal. b) Noise canceller output and mixer output with 100ppm gas cell in the optical path. The modulation signal is suppressed to 22mVpp. Perfect cancellation would remove it completely outside the absorption line. 2f signal peak occur at the absorption line center.

7.8 Noise canceller performance in WMS

The DFB laser is quiet when unmodulated. However, with the current ramp and the modulation signal turned on a sensitivity of approximately 4ppm was achieved in a straight forward method. The etalon noise in the 2f signal comes from the coupling inside the laser module. This noise fluctuates with laser module temperature. Showed in the previous section the common signals can be cancelled. The modulation intensity noise was reduced by approximately 30 times. We test the noise canceller circuit in second harmonic detection. The standard preamplifier circuit in the receiver board is removed. The noise canceller output is directly connected to the mixer input. The direct signal provided by the differential amplifier (NE5534N from Phillips) in the noise canceller is connected to the direct signal input on the receiver board.

To demonstrate the noise canceller performance we test it with the 100ppm gas cell. The second harmonic signal gain is adjusted to $0.93 \times 0.62 \times 133 \times 31.4$. Experimentally a phase correction of 5 degrees in software was needed due to the new preamplifier. Figure 7.15a) shows a 1:1 comparison of the residual noise between single beam and double beam configuration. Single measurement was obtained by blocking the reference beam. 256 scans was averaged to obtain one concentration measurement. The 2f noise has etalon fringing. The fringe tops are separated by 40 samples from each other. In a $0.77cm^{-1}$ (64 samplings in each scan) scan this is equal to approximately $FSR = 0.51cm^{-1}$. The optical surface spacing that give this period is approximately 1cm (FSR = $\frac{1}{2nL}$) in air. No such spacing where identified in our optical system. The noise shape changes when the laser housing temperature was adjusted with the home made temperature controller. Careful study reveals that this noise comes from the light coupling inside the laser module. This noise can therefore not be reduced with external optical components. However, since this noise is present on both fiber outputs of the fiber splitter the electronic noise canceller will suppress it. When the reference beam is unblocked these tops are gone. The 2f signal in this configuration seems to have negative a dc offset. This offset was identified as the etalon fringe from glass windows and lenses (approximately 2-3mm etalon cavities). Figure 7.15b) shows the same comparison, but now the noise with double beam measurement is magnified 12x to give the same noise amplitude as with the single beam measurement. The digital signal processed version of the noise is approximately $400\times$ smaller than the 100ppm signal. This gives a detection limit of 0.25ppm with use of the noise canceller, or 5×10^{-6} in absorbance unit with 0.712m optical path length. The effective noise bandwidth is $ENBW = 134000kHz/256 = 52.3Hz$ and each concentration measurement requires 3.2s acquisition time. Theoretically, by taking more scans for averaging a sensitivity of 4.9×10^{-7} with ENBW=1Hz and 1m optical path length. At these sensitivities careful design of the optical system is necessary to avoid etalon fringing to dominate. In 2004 Engelbrecht[14] reported a sensitivity of 6.4×10^{-7}. For comparison, the theoretical 1Hz rms photocurrent shot noise amplitude with 2.2mA photocurrent is 1.2×10^{-8}. The performance of our instrument relies on effective digital signal processing.

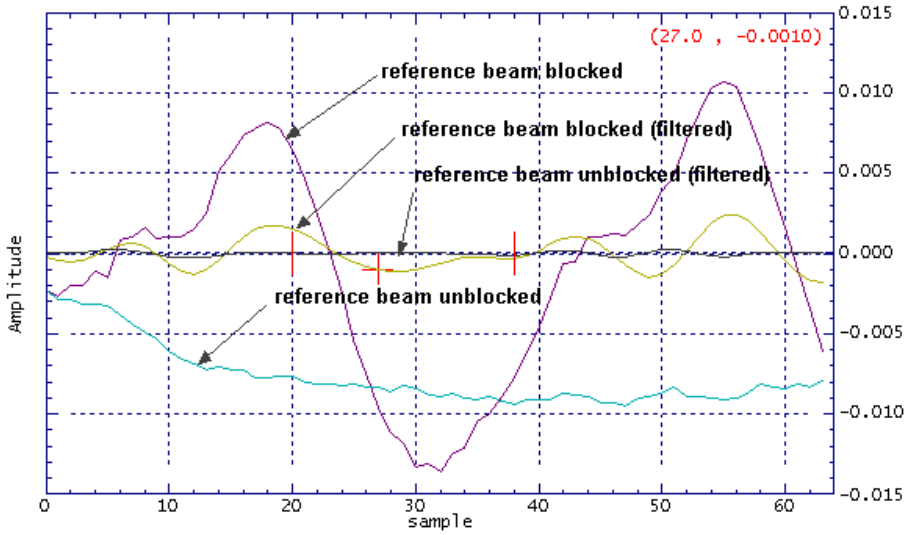

(a)

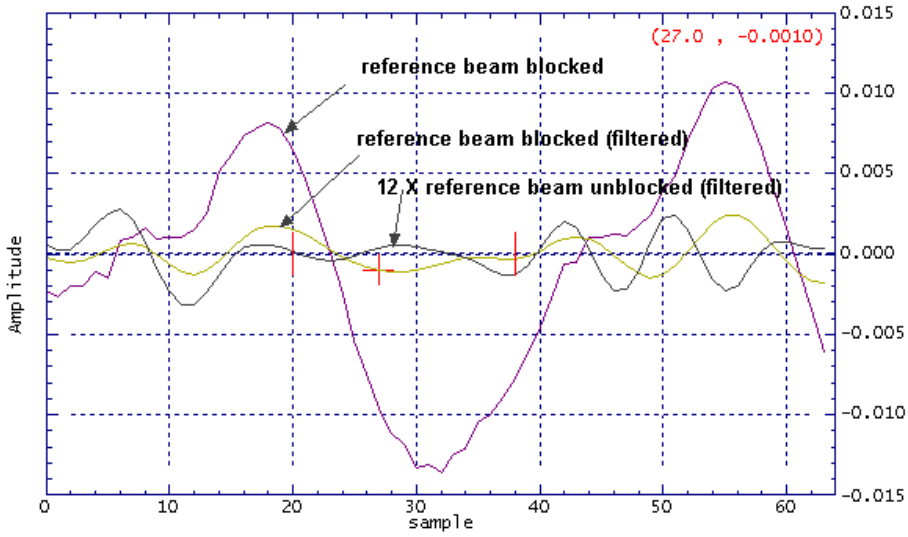

(b)

Figure 7.15: Signal and noise with our current subtractor. 12× reduction in the noise when applying the current subtracter to suppress common noise.

7.9 Electronic noise

It is most common that the preamplifier (front end) dictates the signal to noise ratio in an optical system. At high light levels the photodiode shot noise dominates. At low light levels, VCSEL lasers emit light typically 1/10 of other lasers, larger feedback resistors are necessary and the op amp noise dominates. However, it is not producing noise alone. Later stages in the signal path also produce noise as well. The front end's job is to amplify weak signals, swamped in noise, into larger values. The later gain stages amplify both the noise and signal equally. Additionally, these stages contribute to some additive noise. Since the signal is amplified at the front end making the signal input to later stages relatively large (compared to their noise amplitudes), the noise produced in later stages may not dominate. The preamplifier is adjusted for maximum gain (without creating distortions). This transimpedance gain is 165Ω when no fiber components are used (22mW ramp end output). The noise canceller uses $1k\Omega$ feedback resistor with (22mW/4 fiber output).

7.9.1 Mixer and post-amplifier noise

To characterize the rear end noise we model the rear end stages as a single amplifier with $G = 0.93 \times 0.62 \times 133 \times 31.4 = 2408$. The 0.93 term comes from the amplitude response (187.5kHz) of the first order analog filter at the mixer input. 0.62 term comes from the mixer reflection coefficient defined as the output voltage divided by the input voltage ($\frac{V_{IF}}{V_{RF}}$). It should be mentioned that this constant was measured at 375kHz by Linnerud[31]. We assume that at our 2f frequency this constant is close to this value. The 133 term comes from the 2f signal post-amplifier. This gain is determined by the switch settings in table 6.5. The last amplifier has a fixed non-inverting gain of 31.4. The total gain is therefore a product of all terms above. The analog noise bandwidth was measured to 6.7kHz (theoretically 6.57kHz) [31]. Because of mixing both sidebands contribute to the total noise. Hence, the effective noise bandwidth, encountered for the sidebands, is twice this bandwidth: 13.4kHz. Notice that this is not equal to the 2f signal bandwidth. The signal bandwidth is smaller than the noise bandwidth which is the normalized area under the signal bandwidth. To find the input noise spectral density we divide the output noise (measured) on the total gain and the square root of the bandwidth. Earlier we neglect the impedance of the feedback capacitor. At low frequency it's impedance is big, but at 187.5kHz it's impedance is $Z_c = 1/(2\pi f C_f) \approx 8.5k\Omega$ ($C_f = 100pF$). The feedback resistor is in parallel with the capacitor and the resulting impedance is approximately $Z_f = 900\Omega$. This impedance is what the 2f signal see and it is amplified by this amount. The phase shift is approximately 6.6 degrees. Hence, the equivalent input noise spectral density is

$$i_{in} = \frac{e_{out}}{Z_f G \times \sqrt{B}} = \frac{e_{out}}{2.17M\Omega\sqrt{B}} \tag{7.6}$$

where G is the gain and B is the bandwidth. The total gain is $G_{tot}(187.5kHz) = Z_f \times G = 900\Omega \times 2408 \approx 2.17M\Omega$. The current noise spectral density is referred to the input of the preamplifier. The total input noise is a square sum of noises from

different noise sources, i.e.

$$i_{tot} = \sqrt{i_{in1}^2 + i_{in2}^2 + ... + i_{inN}^2} \tag{7.7}$$

The rear end electronic noise alone is measured by grounding the mixer input. The output noise is then measured at the phase-lock amplifier output (mixer and post amplifiers). The noise amplitude in this configuration is a square sum of the noise from the mixer and following stages, and the transimpedance amplifier noise. However, the noise contributions from later stages is negligible. We can assume that all the noise stems from the preamplifier and the laser beam.

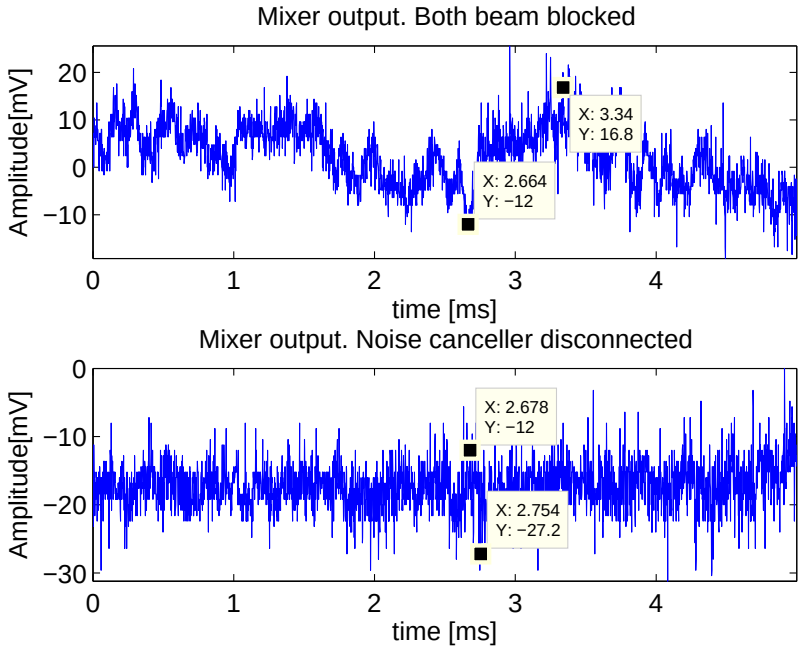

Figure 7.16: Top) Both beams are blocked. The noise is measured at the mixer output (phase lock amplifier output). Bottom) The same measurement, but this time the mixer input is grounded. This noise is the electronic noise floor for our system.

Figure 7.16 (bottom) shows the noise when the mixer input is grounded. A noise amplitude of 5.4mVrms (15.2mVpp) appears at the mixer output. Linnerud reported 4.5mVrms output noise when the mixer was grounded. A numerical application gives the equivalent input noise of $i_{in} = 21.5pA/\sqrt{Hz}$ by use of equation (7.6). This noise comes from the mixer, local oscillator noise, thermal noise in resistors (capacitors and inductors are assumed to be noiseless) and op amp noise. The electronic noise floor is set by this value. For comparison the input voltage noise amplitude of the first op amp after the mixer is $\sqrt{(0.9nV)^2 + (0.92nV)^2}/\sqrt{Hz} = 1.3nV/\sqrt{Hz}$. This noise consists of input resistor thermal noise and op amp intrinsic input voltage noise for the given

amplification. Hence, an equivalent input current noise is $i_{neq} = 1.47pA/\sqrt{Hz}$ (by dividing by the transimpedance gain). From this we see that the noise from the mixer dominates the rear end electronic noise floor.

Figure 7.16 (top) shows the mixer output when the noise canceller output is connected to the mixer input. Both beams are blocked to measure the dark noise. The noise amplitude is roughly 10.2mVrms (28.8mVpp). This gives an equivalent input noise of $i_{eq} = 40.6pA/\sqrt{Hz}$. The noise contribution from the noise canceller is

$$i_{nc} = \sqrt{(40.6pA)^2 - (21.5pA)^2}/\sqrt{Hz} = 34.4pA/\sqrt{Hz} \tag{7.8}$$

When both the detectors are blocked no current flows into the transimpedance input. The $0.4\mu A$ dark current (from the very large shunt resistance of $12M\Omega$) shot noise from the detectors in reverse bias mode is negligible. We can safely assume that the noise appearing at the output is coming from the preamplifier alone. This noise consists of a thermal noise coming from the feedback resistor, the op amp intrinsic voltage noise, the op amp input current noise, and other sources such as power supply noise or noise pickup in the circuitry. Theoretically the preamplifier's equivalent input current noise is (see section 4 for deviations)

$$i_{nA} = \sqrt{(4.07pA)^2 + (2pA)^2 + (0.9nV/1k\Omega)^2}/\sqrt{Hz} = 4.64pA/\sqrt{Hz} \tag{7.9}$$

which comes from thermal noise ($R_f = 1k\Omega$ and 300Kelvin), op amp current noise ($2pA/\sqrt{Hz}$) and op amp voltage noise ($0.9nV\sqrt{Hz}$). We see that the noise canceller has much more noise than the theoretical value, 7.4× (17.4dB above the theoretical value). It should be mentioned that the measurements above have large measurement errors, especially at low output amplitudes, due to the simple measurement setup. However, it gives an indication that the noise canceller electronics are not optimized. We believe that the noise stems from the $\pm 5V$ voltage supplies.

7.9.2 Beam noise without wavelength scan

The same setup is used to measure the beam noise. In this configuration we turn off the current ramp to avoid etalon fringes. The laser wavelength is therefore modulated around a center wavelength outside the absorption line center. Hence, no signal is generated and the output should ideally be zero. Two configurations are compared to each other. First the reference beam is blocked. The mixer output of this measurement is shown in figure 7.17 (bottom). The reference beam is unblocked (top) for comparison. In the double beam configuration the noise amplitude is 47.4mVrms (134mVpp). Using equation (7.6) we find the input noise to be $i_{eqn} = 188.7pA/\sqrt{Hz}$. Referred to the input the beam noise is therefore

$$i_{nB} = \sqrt{(188.7pA)^2 - (34.4pA)^2}/\sqrt{Hz} = 185.5pA/\sqrt{Hz} \tag{7.10}$$

The signal beam photocurrent including the modulation signal is approximately $i_s = i_r/1.8 = 1.5mA$ in this configuration. Hence, a theoretical shot noise amplitude is

$$i_{sn} = \sqrt{4ei_s}/\sqrt{Hz} \approx 31.0pA/\sqrt{Hz} \tag{7.11}$$

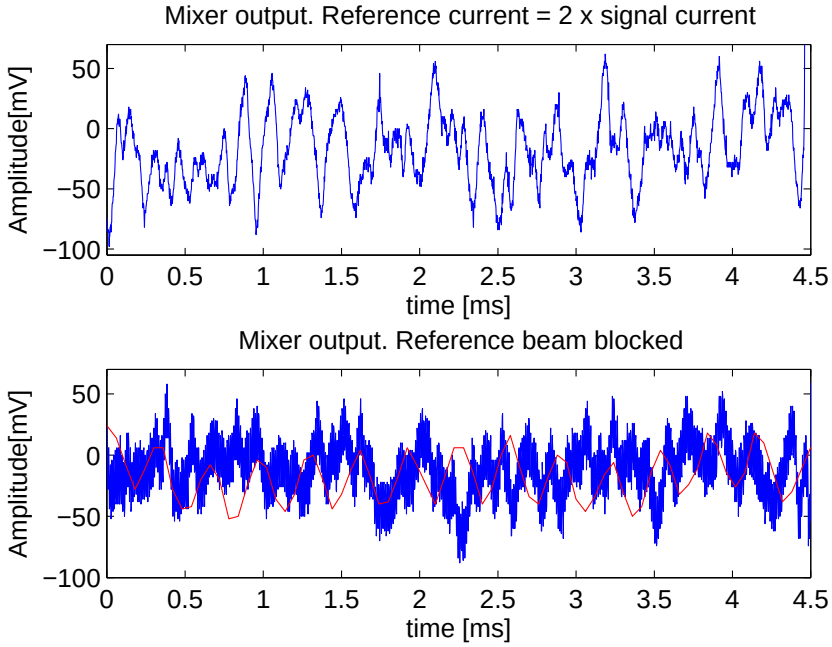

Figure 7.17: Top) Dual beam configuration. Bottom) The same measurement, but this time the reference beam is blocked. The bottom signal has very much contributions of the modulation signal that survives analog filtering. Red graph shows the same signal, but stretched 30× in time to show the 92.75kHz oscillations.

for comparison. Hence, the beam noise is 15.5dB ($i_{nB} = 6 \times i_{sn}$) above the shot noise level of the dual beam configuration or 18.5dB above the signal beam shot noise alone. Remember that the theoretical shot noise floor for the dual beam is 3dB above the single beam configuration.

The reference beam is now blocked for comparison. The noise canceller now works like an ordinary transimpedance amplifier. Figure 7.17 (top) shows one scan capture of the mixer output. The noise amplitude is 36.8mVrms (104mVpp). This corresponds to an input noise of $i_{eqn} = 146.4pA/\sqrt{Hz}$. The single beam noise is

$$i_{nB} = \sqrt{(146.4pA)^2 - (34.4pA)^2}/\sqrt{Hz} = 142.3pA/\sqrt{Hz} \tag{7.12}$$

The noise level in the single beam configuration is 16.2dB above the shot noise level of the signal photocurrent($20log(144.6pA/\sqrt{2ei_s}) = 16.2dB$). This beam noise is identified as the laser excess noise. In the case of perfect noise cancellation the noise level would be 3dB above the signal current shot noise level for the dual beam configuration and above shot noise for the single beam configuration (if the laser beam exhibits excess noise!).

One interesting observation is that the 2f signal in the single beam configuration has contribution from the intensity modulation signal. This signal would be completely

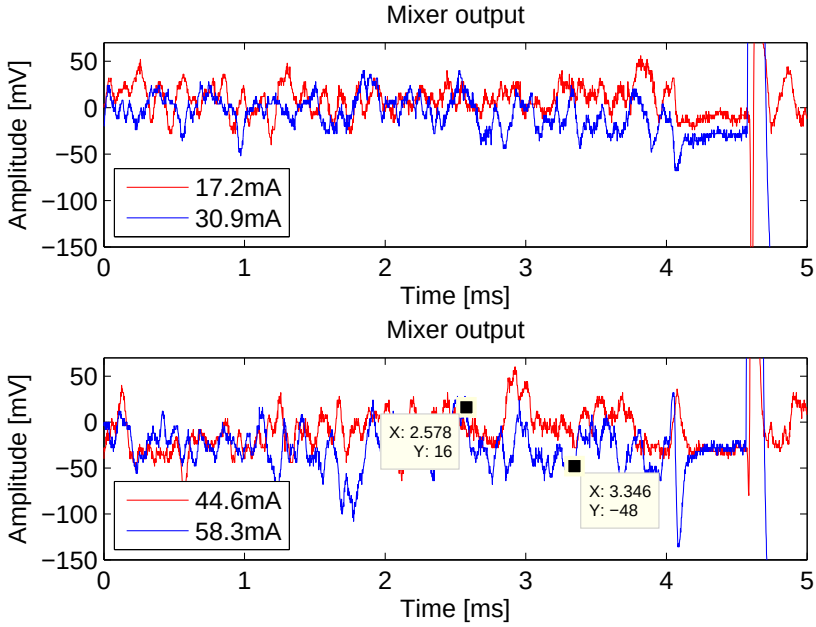

Figure 7.18: Mixer output signal with four different laser injection currents. A 2f noise increase with increasing injection current is observed in this measurement.

removed with a sharp analog filter after the mixer. However, because of the finite attenuation in the stop band some appear at the mixer output. Keeping the same amplitude, but stretching out the time axis of the signal in the bottom graph by 30× reveals this 92.75kHz oscillation signal (The design frequency is 93.75kHz, but the measured frequency is 92.75kHz). It is shown in the red graph in figure 7.17 (bottom). The time between two minima is approximately 10.8μs. This corresponds to one period of the 92.75kHz modulation signal. This amplitude is 46mV at the mixer output, which is of significant amplitude. Fortunately, the sampling frequency is much lower (64 samples within a 2.68ms ramp scan gives 23.9kS/s. Nyquist theorem requires minimum a sampling frequency twice the modulation signal in order to capture it). When using signal averaging of 256 ramp scans and using effective digital filtering there is no trace left from this modulation signal in the digital 2f signal. As a bonus the dual beam subtraction technique removes this modulation signal. Even before sampling and averaging it is far gone as shown in the top figure.

7.9.3 Beam noise with dc injection current

In this measurement we turn off both the wavelength scan and the wavelength modulation. The laser injection current and thus the laser beam is dc. If the laser is quiet the beam only has shot noise. This measurement directly measures the laser excess noise at a 13.4kHz bandwidth near 187.5kHz. Four dc injection currents are compared to

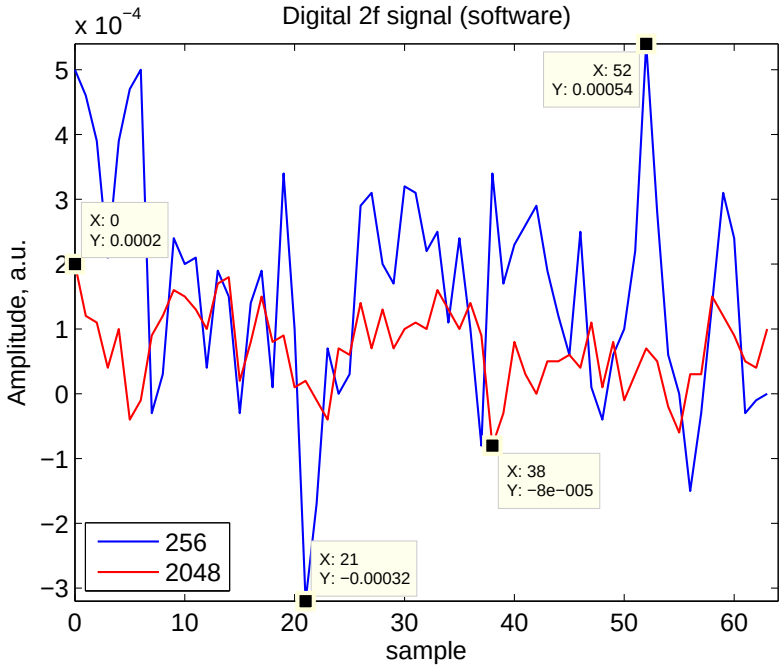

Figure 7.19: Digital 2f residual noise signal for two effective noise bandwidths. Blue graph shows the 256 scans averaged signal before digital signal processing. 2048 scans is averaged to get the red graph. Hence the effective noise bandwidths are ENBW=52.3Hz and ENBW=6.5Hz, respectively

see the effect of increasing shot noise with increasing photocurrent. Figure 7.18 shows four single scans of the mixer output signal. In this double beam configuration we have $i_r = 1.8i_s$. At 58.3mA laser injection current with modulation and ramp turned off the photocurrent is approximately 1.6mA. The theoretical photocurrent shot noise is $i_{sn} = \sqrt{2ei_s} = 22.6pA/\sqrt{Hz}$. The measured rms noise amplitude of the laser beam is $22.6mV$ rms (64mVpp) and corresponds to a noise density of $90.0pA/\sqrt{Hz}$. The equivalent input noise density is therefor

$$\sqrt{(90.0pA)^2 - (34.4.5pA)^2}/\sqrt{Hz} = 83.2pA/\sqrt{Hz} \tag{7.13}$$

Now the noise is 11.6dB above the theoretical signal beam shot noise.

7.9.4 Acquisition time and noise bandwidth

The shot noise, thermal noise and electronic noise can be reduced by increasing the measurement time (acquisition) by averaging single scans. A larger number of ramp scans must be used to produce the digital 2f signal. In the software we can change this number (software parameter: "ramp accumulations") to reduce the effective noise bandwidth. The effective noise bandwidth is given by

$$\text{ENBW} = \frac{13400Hz}{N} \tag{7.14}$$

where N is the number of ramp scans to be averaged. To verify we change the standard value (256) to 2048 thus reducing the effective noise bandwidth by a factor of 8. We could expect a noise reduction with a factor of $\sqrt{8} = 2.8$. Figure 7.19 shows two digital noise signals for two software settings. With 256 ramp scans the effective bandwidth is 52.3Hz. With 2048 ramp scans the effective bandwidth is 6.5Hz. 256 or 2048 acquisitions are averaged to represent the signals in figure 7.19. The noise is reduced by a factor of 3.07. This is in well agreement with the predicted value of $\sqrt{2048/256} = 2.8$

7.9.5 Electronic noise in WMS

How do these noise amplitudes translate in measurement sensitivities with the digital signal processing applied? The digital signal processing improves the signal to noise ratio by filtering the input signals with matched filters. With dc photocurrent of $i_r = 1.8i_s = 1.6mA$ the analog signal at the mixer output has an equivalent input current noise level 11.6dB above the shot noise. When the mixer input is grounded the noise density is $21.5pA/\sqrt{Hz}$. This is the noise floor of our system. When the ADC is used to convert the analog signal to digital form ADC noise will be added to the digital signal. The theoretical ADC noise is 1.4mV referred to the ADC input with 10V scale(component choice). Figure 7.20 compares two noise measurements. The noise amplitude in software is $\sim 1.29 \times 10^{-4}$ for the dc laser beam (ramp and modulation off) and $\sim 1.6 \times 10^{-5}$ with mixer input grounded at an effective noise bandwidth of 52.3Hz. Relative to the 100ppm line amplitude (1.02×10^{-1}) these values correspond to SNR $\approx$ 790 and SNR $\approx$ 6375. The gas concentration sensitivities are 0.13ppm and 0.016ppm respectively. These values correspond to sensitivities of 2.5×10^{-6} and 3.1×10^{-7} in absorbance units respectively with ENBW=52.3Hz and 0.712m optical path length. Notice that these values are the digital signal to noise ratio and absorbance equivalent unit respectively.

7.9.6 Summary

The results in this section show that the laser is relative quiet at a narrow bandwidth centered at the 2f frequency (187.5kHz) when it is not modulated. The noise density near the detection bandwidth is 11.5dB above the shot noise of the signal photocurrent alone. The noise level rises to 18.5dB when a 92.75kHz modulation signal is added to the dc injection current(dual beam configuration). When the ramp is applied etalon effects due to the wavelength scan become the limiting factor. This noise easily exceeds 30dB above the shot noise as we will see later. The coupling inside the laser module contributes to very much noise when the normal modulation scheme is applied. Since the noise source is inside the laser module, external components such as optical isolators can not reduce the noise amplitude. The only choice is noise suppression in the electronic domain.

In single beam measurements the modulation signal is not fully suppressed by analog filtering. Dual beam measurements have larger shot noise due to uncorrelated

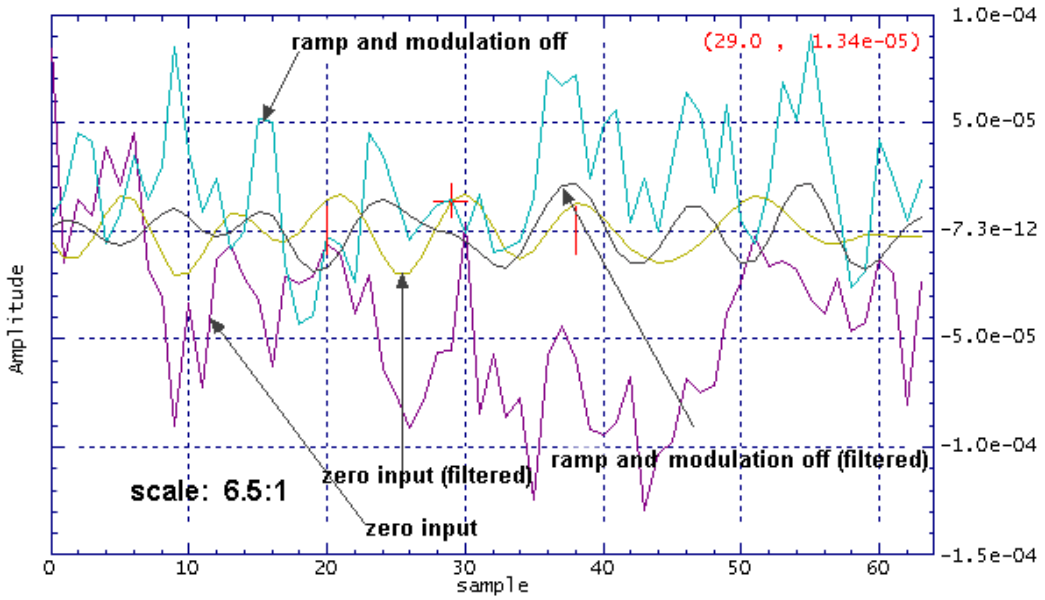

Figure 7.20: 2f noise for dc laser beam and mixer input grounded.

shot noise in the signal and reference channel. Their power adds, rather than their amplitude! The noise canceller electronics are not optimized and can be improved more. It's noise amplitude is more than 10dB above the theoretical limit from the op amp datasheet. The ADC noise and the effective noise bandwidth can be reduced by averaging more single measurements. An effective noise bandwidth of 5.6Hz requires an acquisition time of 30s. To achieve an effective noise bandwidth of 1Hz the acquisition time would be 167.5s. The noise reduction roughly follows equation (7.14)

7.10 Optimization of the current domain noise canceller

The basic noise canceller based on current domain subtraction suppresses the intensity modulation signal from 800mV to 22mV and reduces the mixer requirements. If the amplitude balance in the current splitter is perfect (i.e. $i_s = i_r$) only the phase prevents perfect cancellation of the common signals. The dc level balance was observed to be very good and we can neglect amplitude unbalance. A phase shift difference of 1.6° limits the minimum amplitude to 2.8%. The goal of this section is to eliminate the phase difference to achieve high cancellation strengths ($i_s/\Delta i$).

The current into the op amp's negative input pin is given by

$$\Delta i = i_s \cos(\omega_m t + \varphi_1) - i_r \cos(\omega_m t + \varphi_2) = -2i_s \sin(\omega_m t + \frac{\varphi_1 + \varphi_2}{2}) \sin(\frac{\varphi_1 - \varphi_2}{2}) \tag{7.15}$$

where we have used perfect balancing and a trigonometric relation in the last step. The intensity modulation signal phase at the output is shifted, but the amplitude is given by $-2i_s \sin[(\varphi_1 - \varphi_2)/2]$ which is the minimum intensity modulation signal amplitude at the noise canceller input. All other signals cancel in the similar fashion (only the phase and thus the cancellation strength differ). If the phase shifts in the signal and the reference path are not identical the ac signal at the output is not zero.

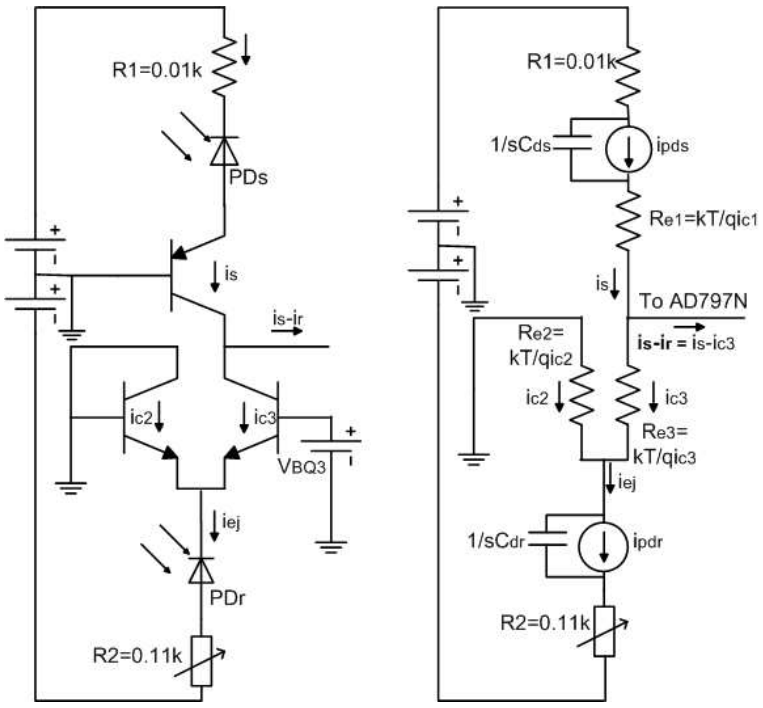

Figure 7.21: Noise canceller equivalent circuit.

The equivalent circuit for the noise canceller is shown in figure 7.21. In the basic

noise canceller circuit $R_2 = 0\Omega$ (it turned out to be a bad choice!). The difference amplifier attached to the R_1 resistor is ignored in the analysis because of it's little influence on the phase shift. We look at the circuitry around the signal photodiode. The photodiode is modeled as a current source with it's shunt capacitance in parallel. At high frequencies the shunt capacitor becomes a problem and more photocurrent takes the way through the shunt capacitance. Hence, less signal current goes out of the photodiode anode while the voltage across the photodiode jiggles. The current flowing out of the pnp transistor's collector is given by current division between the shunt capacitance and the load resistor seen by the photodiode

$$i_s = i_{c1} = \frac{i_{pds} \cdot 1/j\omega C_{ds}}{R + 1/j\omega C_{ds}} = \frac{i_{pd}}{j\omega R C_{ds} + 1} \tag{7.16}$$

where C_{ds} is the signal photodiode shunt capacitance and $R = R_1 + kT/qi_{c1}$. According to the Ebers-Moll model the emitter resistance of pnp/npn transistors are given by kT/qi_c. i_{c1}, i_{c2} and i_{c3} are the large signal dc currents. i_{ej}, i_s, i_r and Δi are the ac small signal currents (harmonic signals). The phase shift of the signal current at the summation node is found by taking the phase of equation (7.16) and is

$$\varphi_1 = -\tan^{-1}[\omega C_{ds}(kT/qi_{c1} + R_1)] \tag{7.17}$$

We now look at the circuitry around the reference photodiode. The npn transistor pair is modeled as two resistors in parallel. The equivalent resistance seen by the reference photodiode is given by

$$R_{eq} = R_{e2}||R_{e3} + R_2 = \frac{R_{e2}R_{e3}}{R_{e2} + R_{e3}} + R_2 = \frac{(kT/q)^2/(i_{c2}i_{c3})}{kT/qi_{c2} + kT/qi_{c3}} + R_2 = \frac{kT}{q(i_{c2} + i_{c3})} + R_2 \tag{7.18}$$

The reference photocurrent going into the common emitter junction is

$$i_{ej} = \frac{i_{pdr}}{j\omega R_{eq} C_{dr} + 1} = \frac{i_{pdr}}{j\omega[\frac{kT}{q(i_{c2}+i_{c3})} + R_2]C_{dr} + 1} \tag{7.19}$$

and the rest takes the way through the shunt capacitance C_{dr}. The current going into the collector of transistor Q3 is given by the current division. Putting equation (7.18) into (7.19) and use current division between Q3 and Q2 yields:

$$i_r = i_{c3} = \frac{i_{ej}R_{e2}}{R_{e2} + R_{e3}} = \frac{i_{pdr}}{j\omega[R_2(1 + i_{c2}/i_{c3}) + R_{e3}]C_{dr} + 1 + i_{c2}/i_{c3}} \tag{7.20}$$

Notice that $R_{e3}/R_{e2} = i_{c2}/i_{c3}$. In the case of $i_{pdr} \approx i_{pds}$ Q2 is off and $i_{c2}/i_{c3} = 0$ and we have symmetry if $R_2 = 10\Omega$. i_s and i_r are signal current and reference current respectively. The phase shift in the current into the collector of transistor Q3 is found by taking the phase of equation (7.20) or equation (7.19) and is given by

$$\varphi_2 = -\tan\{\omega C_{dr}\frac{[R_2(1 + i_{c2}/i_{c3}) + kT/qi_{c3}]}{1 + i_{c2}/i_{c3}}\} = -\tan[\omega C_{dr}(\frac{kT}{qi_{pdr}} + R_2)] \tag{7.21}$$

The phase shift is therefor a function of the reference photocurrent. This phase is only a function of the reference photocurrent and is independent of the signal current. It is important to notice this result. If we adjust R_2 such that maximum cancellation is achieved at the dc level the cancellation is not maximum at the current ramp since the signal photocurrent and the reference photocurrent change. In our scheme the relative photocurrent change is $i_{ramp}/i_{dc} = 31.6mA/52.3mA = 0.6$ (laser injection currents). We could chose the maximum cancellation point where the absorption line peak appears, but when the signal beam is attenuated due to loss or scattering the optimum cancellation point shifts to an another point. φ_1 and φ_2 are the phase shifts of the signal current and the reference current respectively. If we have symmetry these quantities are identical thus no phase error. The phase shift difference is zero only when Q2 is off and $R_2 = 10\Omega$. The relative change due to a capacitor mismatch ($C_{dr} \neq C_{ds}$) also contributes to this phase error and limits the cancellation. Cancellation strength also vary with frequencies. It is important to notice that adjusting R_2 can compensate for the mismatch in C_{dr} and C_{ds}. Unfortunately, the relative phase shift changes with reference and signal current amplitudes. Figure 7.22 and 7.23 show a graphical illustration of these effect.

In the first measurements the signal current $i_s = 1.5mA$. The phase is $\varphi_1 \approx -0.18°$ according to equation (7.17) with $C_{ds} = 200pF$ (5V reversed biased) and $\omega = 2\pi \times 93.75kHz$. The reference current is $i_{pdr} \approx 2i_{pds}$. In the first version of the noise canceller circuit R_2 was not implemented. Hence, $R_2 = 0$ and the reference signal phase shift is $-0.056°$ according to equation (7.21). The phase difference is therefor $|\varphi_1 - \varphi_2| = 0.18 - 0.056 = 0.124°$. Using equation (7.15) the output amplitude is $\Delta V_{out} = \Delta i \times R_f = (2.16i_s \times 10^{-3}) \times R_f$. The theoretical cancellation strength is 447×. That means the 800mV intensity modulation signal would become 1.68mV at the output. However, the observed output is much more (22mV). It turned out that the optical effects limit the cancellation. The two unmatched coax cables also contribute to a difference in the effective capacitance difference, which in turn affects the relative phase shift.

To eliminate all sources of errors we remove the coax cables used to transmit the photocurrents, R_2 is implemented as a 10Ω resistor and a 100Ω potensiometer in series. R_2 is in series with the reference photodiode for phase adjustment (R_2 adjustable from 10Ω to 110Ω). The optical path difference is small (0.5m in air causes 0.06° at f=93.75kHz). The transistors are 2N3904(npn) and 2N3906(pnp) with beta close to 70 at the collector currents of interest (1mA-10mA). The reference beam is directly focused on the photodiode from the fiber end. The fiber end is $L = 1.27mm$ from the photodiode active surface and the mode field diameter (ω_0) from the single mode fiber end is approximately $9\mu m$. The spot size onto the active area is given by diffraction when the light exits the fiber end. The spot diameter[40] is approximately $d = \frac{4\lambda L}{\pi\omega_0} = 270\mu m$ which is much smaller than the active region of the photodiode (2mm). This also eliminates the problem of strange responses near the photodiode edges where the response is not linear. Two configurations are tested with respect to the focusing of the signal beam. One is to directly focus the beam from the fiber

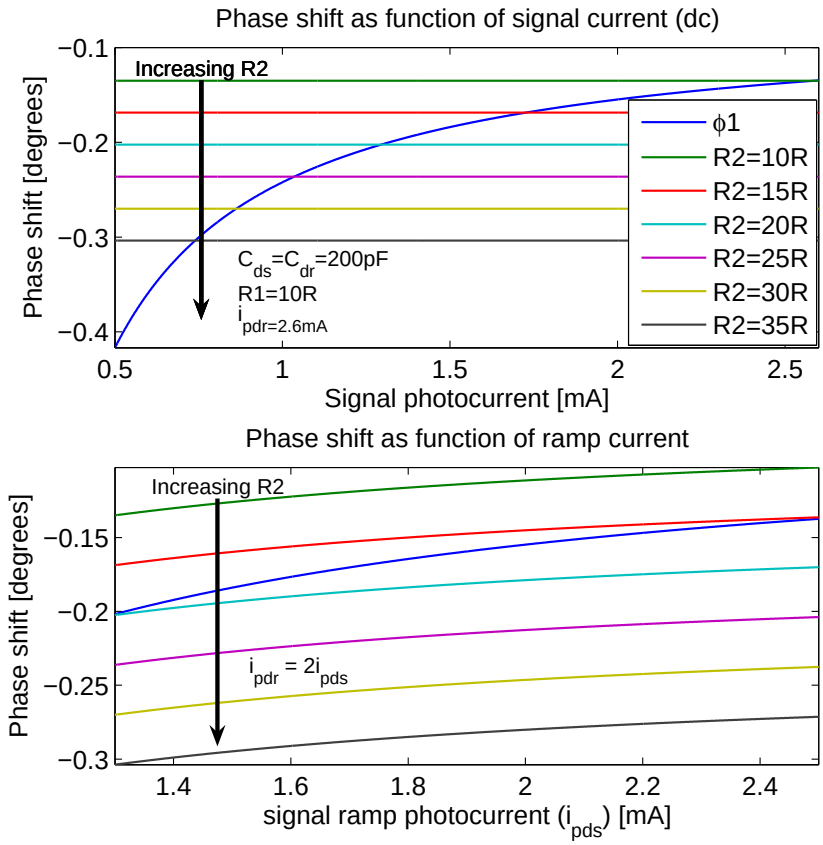

Figure 7.22: Blue plot shows φ_1 and all other plots show φ_2. Top: Phase shifts φ_1 and φ_2 as function of signal photocurrent when the reference photocurrent is fixed at 2.6mA. Bottom: Assuming $i_{pdr} = 2i_{pds}$ during the entire ramp scan which starts at $i_{pds} = 1.3mA$ and ends at $i_{pds} = 2.5mA$. Best cancellation is achieved with $15\Omega < R_2 < 20\Omega$

onto the signal photodiode to achieve similar response as for the reference beam. The other configuration focuses the beam onto the signal photodiode using a 10cm focal length lens (standard receiver unit used in ammonia instruments). Careful alignment was necessary to focused the d=1.6cm signal beam onto the signal photodiode.

When using the standard receiver unit the base voltage of transistor Q3 is -2mV. Hence, the dc reference current is approximately $i_{pdr} \approx 2.08 i_s = 2.6mA$ ($i_s = 880mV/680\Omega \approx 1.3mA$)). The power loss is because of beam spill off at the collimation lens and 8% loss at each optical windows (one lens and one glass window). The ramp is turned off to avoid etalon effects to limit the amplitude balance. $R_{e3} \approx R_{e2} \approx R_{e1} = kT/qi_{c1} \approx 19.3\Omega$. The intensity modulation signal at the output of the noise canceller is measured to approximately 1mV (412mV without cancellation). The real cancellation strength is therefor 412× or 52dB. According to equation (7.17) the signal current phase shift is 0.2° and according to equation

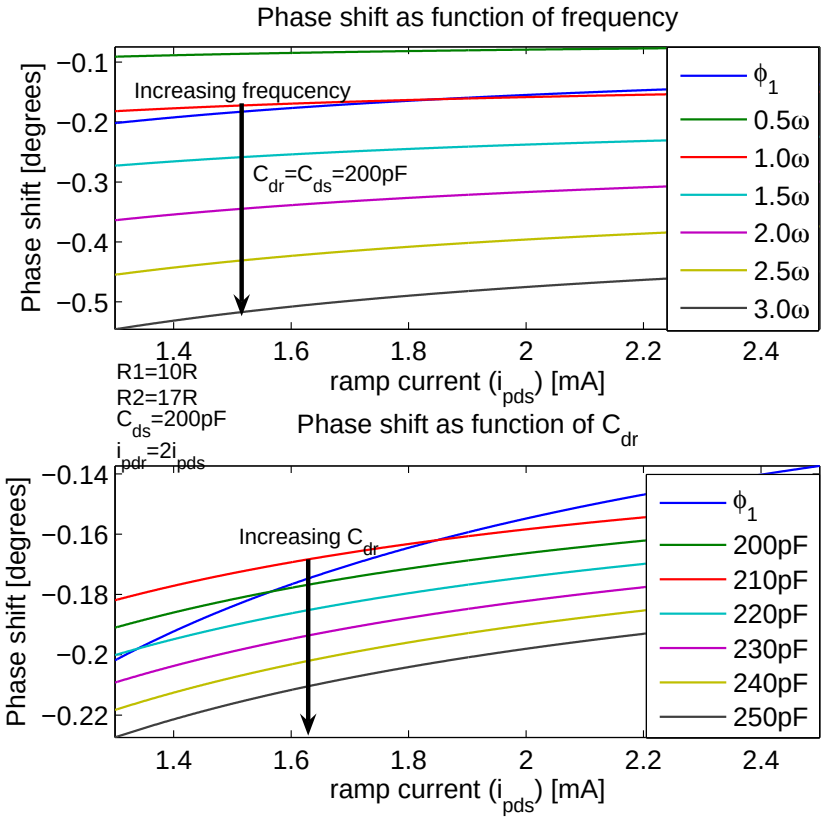

Figure 7.23: Blue plot shows φ_1 and all other plots show φ_2. Top: Phase shifts φ_1 and φ_2 as function of signal photocurrent. Bottom: Phase shift due to mismatch between C_{dr} and C_{ds}. All plots assumed $C_{ds} = 200pF$.

(7.21) the reference current phase shift is 0.13°. A theoretical output is therefor $412mV \times 2\sin(\Delta\varphi = 0.035°\pi/180) \approx 0.5mV$. Hence, the theoretical cancellation strength is 819× or 58dB. The actual output is very close to this value, even not countering for the capacitance mismatch. Experimentally the intensity modulation signal is gone ($< 100\mu V$ yields a cancellation strength of more than 72dB) if R_2 is adjusted to approximately 25Ω. When $R_2 = 25\Omega$ the reference current phase shift is changed to $\varphi_2 = 0.23°$ and the relative phase shift becomes smaller, 0.03°. Assuming no optical effects, perfect amplitude balance and signal/reference photodiode load resistance symmetry the remaining $\Delta\varphi$ is caused by the shunt capacitance mismatch of $C_{dr} - C_{ds} \approx 30pF$ (encountered for all parasite capacitance in the wires). By adjusting R_2 somewhat larger than R_1 compensates for the shunt capacitance mismatch. For a random pair of InGaAs photodiodes from Fermionics the capacitance mismatch is $C_1 - C_2 = 627pF - 588pF = 39pF$ at zero reverse bias voltage (test results are provided by Fermionics' datasheet). As noted earlier the phase mismatch changes with signal and reference photocurrents.

In the other configuration the signal beam is directly focused on the signal photodetector from the fiber end. Now the potensiometer must be adjusted to zero for maximum signal cancellation. The signal photocurrent and the reference photocurrent are almost equal in magnitude in this setup. Hence, Q2 is off and $i_{c2}/i_{c3\to 0}$. The intensity modulation signal amplitude at the noise canceller output is now $0.8\mu V$ (initially 780mV), 60dB cancellation. The best 2f noise results were achieved with this configuration since we no longer have troublesome etalon fringing in the signal path.

Other effects were also observed. When using with the receiver unit different cancellation strengths were observed as different parts of the beam were blocked. We believe this effect is caused by non-uniform distribution of the signal information in the signal beam and the spatial non-uniform response of the InGaAs PIN photodiodes. If the signal beam is not tightly focused on the signal photodiode these effects becomes more pronounced since the spot size fills more of the active area, enhancing the spatial non-uniform effects. Real transistors does not follow Ebers-Moll model exactly. The small signal current gain $h_{fe} = \frac{\partial i_c}{\partial i_b}$ and the large signal current gain $h_{FE} = \frac{i_c}{i_b}$ are not equal. In real transistors the current gain is a function of the collector current. The 2N3904 used in the prototype has 140% change in the i_c/i_b curve over a collector current range from 0.1mA-10mA (not optimum component choice!). The dc and the ac signals split differently and we have amplitude error in the ac signal even though the dc level is exactly zero. The relative amplitude is given by[23]

$$\frac{\Delta i}{i_s} = \frac{1}{h_{FE}} \times |1 - \frac{h_{FE}}{h_{fe}}| \tag{7.22}$$

Transistors with large current gain and which is not strong functions of collector current are best devices. Additionally the negative feedback caused by the emitter bulk resistance also contributes to amplitude errors due to splitting errors in the npn transistor pair. The feedback depends on ΔV_{BE} and on collector currents of Q2 and Q3, so their transconductances are no longer proportional to their collector currents. This causes the ac to split differently than the dc. The effect of this is an additional voltages across the emitter bulk resistances that appear in series with the base-emitter voltages. A modification to the Ebers-Moll equation include this effect.

$$\frac{i_{c3}}{i_{c2}} = \exp(\frac{qV_{BQ3}}{kT}) \exp[\frac{q(i_{c2}r_{E2} - i_{c3}r_{E3})}{kT}] \tag{7.23}$$

Hobbs showed that the limit is[23]

$$\frac{\Delta i}{i_s} = \frac{q}{kT} \frac{i_{pdr} - i_{pds}}{i_{pds}} \times [r_{E2}(i_{pdr} - i_{pds}) - i_{pds}r_{E3}] \tag{7.24}$$

Notice that the emitter bulk resistance is not the emitter resistance, i.e. $r_E \neq R_e = kT/qi_c$. The $r_E \approx 0.3 - 1\Omega$ for small signal transistors (MAT02F has $r_E = 0.3\Omega$, 2N4904 has $r_E = 0.9\Omega$, 2N3906 has $r_E = 1\Omega$). The base spreading resistance has Johnson noise amplitude of approximately $1nV/\sqrt{Hz}$ ($r'_b \approx$ 40-100Ω) on each base and limits the signal-to-noise ratio to approximately $2kT/\sqrt{2}q \approx 3.5 \times 10^7$ (151dB)[24].

In absorbance unit this is equal to 0.29×10^{-8} with 1Hz noise bandwidth. Several transistors can be connected in parallel to reduce the base Johnson noise. Most of the results in this thesis are achieved with the basic noise canceller, i.e. $R_2 = 0$.

7.10.1 Linear and log outputs

The log output (servo amplifier output) provides a output voltage given by

$$V_{log} = \frac{R_1 + R_2}{R_2} \times \frac{kT}{q} \ln(\frac{i_{pdr}}{i_{pds}} - 1) \approx \ln(\frac{i_{pdr}}{i_{pds}} - 1) \tag{7.25}$$

where i_{pdr} is the reference photocurrent and i_{pds} is the signal photocurrent. R_1 and R_2 are shown in the schematic diagram of the noise canceller (figure 5.7). The log output shown in figure 7.24 shows the linear output with and the log output with a feedback time constant of $RC = 0.47\mu F \times 1k\Omega = 4.7 \times 10^{-4}s$. It was experimentally observed that when turning off the modulation signal the shape of the log output signal becomes more like the absorption line profile. The log output shown in the figure is smeared out because of the modulation signal. The bottom graphs show the lock-in-amplifier output (mixer) with two different feedback time constants. Blue: $\tau = 4.7 \times 10^{-4}s$ and red: $\tau = 0.33ms$.

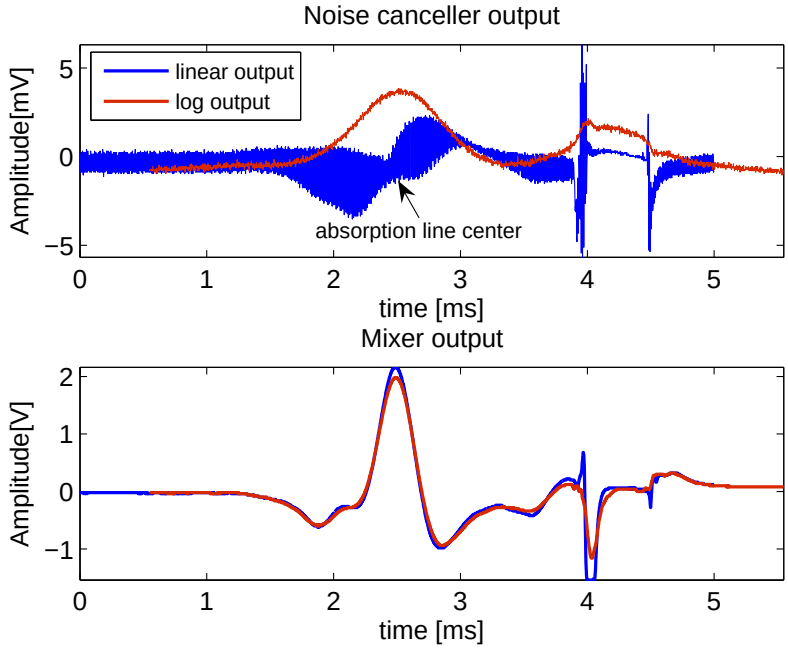

Figure 7.24: Top: Blue curve shows the standard linear output. Red curve are acquired from the servo amplifier output. The servo amplifier feedback capacitor is $0.47\mu F$. Hence, the time constant of the feedback loop is $RC = 4.7 \times 10^{-4}s$. Bottom: the lock-in-amplifier output (mixer) with two different feedback time constants. Blue: $\tau = 4.7 \times 10^{-4}s$ and red: $\tau = 0.33ms$

7.10.2 Information signals in wavelength modulation spectroscopy

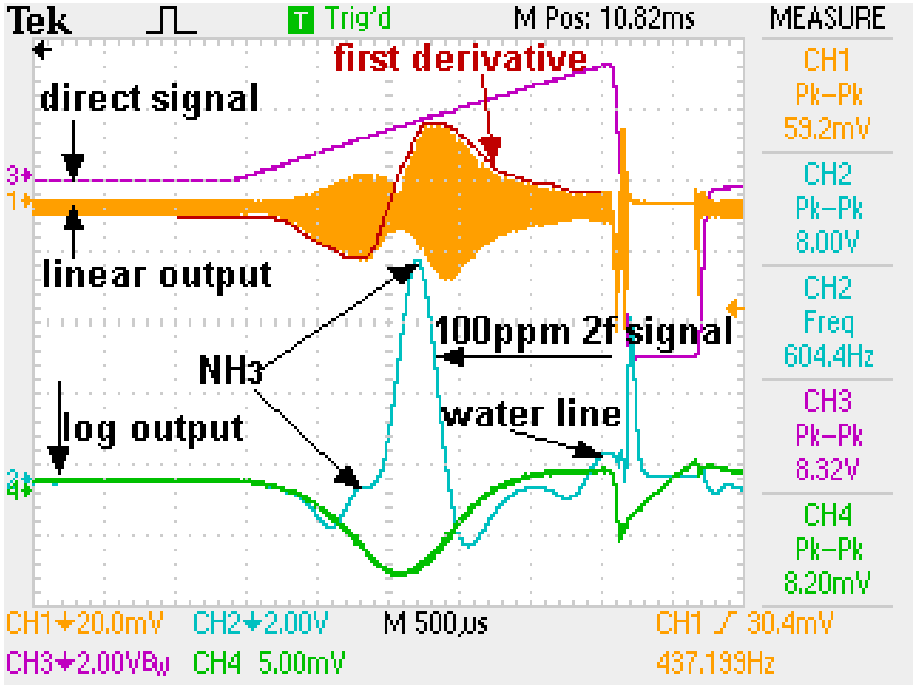

Figure 7.25: Screen capture of four signals. The first derivative ($\frac{\partial\alpha(\lambda)}{\partial\lambda}$) is drawn in to illustrate the dominating signal at the linear output. This signal is generated in the signal path and is not common. Rf=5.1k and Cf=33pF. With such large feedback resistor the instrument will not operate with single beam. This is because the 1.3mA dc signal photocurrent current will become 6.63V and saturate the output which can stand maximum $3V_{pp}$ because of $\pm 5V$ voltage supplies.

When using single beam and second harmonic detection the intensity modulation signal dominates the mixer input signal as shown in the blue graph in figure 7.14 (top). Figure 7.25 shows four signals from four outputs. Figure 7.26(a) shows the noise canceller output and the mixer output when the signal photodetector was carefully aligned for maximum intensity modulation suppression. An acquisition time of 12.5ms (one scan) was used to record the signals above. Figure 7.26(b) shows the the noise canceller output and the mixer output when scanning the same absorption line. This time we record only a small portion of the ramp scan near the absorption line center. At the noise canceller output in the top figure we can see the envelope of the second harmonic signal. In the bottom figure we see little contribution from the 1f oscillations and large contribution of the 2f oscillations near the absorption line center (ideally the 1f signal is zero at the line center).

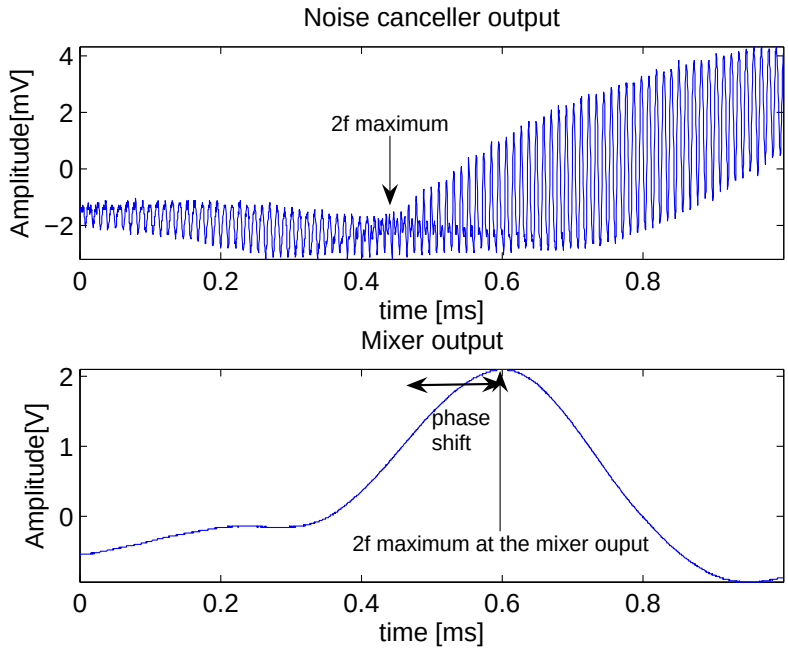

(a)

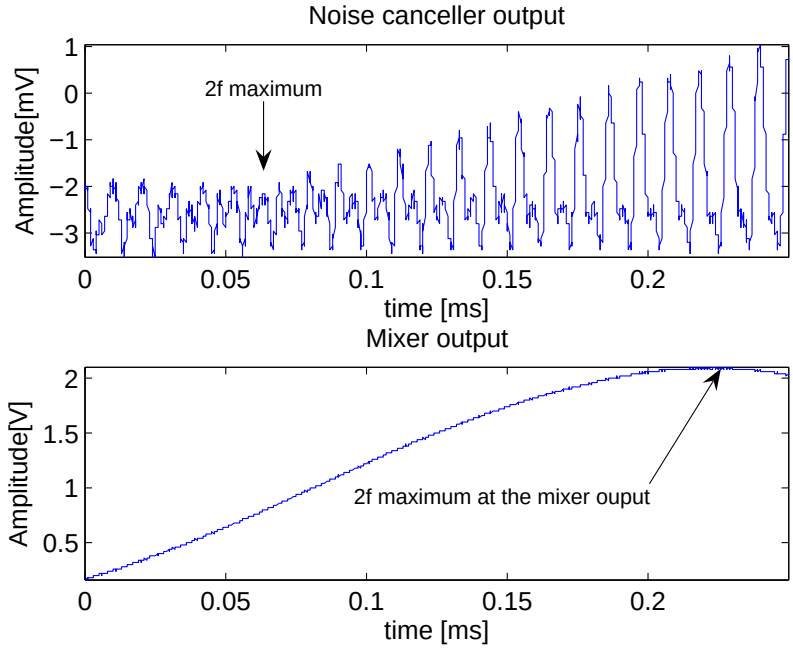

(b)

Figure 7.26: a) A small portion of the ramp scan. Top graph shows the noise canceller output and bottom graph shows the mixer output. b) The noise canceller output and the mixer output near the absorption line center. Notice a phase shift cause by the mixer and post amplifier stages on the 2f signal (top graph). The acquisition time is 0.8ms (averaging of 64 scans.)

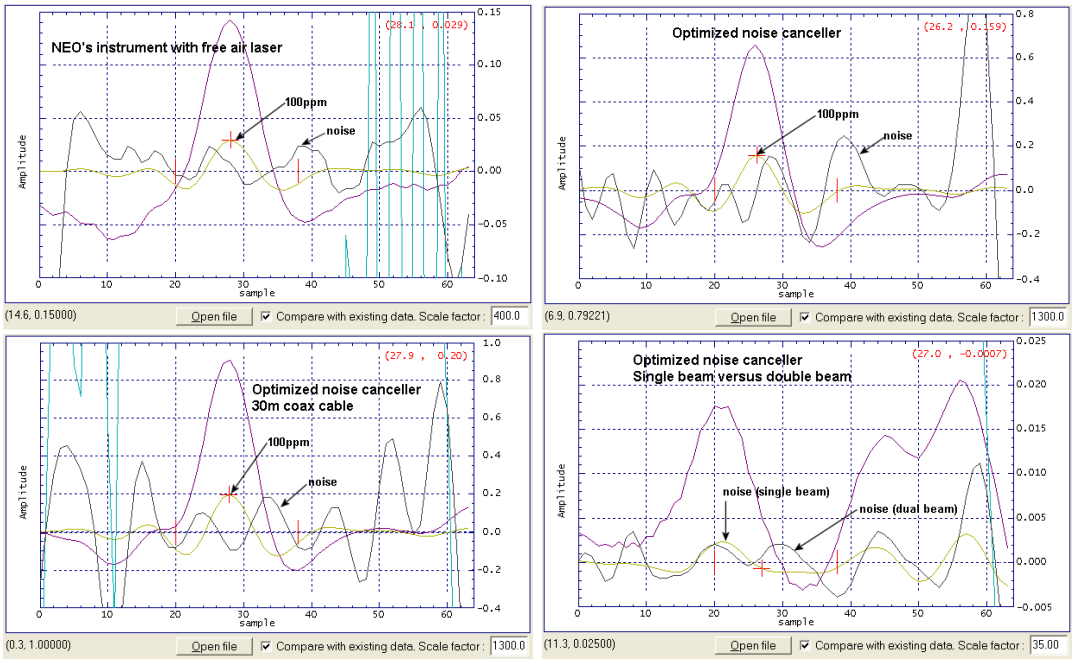

Figure 7.27: Three measurements with the optimized version of the noise canceller. These results are compared with the existing instrument from which uses free air laser and single beam detection. The sensitivity is now more than 2× better than the standard instrument. The double beam signal to noise ratio is improved by more than 15dB compared to the single beam which has much etalon noise coming from the fiber coupling inside the laser module.

7.10.3 Signal to noise ratio with the optimized noise canceller

The noise optimized version of the noise canceller can suppress the intensity modulation signal by more 60-70dB. It is therefore interesting to test it with second harmonic detection. Figure 7.27 shows four measurements for comparison. The sensitivity of the standard instrument is approximately 0.2ppm (SNR=500). The optimized noise canceller achieves a sensitivity less than 0.1ppm (SNR>1000). We also separated the preamplifier from the receiver electronics by using 30m coaxial cable. The feedback resistor was increased from 680Ω to 5.1$k\Omega$ to have a strong 2f signal. The mixer gain was set to 33× to reduce noise pickup from the coax cable. Since the feedback resistor is large, the output will saturate if the reference beam is blocked. We achieve approximately the same sensitivity of 0.1ppm or 2×10^{-6} in absorbance unit with ENBW=52.3Hz and 0.712m optical path length. With such sensitivities the etalon noise from the signal beam is the dominating noise. Earlier we improved the signal to noise ratio by a factor of 12× with the noise canceller. Optimizing it improves this factor to $35 - 40\times$. In real applications a cancellation strength of 40dB or more for the 2f signal is typical. However, any noise in the signal path will show up in the 2f signal. To reduce the 2f noise further the optical system must be optimized.

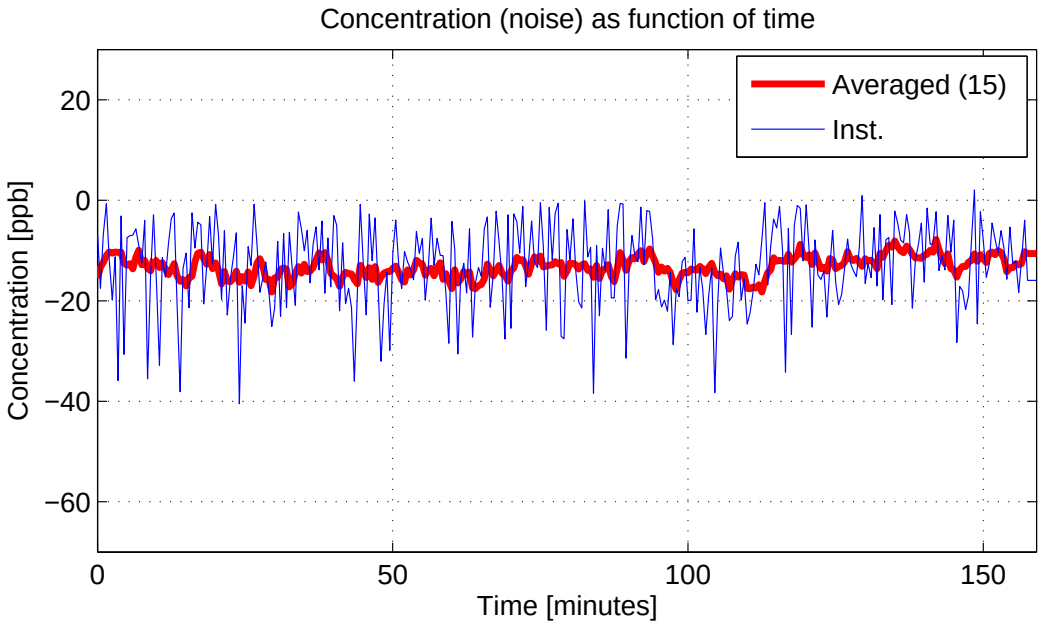

Figure 7.28: The gas cell is removed and the concentration as function of time is plotted. 15 concentrations are averaged to give the red trace. Hence, ENBW=3.5Hz and a sensitivity of 18ppb with 1m optical path length.

7.10.4 Detection limits

We have seen that the relative signal to noise ratio (relative to the 100ppm gas cell) is more than 1000 × . Figure 7.28 shows the noise (in concentration) as function of time over a 160 minutes period. The optical path length is 1m and the effective noise bandwidth is 52.3Hz (256 scans averaging). To reduce the noise bandwidth we average 15 concentration measurements to achieve a noise bandwidth of $52.3Hz/15 = 3.5Hz$. With a relative signal to noise ratio more than 1000× the detection limit is less than $100ppm/(1000 \times \sqrt{15}) = 25.9$ppb. This is in great agreement with the experimental result of 19ppb over almost three hours. This result is surprising and is 8 times lower than the existing limit of NH_3 gas instruments. To verify the result we do an another concentration log several hours later. Figure 7.29 shows a 250 minutes log of the noise as function of time. This result is still very good, 4 times better than the standard instrument (150ppb) which is limited by etalon and laser feedback noise. The reason why our prototype this good is because of the very effective noise canceller circuit that removes much of the common noise such as etalon noise, laser feedback noise and laser diode power supply noise pickup. We believe that our detection sensitivity is limited by the etalon noise between the fiber end and the collimation lens. By tilting it the fast oscillating fringes changes. An AR coated lens would reduce this noise.

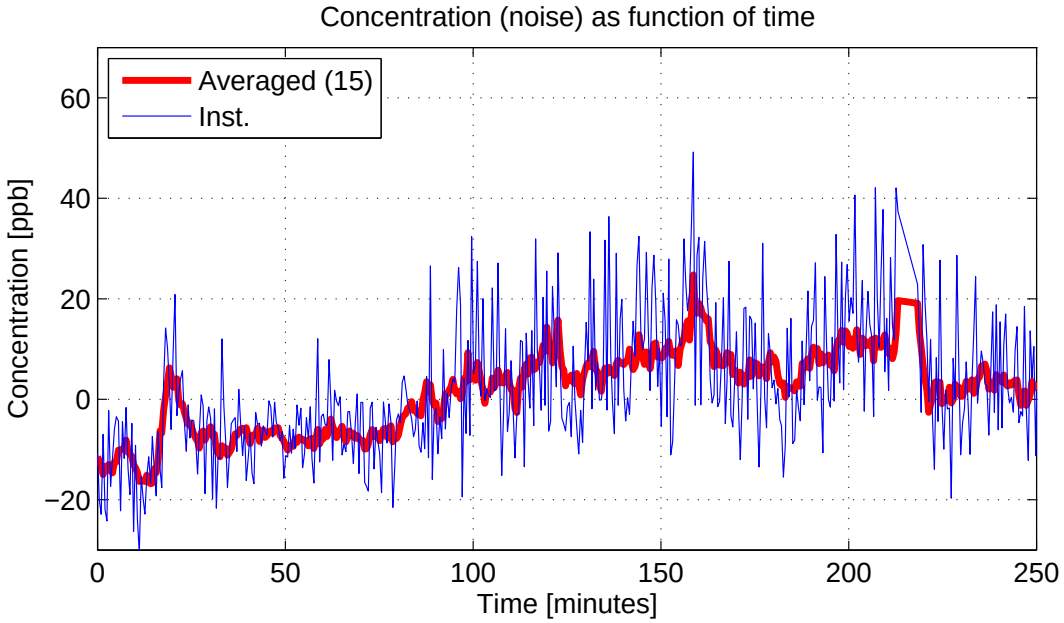

Figure 7.29: ENBW=3.5Hz for the red trace and ENBW=52.3Hz for the blue trace. The detection limit is 40ppb.

7.10.5 Noise during the temperature ramp

With single beam measurement the concentration fluctuation was more than 10ppm during the temperature ramp set by the temperature controller. During the laser case temperature ramp the laser diode temperature(inside the laser module) fluctuates. This temperature fluctuation in turn cause the laser wavelength to fluctuate. With single beam the etalon noise amplitude was about 3-5ppm. These etalon fringes moves accordingly to the laser wavelength. With linear superposition of all 2f signals this caused a 10ppm fluctuation in the concentration.

To really push the noise canceller to the limit we use the temperature ramp to produce common noise. Figure 7.30 shows the concentration and the laser module (case) temperature. The concentration fluctuation is approximately 100ppb. This sensitivity is comparable with the standard instrument with free air lasers. Hence, the noise is suppress approximately 100× compared to the single beam configuration. We observed that the water absorption line position near the end of the ramp scan fluctuates when the case temperature was ramped. This means that the temperature stabilization of the laser diode is not optimal resulting in laser wavelength fluctuation. AR coated lenses to remove etalon noise and better laser diode temperature stabilization will give better sensitivity. Due to the time limit of this thesis these modifications was not tested.

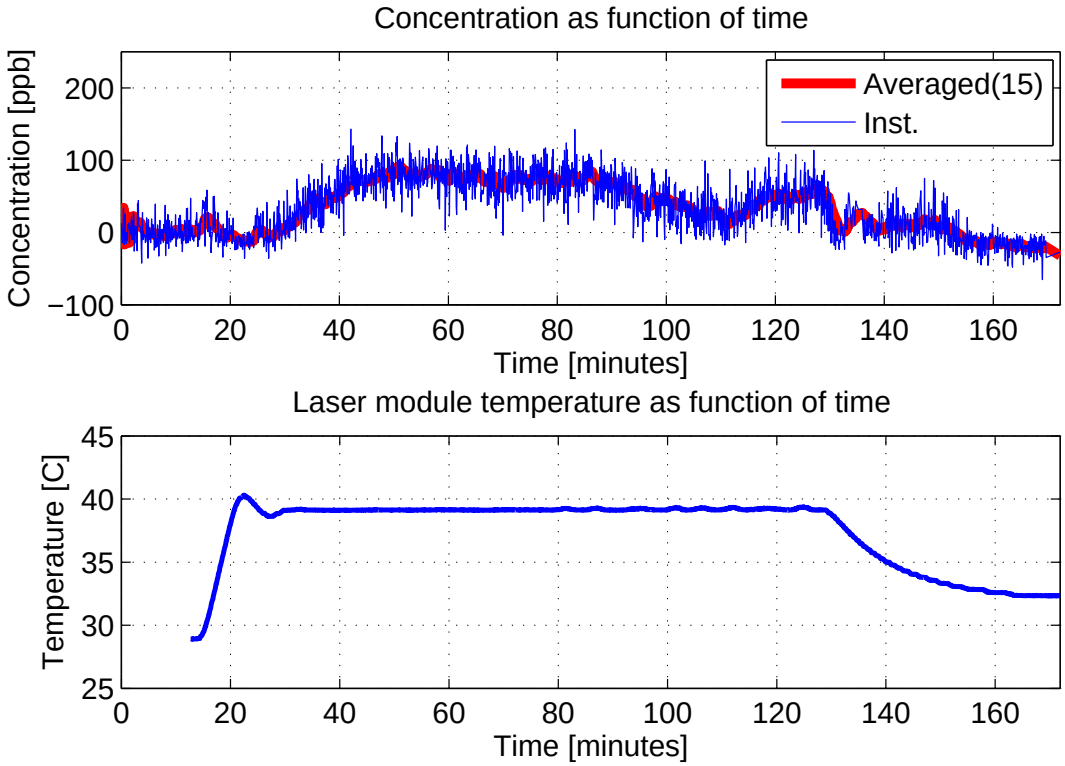

Figure 7.30: The detection limit is 150ppb and is comparable with existing instruments. 1m optical path length and ENBW=52.3Hz for the blue trace and ENBW=3.5Hz for the red trace.

7.11 Harmonic distortions and nonlinear effects

The photodiode linear range is increased in reversed biased mode. With 5V reversed biasing the detector nonlinear effects were not a problem with the beam intensities of interest, less than 20mW. However, nonlinear effects were observed when the light beam hits the edges of the photodiode active region. Offset or strange nonlinear 2f signal shapes were observed. Too large signal beam power can cause three problems: 1) op amp saturation or/and harmonic distortion. 2) too large modulation signal amplitudes into the mixer (max $600 - 700mV_{pp}$) give distortion, even without op amp saturation. 3) photodetector nonlinear response. All three problems must be avoided! Following we demonstrate some effects that can give many hours of troubleshooting.

Figure 7.31 shows the noise canceller output and the mixer output when the current ramp was turned off. The photocurrent was adjusted by defocusing the laser beam (A grey filter should be used, indeed!). By doing this the beam fill more of the active region and enhances the spatial nonlinearity of the photodetector. This effect limits the cancellation strength discussed above. The modulation amplitude is very large ($900mV_{pp}$, red plot) and exceed the linear region of the mixer. Op amp saturation is not met yet, but we see a offset in the 2f signal. Notice that the 2f noise amplitude

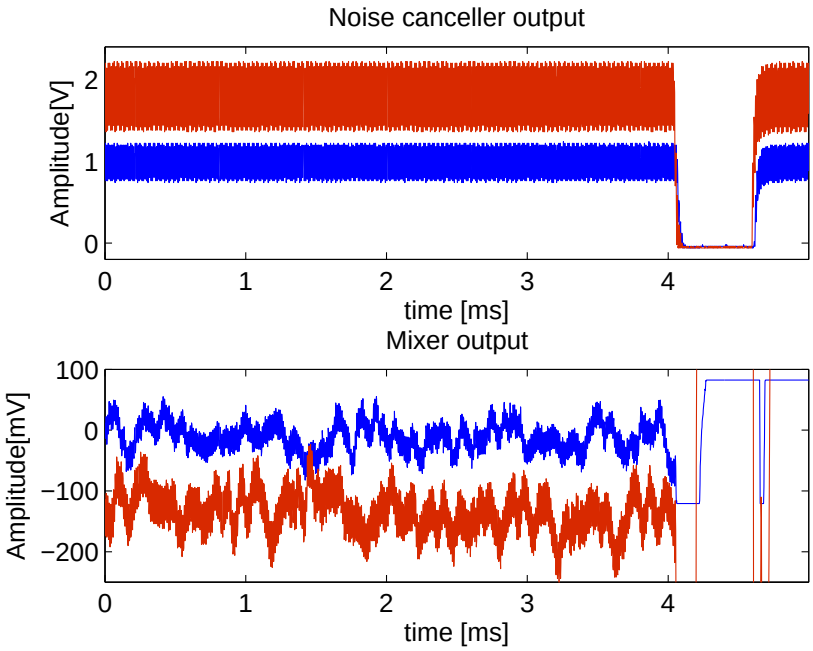

Figure 7.31: Blue graph shows the noise canceller output with a defocused laser beam and the red graph shows a focused laser beam onto the photodetector active area. The current ramp is turned off.

is larger when the photocurrent is increased. The other effect is harmonic distortion when the output voltage approaches the power supply voltage. If the photocurrent and the feedback resistor is too large, the preamplifier output will saturate. Second harmonic distortions are picked out by the mixer and show up in the 2f signal.

Figure 7.32 shows two measurements with the same setup, but this time the current ramp is turned on. At the noise canceller output we can see a saturation voltage of approximately 3.5V at the ramp end. The nonlinear effects dominate the 2f signal at the mixer output. Notice the 2f output saturation at 14V, because of $\pm 15V$ voltage supplies of the 2f signal amplifiers.

7.12 Determining the absorption linewidth

The noise canceller is actually a balance receiver. The linear/log output provides us a direct spectrum signal when the modulation is turned off. If the linear output is used the feedback loop time constant must be increased to not cancel the spectrum signal. If the log output is used the time constant must be decreased to let through the spectrum signal. Our absorption line width is approximately FWHM $\approx 0.19cm^{-1}$ as shown in figure 7.33.

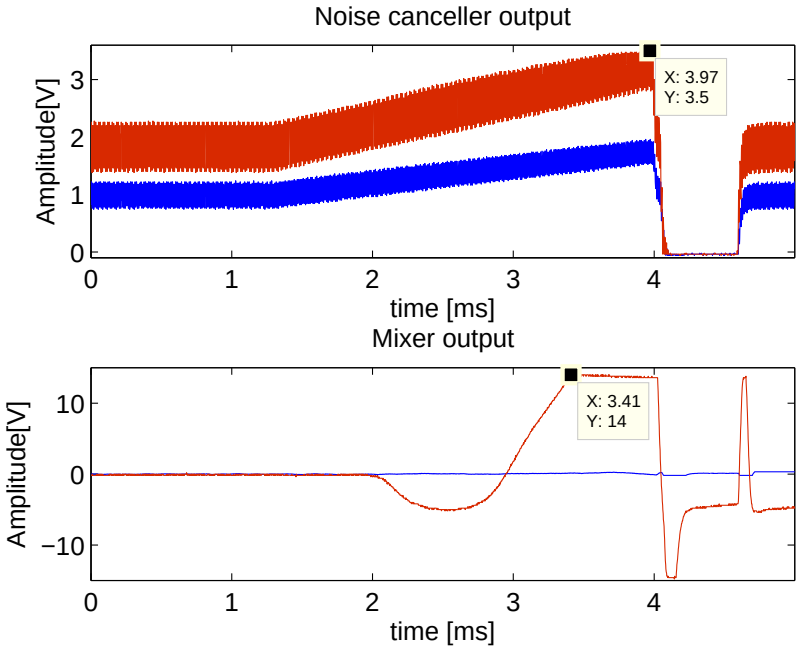

Figure 7.32: Photodetector nonlinear effects. Blue graph shows the noise canceller output with a defocused laser beam and the red graph shows a focused laser beam onto the photodetector active area. Both the modulation and the current ramp is turned on.

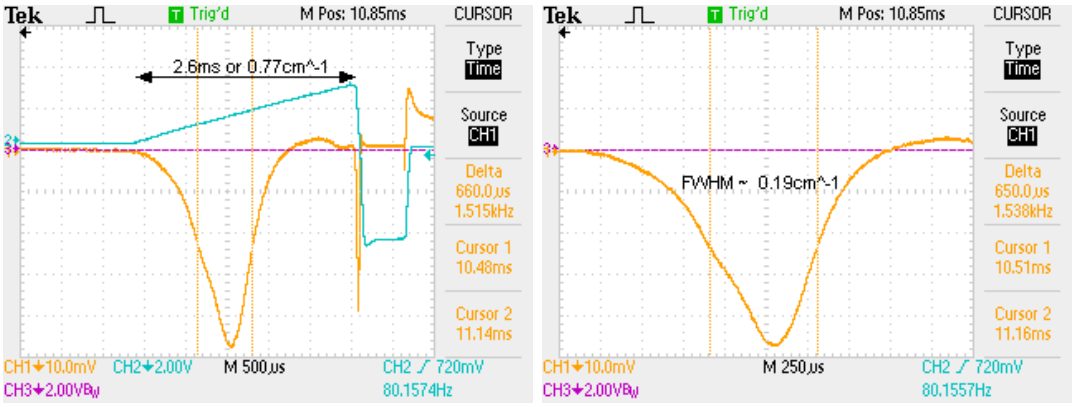

Figure 7.33: Full width at half maximum (FWHM) measurement with the noise canceller linear output. We reduce the feedback loop bandwidth to prevent cancellation of the absorption spectra signal. $\tau = R_{in}C_1 = 15k \times 2.2\mu F = 33ms$.

7.13 Measurements with the voltage subtracter

The voltage subtracter circuit was built first to investigate the noise cancellation possibilities. The working principle and the noise is discussed in section 5. This circuit is simple to build and is more straight forward in the analysis. The advantage with this circuit is that the phase shift does not change with signal photocurrent. However, the the phase error is larger because of two independent op amps and external components. In production component values will vary and small phase error guarantee is not possible. Here the phase control of the current domain subtraction circuit is more attractive. This circuit also has less cancellation bandwidth than current domain subtraction circuit which is limited by the transistor bandwidth, f_T.

To demonstrate the performance of the subtraction circuit the reference beam is blocked with a piece of black paper. The laser feedback noise can easily be seen in the raw signal in figure 7.34. When filtered the signal to noise ratio is approximately 25 times. We believe our electronics is not good as the standard preamplifier on the receiver board. Now when the black piece of paper is removed the common signals in the signal detector and the reference detector are canceled and only second and higher harmonic signals appear at the input to the mixer. With this double beam setup we achieve a signal to noise ratio of approximately 500 times relative to the 2f signal with 100ppm gas cell. This is equal to a detection sensitivity of 0.2ppm NH_3 or $4 \cdot 10^{-6}$ expressed in absorbance unit. This result is comparable with the first version of the current domain subtraction.

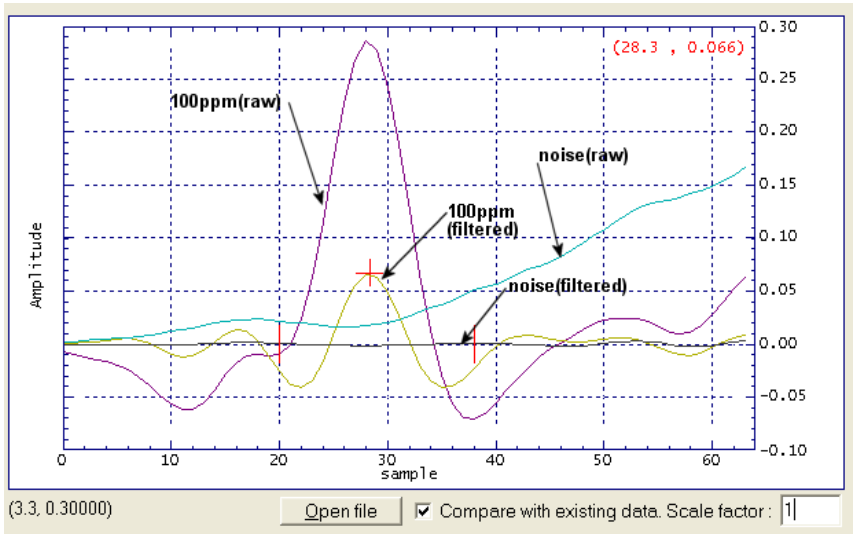

(a)

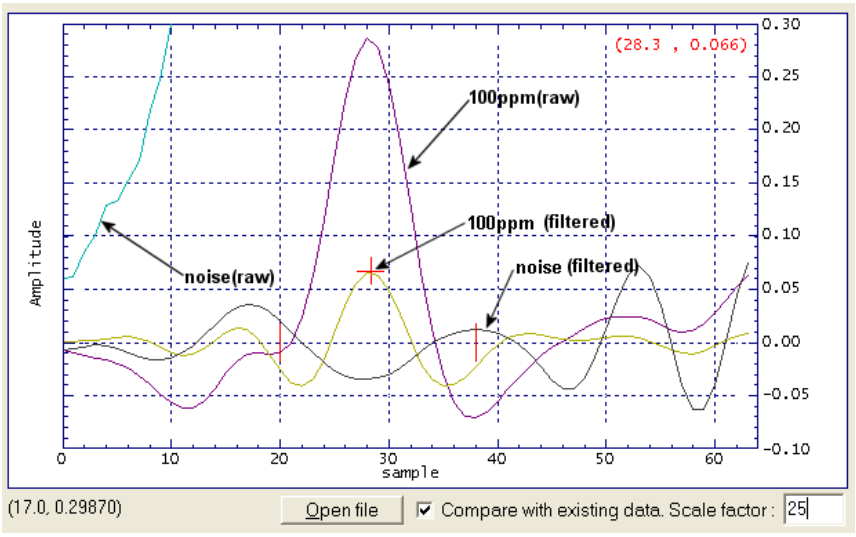

(b)

Figure 7.34: 2f signal with and without the gas cell. Measured with the noise canceler and two detectors. Top) 1:1 comparison. Bottom) Noise is magnified 25 times

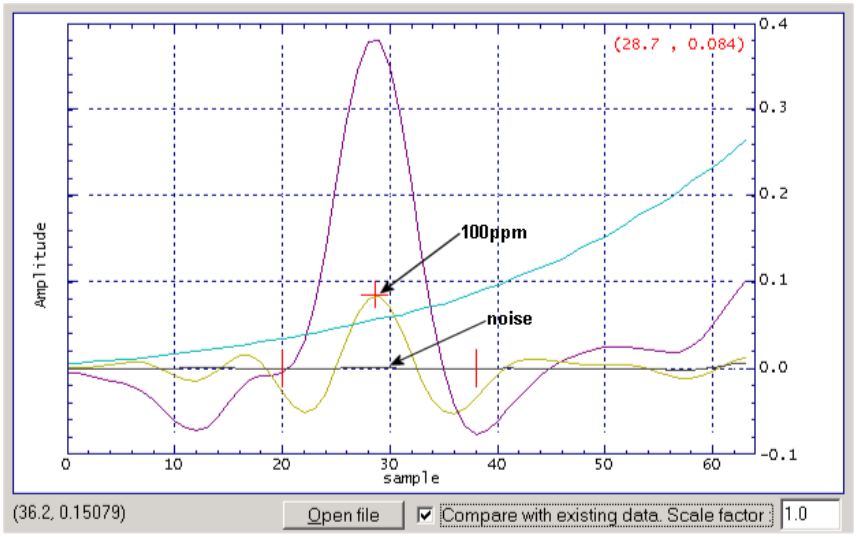

(a)

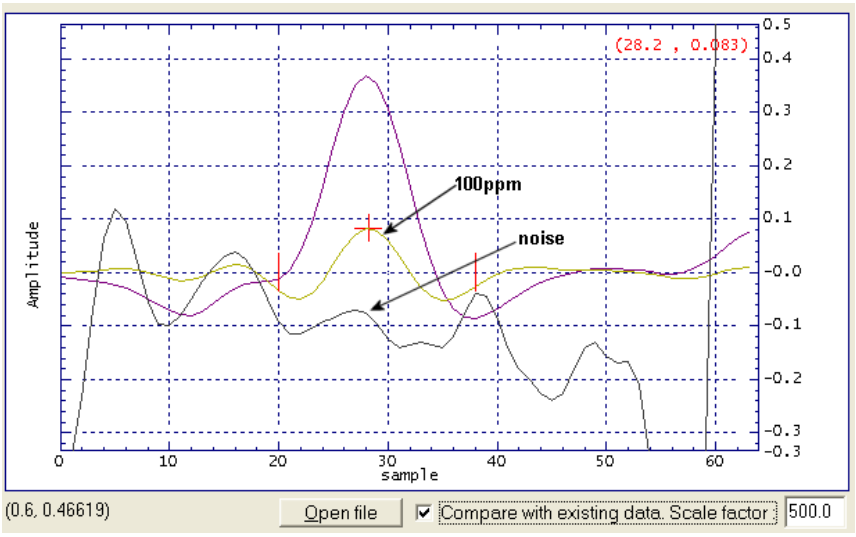

(b)

Figure 7.35: 2f signal with and without the gas cell. Measured with the noise canceler and two detectors. Top) 1:1 comparison. Bottom) Noise is magnified 300 times

7.14 Measurements with 3200m SMF fiber

The most interesting results is to test the noise canceller performance with long length fibers. From last semester we achieved a signal to noise ratio of 8× when 3200m fiber was used. The noise was induced in the fiber length. To overcome this problem we insert the fiber reel between the fiber splitter and the laser output. The light from the laser goes through 3200m of single mode fiber from Cornings. FC/APC connectors and fusion splices are used for minimum back reflections. We splits the laser beam from the single mode fiber into two beams using a 2x2 fiber splitter from Diamond. The reference beam is, again, directly pointed at the reference photodiode without any focus lens for minimum etalon effects. The signal beam is collimated and sent through the gas cell. The optical path difference is approximately 1 meter.

This configuration offers most noise cancellation, but both photodiodes must be placed at the measurement site. The other configuration that is practically more attractive is to split the light before guiding it to the measurement site by fibers. The signal beam is guided by one separate fiber to the measurement path. The reference beam is sent through bare fiber without protection for minimum space requirement. The idea is to place this fiber inside a control box with the reference photodetector. This allows a reference cell to be placed in the optical reference path for difference measurements. This configuration enables us to track the absorption line and adjust the laser temperature to keep the line position constant. This can be a problem with lasers where the wavelength drifts much over time. Laser intensity drift can also be corrected for. Since the reference beam intensity is constant, intensity drift can be monitored and controlled. Noise cancellation is only possible if the noise in the two fiber are identical, otherwise the result can be worse: 3dB up if the noise in the signal fiber and the reference fiber are stochastic.

We test the basic (not optimized yet) current domain noise canceller with 3200m of single mode fiber between the fiber splitter and the laser. Figure **??**a) shows the signal and the noise from a single beam measurement from last semester, using standard components. The fiber noise limits the detection sensitivity to 12.5ppm with ENBW=52.3Hz and 0.712m optical path length. Figure 7.36b) shows a measurement with the double beam prototype. The relative signal to noise ratio is now improved to 180×. Hence, a detection limit of 0.55ppm with 3200m single mode fiber is incredible. We believe the optimized version of the noise canceller will push this limit down to the limit of free air laser instruments.

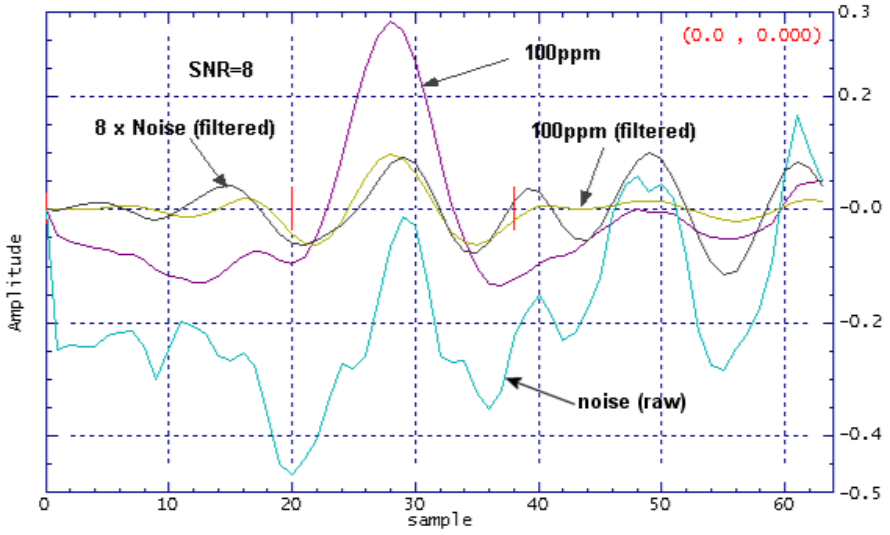

(a)

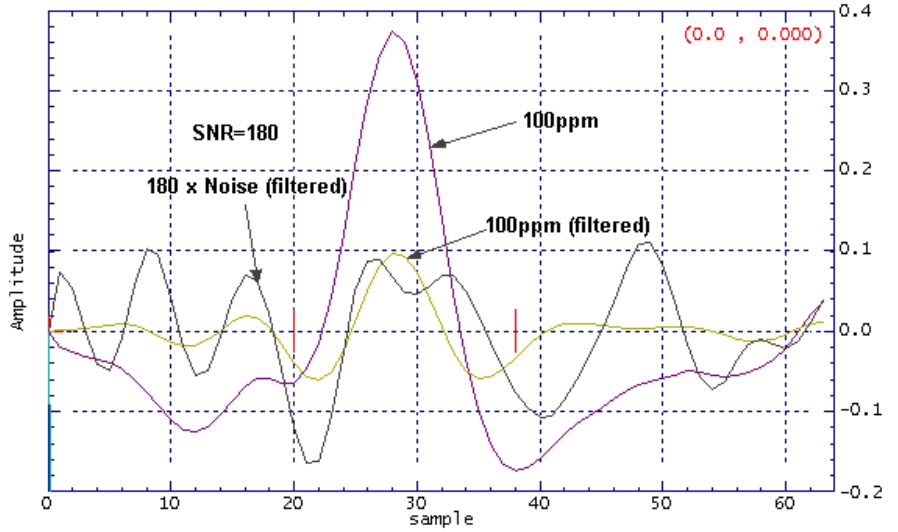

(b)

Figure 7.36: a) single beam measurement with standard components (optics and electronics). b) 3200m SMF between the fiber splitter and the laser. The detection limit is improved to 0.55ppm.

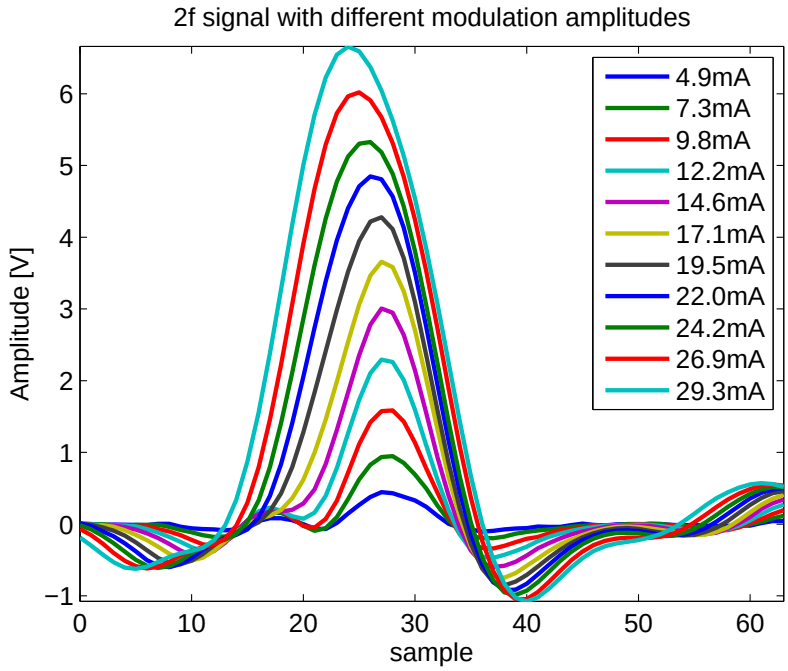

Figure 7.37: 2f signal amplitude versus modulation amplitudes. The plot show the digital 2f signal for several laser injection currents, thus modulation amplitudes.

7.15 Modulation amplitudes and 2f signal shapes

In the standard configuration, i.e. transimpedance mode, the modulation amplitude is limited by the mixer linear range. The maximum modulation amplitude was set by 2.992V in software which corresponds to 14.6mA laser current. With this setting the 93.75kHz modulation signal amplitude was 600mVpp (preamplifier output). The maximum output voltage at the ramp end including the modulation signal was approximately 3V, within the dynamic range of the op amp preamplifier with $\pm 5V$ supply voltages (keeping below around 3V to avoid nonlinear effects).

When using with the noise canceller the ramp is removed and does not limit us to the dynamic range of the op amp (in current the subtraction circuit). The modulation signal amplitude is suppress as well and does not limit us by the linear region of the mixer. The only limitations in this scheme is how much injection current the laser can stand and how much power the photodiode can absorb without generating harmonic distortions . Figure 7.37 shows some 2f signal amplitudes with different laser injection currents, thus difference modulation amplitudes. We can see from the plot that with increasing injection currents the 2f signal amplitudes increase. Theoretically the 2f signal increases with increasing wavelength modulation amplitudes. When the maximum value is reached at $m = 2.2$ and after this the 2f signal amplitude will decrease with increasing modulation amplitudes. The 2f signal kept increasing with

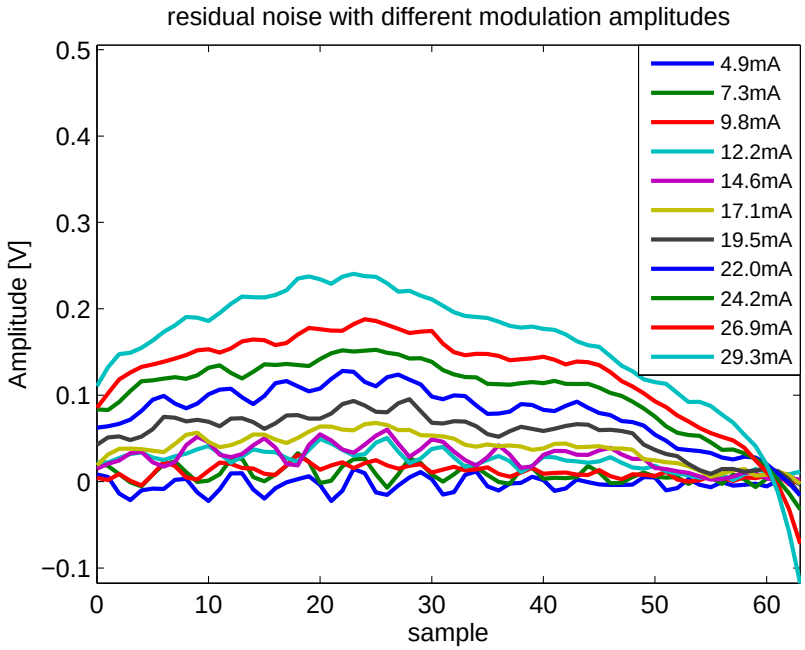

Figure 7.38: The residual noise with the same collection of modulation amplitudes

increased laser modulation currents. The maximum point is not met and indicates that the wavelength modulation index is less than $m_0 = 2.2$.

Figure 7.38 shows the residual noise the for the same modulation amplitudes when the gas cell is removed. For small modulation amplitudes the etalon effects from far spaced optical interfaces dominates. The wide etalon fringe from reference path becomes dominating at higher modulation currents. This agree with our predictions. When we increase the modulation current the small FSRs , due to optical facets far spaced from each other(7.6cm from collimation and 10cm from focusing), is much smaller than the modulation amplitude and their 2f signal are decreased. Unfortunately, the etalon effects from near spaced optical windows dominates.

7.16 Fiber temperature gradients and 2f noise

Under operation in a remote monitoring setup the fiber which is used to guide the laser light from the control station to a remote location will experience temperature gradients. The fiber can go through a location with very high temperature and thus has temperature gradients, i.e. the temperature vary with fiber length. The back-scattered light, which disturbs the coherent light generation inside the laser cavity grows, with increasing refractive index gradients. The fiber core refractive index has a dependence on the fiber temperature. Usually this dependence is weak. Toyoda and Yabe[46] showed that the refractive index dependence is $\frac{dn(\lambda,T)}{dT} \approx 12 \times 10^{-6} K^{-1}$

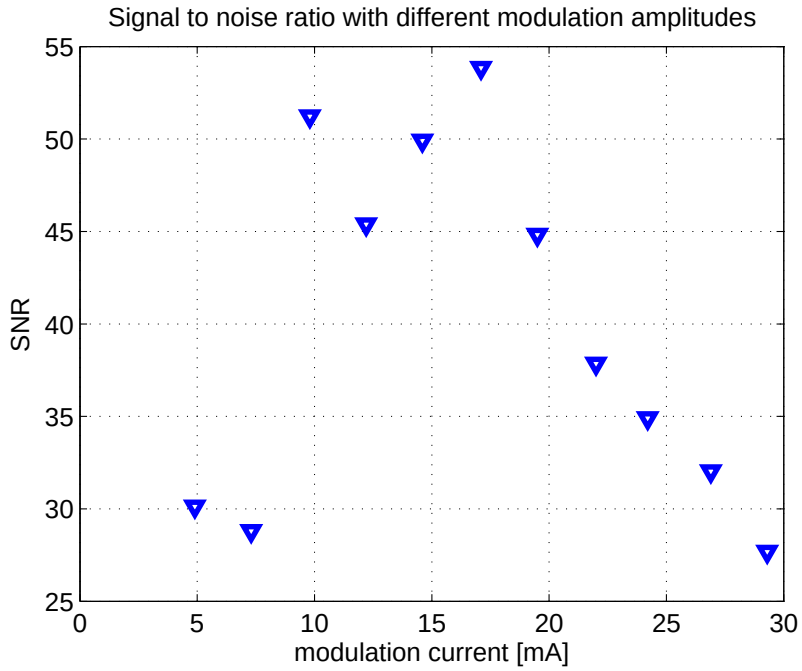

Figure 7.39: The signal to noise ratio with the same set of modulation amplitudes. The values are calculated by taking ratio of the maximum values of the 2f signals and the maximum values of the noise signals.

near $1500nm$. To test the temperature effects on the 2f signal shape we use single beam configuration and 50m single mode fiber. The fiber is connected between the laser and the collimation lens. A small portion of the fiber coil is heated with a air heater. Hence, there is a periodic temperature profile in the fiber length with approximately 50cm between each maxima. This increases the effects of backscattering since we have many temperature gradients in the fiber length. A small portion of light is backscattered near each temperature maxima. The 2f signal before and after heating are recorded for comparison. Figure 7.40 shows a comparison between heated and not heated fiber. Blue and green graph shows the raw noise (ADC value of the 2f signal divide on the ADC value of the direct signal). The two remaining graphs shows the filtered version of 2f noise. The result shows that the noise is much smaller than the etalon effects from the fiber coupling.

7.17 Multiple gas path measurements with one laser

Free air instruments achieve high sensitivity. A complete wms instrument is quite expensive. Traditionally NEO's gas monitors can only measure one gas path with one instrument. With fiber components the laser beam can be split and guided to many measurement paths. Imagine one control box that have all necessary electronics. The laser light from the laser inside this box is split by a fiber splitter and guided to

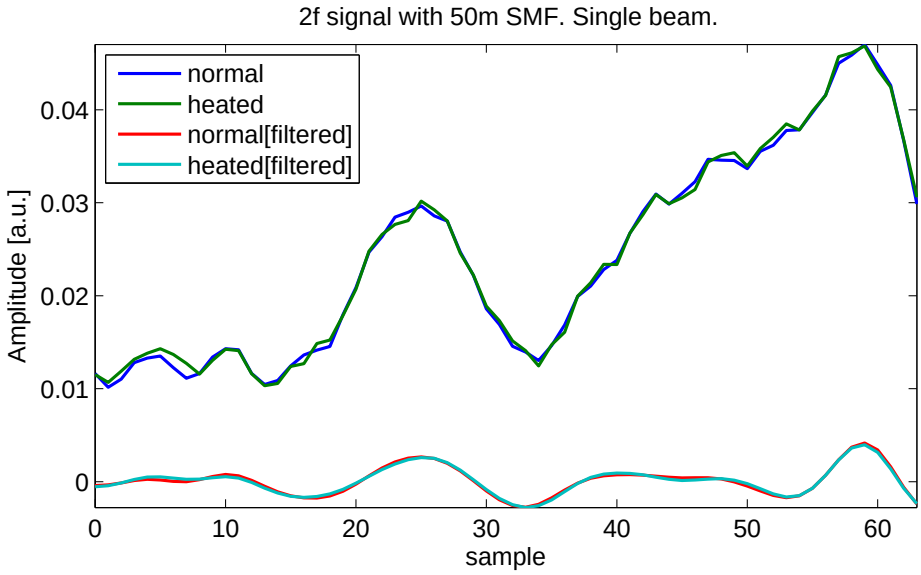

Figure 7.40: 2f noise with 50m of heated and unheated single mode fiber. The fiber coil is heated with a hair dryer.

two pipes spaced far from each other. Each photodetector generates photocurrents and is transferred back to the control box with coaxial cable. Using two independent preamplifiers and lock-in-amplifiers two independent measurements can be done simultaneously.

In this section we demonstrate a measurement of two independent gas paths. We use the same home made gas cell that we used to record the NH_3 spectrum. The light from the laser is split with a 1x4 fiber splitter from Diamond. The power from each output is 25% of the input power. The peak light intensity is approximately 5mW at each output. Channel 1 and 2 is used as the signal and reference beam respectively. The signal beam is sent through a 100ppm gas cell and the reference beam is used to cancel noise. In the second measurement configuration we use the light from channel 3 and use single beam measurement. The receiver unit consisting of a focus lens and a reverse biased photodiode connected to NEO's preamplifier, mixer, etc. The receiver unit is connected to a separate mainboard. A dummy laser is used to bypass the test procedures of the mainboard (it detects the peltier element and the NTC resistor). This board is connected to a RS232 port and a different instance of the LaserGasII software is used to communicate with the mainboard. Preamplifier gain and post-mixer gain are adjusted for sufficient signal amplitudes. Because of coherent detection the local modulation signal used to modulate the laser must be connected to the other mixer. To do this we removed the local oscillator and feed the mixer with the laser modulation signal (187.5kHz square pulses with 50% duty cycle). 50Ω coaxial cable is used for minimum noise. Because of the implementation the mixer input phase can not be controlled independently in software. This phase is implemented as a phase shift to the laser current. Hence a different mixer phase in software will change the

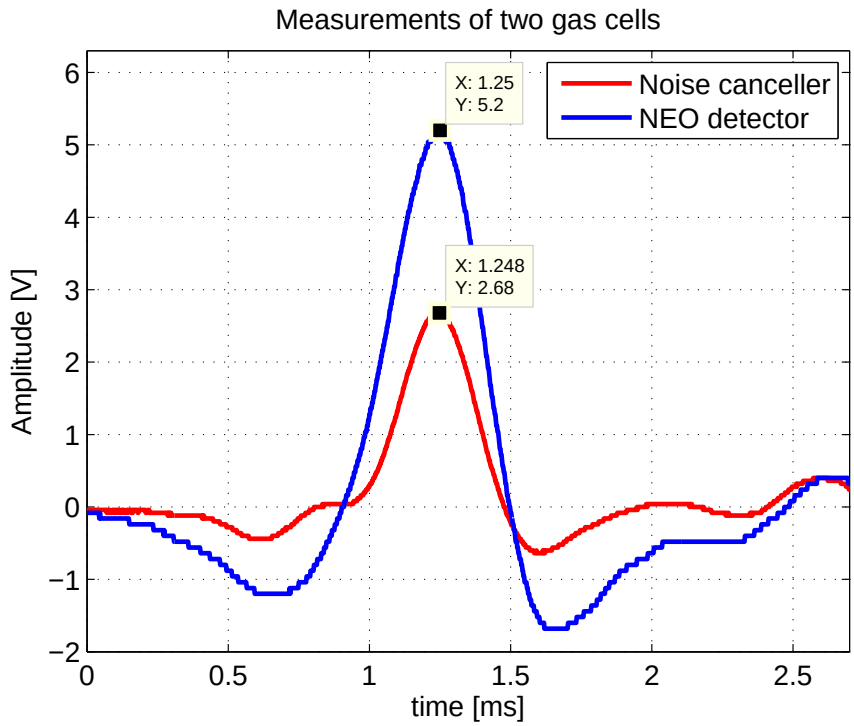

Figure 7.41: Two gas paths are simultaneously and independently measured by using three detectors and a 1x4 fiber splitter. Red curve shows the 2f signal from the 100ppm gas cell. Blue curve shows the 2f signal from the home made gas cell.

laser current phase and will be seen by both detectors. In real applications the fiber lengths to two measurement paths are not necessary the same, and a phase shift in the demodulation will occur. To control the phase independently the fiber length of the channel of interest can be changed.

Figure 7.41 shows a measurement with the prototype. A 50m SMF fiber is used to guide the light from channel 3 of the fiber splitter to the home made gas cell. We use 5cm focal length lens (that was available) and set the beam waist to the middle between the collimator lens and the focus lens. Labview software is used to capture and Matlab is used to plot the 2f signals. All software parameters remain the same. The calibrated 2f signal peak is 2.68V at the absorption line center and corresponds to 100ppm. The other mixer output is 5.6V and corresponds around 200ppm NH_3. The 50m fiber length adds a intensity lag of $\varphi_f \approx 8$ degrees compared to the main beam. The electronics also add a little phase shift due to component variations, but of negligible amount.

8 Conclusions

A prototype of a fiber based wavelength modulation spectroscopy instrument is built and tested on real gases. The DFB fiber pigtailed laser from NEL electronics is quiet at dc injection current, 11.6dB above shot noise near 187.5kHz. The etalon fringing from the fiber coupling inside the laser module limits the instrument sensitivity to approximately 5ppm. Thermal effects caused these etalon fringing to fluctuates and limit the zero point drift to ±5ppm. These effect were identified with the home built temperature controller based on an Atmel AVR microcontroller, ATMega16.

Due to high laser beam intensity the shot noise is much more than the electronic noise. Two noise canceller circuits are designed to cancel common signals in the signal and the reference beam. The voltage domain subtraction circuit achieved a sensitivity of 0.2ppm. After optimizing the current domain subtraction circuit we achieved a record sensitivity of 0.05ppm with 256 scans averaging with an acquisition time of 3.2s (ENBW=52.3Hz). The etalon fringing in the signal beam limits the zero point drift (when measuring no absorption lines) to approximately ±20ppb.

We also demonstrate multiple gaseous path measurement with one single fiber based laser. Two absorption lines with different shapes and absorption strengths are simultaneously measured with two lock-in amplifiers. The remote sensing possibility is tested by separating the balanced preamplifier from the main electronics. 30m coaxial cable is used to carry the second harmonic signal from the preamplifier output to the mixer input. A noise level more than 1000× smaller than the 100ppm line amplitude was achieved with this setup. Hence the sensitivity is 0.10ppm with 3.2s acquisition time.

Fused biconical taper(FBT) couplers from Diamond exhibit very linear response and split the laser light equally with negligible noise. With great repeatability and absence of nonlinear effects, the common noise, such as etalon noise and laser excess noise, was also equally split between the coupler outputs. The residual intensity modulation signal was suppressed more than 70dB and relaxes the mixer requirements.

This project has been very interesting and exciting. The author has learned very much about instrumentation and noise analysis. After long time with hard work we are satisfied with the results presented in this thesis. The results shows that we have achieved a lower detection limit with a noisier laser. This is possible because of the very linearity response of the optical system and effective electronic noise cancellation. We have learned a lot of wavelength modulation spectroscopy and modulation techniques. In the end of this project we came up with an idea to measure the Doppler shift of absorption lines with the wavelength modulation spectroscopy technique. This technique is presented in the appendix F.

9 Outlook and future work

Because of the time limit there is many things that is left out. In the list below we suggest some future work. The intensity modulation signal is suppressed so modulation current can be increased to achieve higher signal to noise ratio. We observed that our system has much high frequency etalon fringing.

- Implement the noise canceller on a print board and use surface mount components
- Test with AR coated collimation lens to reduce the high frequency etalon fringing.
- Test noise cancellation with two separate fibers for the signal beam and reference beam.
- Optimize the preamplifier electronics to achieve lower noise floor and better cancellation.
- Test the instrument in real application under different transmission amplitudes to characterize the performance of the noise canceller electronics.

References

[1] John Andrews and Paul Dallin. "Frequency modulation spectroscopy". *Spectroscopy Europe*.

[2] John Andrews and Paul Dallin. Wavelength modulation spectroscopy. *wwww.spectroscopyeurope.com*.

[3] P.W. Atkins. *Physical Chemistry*. W.H. Freeman and Co., 1978.

[4] L. Bjerkan, K. Johannessen, and X. X. Guo. Measurements of frequency responses of three-section distributed bragg reflector lasers and application to modulation spectroscopy. *Optics and Laser Technology*, 30(6-7):417–423, 1998.

[5] D. E Cooper C. B. Carlisle and H. Prier. "Quantum noise limited FM spectroscopy with a lead salt diode laser". *Applied Optics, Vol.28, 2567-2576*, 1989.

[6] D.T. Casidy and J. Reid. "Atmospheric pressure monitoring of trace gases using tunable diode laser". *Applied Optics*, Vol. 21:1185–1190, 1982.

[7] R. Claps, F. V. Englich, D. P. Leleux, D. Richter, F. K. Tittel, and R. F. Curl. Ammonia detection by use of near-infrared diode-laser-based overtone spectroscopy. *Applied Optics*, 40(24):4387–4394, 2001.

[8] C. Corsi and M. Inguscio. "High sensitivity trace gas mornitoring using semiconductor diode lasers". *Optical Sensors and Microsystems*, 2000.

[9] A. C. Stanton D. S. Bomse and J. A. Silver. "Frequency modulation and wavelength modulation spectroscopies: comparison of experimental methods using a lead salt iode laser". *Applied Optics, Vol.31, 718-731*, 1992.

[10] Dung Do Dang. "Wavelength modulation spectroscopy with single mode fiber". Student project, NTNU - Department of Electrical and Telecommunication, desember 2005.

[11] E. L. Dereniak and G. D. Boreman. *"Infrared Detectors and Systems"*. John Wiley and sons, 1996.

[12] A. N. Dharamsi. "A theory of modulation spectroscopy with applications of higher harmonic detection". *Applied Physics B*, 29, 1996.

[13] L. Dong, W. G. Ma, W. B. Yin, C. Y. Li, and S. T. Jia. Experimental study on harmonic detection of methane by use of a digital lock-in amplifier. *Spectroscopy and Spectral Analysis*, 25(3):473–476, 2005.

[14] R. Engelbrecht. "A compact NIR fiber-optic diode laser spectrometer for CO and CO2: analysis of observed 2f wavelength modulation spectroscopy line shapes". *Spectrochimica Acta Part A*, Vol. 60:3291–3298, 2004.

[15] M. C. Nuss et al. "Amplitude noise reduction of 50dB in colliding-pulse mode-locking dye lasers". *Optics letters*, Vol. 15:1026–1028, 1990.

[16] Ricardo Claps et al. "Ammonia detection by use of near-infrared diode-laser base overtone spectroscopy". *Applied Optics*, Vol. 40, no.24:4387–4394, August 2001.

[17] Jerald Graeme. *PHOTODIODE AMPLIFIERS - op amp solutions*. McGraw-Hill, 1995.

[18] Magnus Haakestad. "Gaussisk tilnærmelse".

[19] Eugene Hecht. *Optics*. Prentice Hall, 2001.

[20] Jeff Hecht. *Introduction to fiber Optics*. Prentice Hall, 2002.

[21] Philip C. D. Hobbs. Reaching shot noise limit for 10. *Optics & Photonic News*, 1991.

[22] Philip C. D. Hobbs. Shot noise limited optical measurements at baseband with noisy lasers. *Proc. SPIE Vol. 1376, p. 216-221*, 1991.

[23] Philip C. D. Hobbs. "Ultra sensitive laser measurements without tears". In *Applied Optics, Vol.36, 903-920*, 1997.

[24] Philip C. D. Hobbs. *Building electro-optical systems : making it all work*. Wiley, New York, 2000.

[25] Philip C.D. Hobbs. Photodiode front ends - the real story. In *Optics & Photonics News*, pages 42–45, april 2001.

[26] P. Kaspersen I. Linnerud and T. Jæger. "Gas mornitoring in the process industry using diode laser spectroscopy". *Applied Physics B*, 67, 1998.

[27] Texas Instruments. *OPA657 datasheet from Texas Instruments (Burr Brown). p.11-12*.

[28] P. Kluczynski and O. Axner. Theoretical description based on fourier analysis of wavelength-modulation spectrometry in terms of analytical and background signals. *Applied Optics*, 38(27):5803–5815, 1999.

[29] Me Koy. "Optoelectronic devices". Nanyang Technological University, 2004.

[30] H. Riris L. G. Wang, D. A. Tate and T. F. Gallagher. "High sensitivity frequency modulation spectroscopy with a GaAlAs diode laser". *J. Opt. Soc. Am. B6, 871-876*, 1989.

[31] Ivar Linnerud. "Noise test with FET input transistor. Internal note.". Technical report, Norsk Elektrooptikk, 2004.

[32] F.S. Pavone M. Gabrysch, C. Corsi and M. Inguscio. "Simultaneous detection of CO and CO2 using a semiconductor DFB diode laser at 1.578 μm". *Applied Physics B*, 65, 1997.

[33] D. Marcuse. Loss analysis of single-mode fiber splices. *The Bell Syst. Tech.J.,*, vol. 56, May-Jun. 1977.

[34] R. T. Menzies. *"Laser heterodyne detection techniques"*. Springer,New York, 1976.

[35] C.D. Motchenbacher and J.A. Connelly. *Low-noise electronic system design*. Wiley, New York, 1993.

[36] John Ngo. "Fundamentals of optical fibers". Nanyang Technological University, 2004.

[37] P. Kluczynski, Jorgen Gustafson, Åsa M. Lindberg, Ove Axner. "Wavelength modulation absorption spectrometry- an extensive scrutiny of the generation of signals". *Soectrochimica Acta Part B 56*.

[38] David M. Pozar. *Microwave and RF wireless systems*. John Wiley and Sons, INC, 2001.

[39] Giogio Rizzoni. *Principle and applications of electrical enginering. 3th edition*. McGraw Hill, 2000.

[40] B.E.A. Saleh and M.C. Teich. *Fundamental of optics*. John Wiley and sons, 1991.

[41] K. Sap. *Optoelectronic devices*. Prentice Hall, 2002.

[42] Stephane Schilt and Luc The´venaz. Wavelength modulation photoacoustic spectroscopy: Theoretical description and experimental results. *Science Direct*, april 2005.

[43] J. A. Silver. Frequency-modulation spectroscopy for trace species detection: theory and comparison among experimental methods. *Applied Optics, Vol.31, 707-717*, 1992.

[44] Luc Thevenaz Stephane Schilt and Philippe Robert. "Wavelength modulation spectroscopy: combined frequency and intensity laser modulation ". *Applied Optics*, Vol. 42, No. 33:6728–6738, November 2003.

[45] Ben G. Streetman and Sanjay Banerjee. *Solid state Electronic devices*. Prentice Hall International, Inc., 2000.

[46] T Toyoda and M Yabe. "The temperature dependence of the refractive indices of fused silica and crystal quartz". *Applied phys.*, 16:97–100, 1983.

[47] Endel Uiga. *Optoelectronics*. Prentice Hall International, Inc., 1995.

[48] J.B. Jeffries X. Zhou and R.K. Hanson. "Developement of a fast temperature sensor for combustion gases using a single tuneable diode laser". *Appl. Phys. B*, 81:711–722, 2005.

[49] Zhi Xu and David W. Larsen. "Development of Ultra-Low-Noise Spectrophotometry for Analytical Applications". *Anal. Chem.*, 77:6463–6468, 2005.

[50] Young and Freedman. *University physics. 10th edition*. McGraw Hill, 2000.

[51] Xiang Zhu and Daniel Cassidy. Electronic subtracter for trace-gas detection with ingaasp diode lasers. *Applied Optics*, Vol. 34, No. 36, 1995.

A

Project description (in Norwegian)

Laserspektroskopi med optiske fibre

Bakgrunn: Norsk Elektro Optikk AS har utviklet en serie gassmålere basert på avstembare diodelasere og enkeltlinjespektroskopi. Disse kan benyttes til måling i piper og kanaler i prossesser samt til måling i industrihaller over lengre avstander (100-500m). NEOs gassmålere har elektronikken samlet i en sender- og en mottaker-modul montert i hver sin ende av den optiske måleløypa. For noen applikasjoner vil det være gunstig med fiberoptisk kobling mellom laser/detektor/elektronikk og optisk måleløype. Dette kan gjelde områder med høye temperaturer eller områder med tilstedeværelse av eksplosive gasser.

Praktisk gjennomføring av oppgaven: Prototypesystemet tenkes laget basert på eksisterende deler fra dagens gassmålere kombinert med egnede optiske og fiberoptiske komponenter. En del av oppgaven vil gå ut på å finne passende optiske komponenter eventuelt med alternativer. Oppgaven vil videre omfatte bygging av et prototypeoppsett som vil bli brukt til målinger på reelle gasser. Resultatene vil bli sammenlignet med dagens gassmålere og vurdert med hensyn på deteksjonsgrense og ulike støybidrag slik som etalonstøy og speckle.

B

The Software

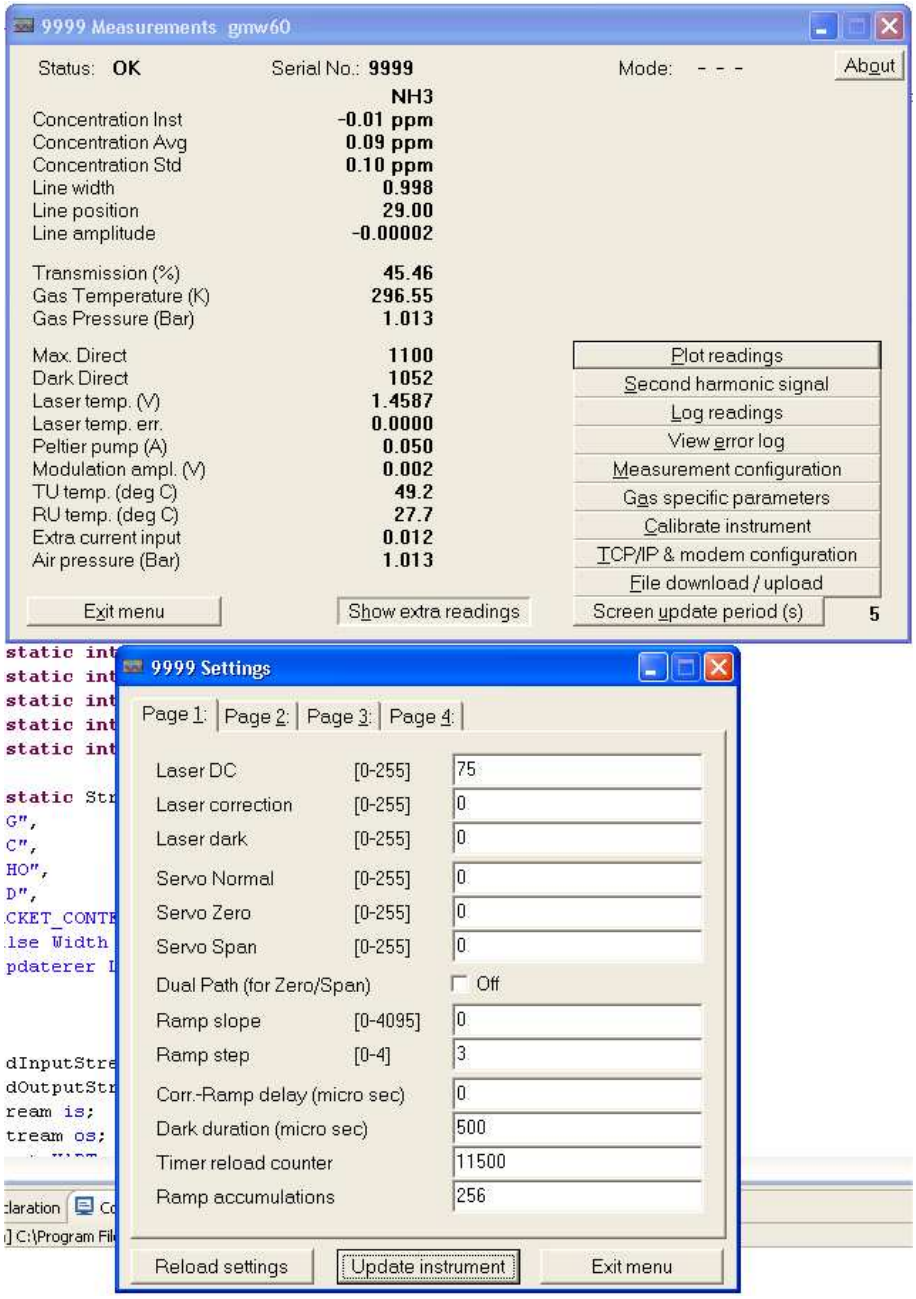

Figure B.1: LaserGasII software

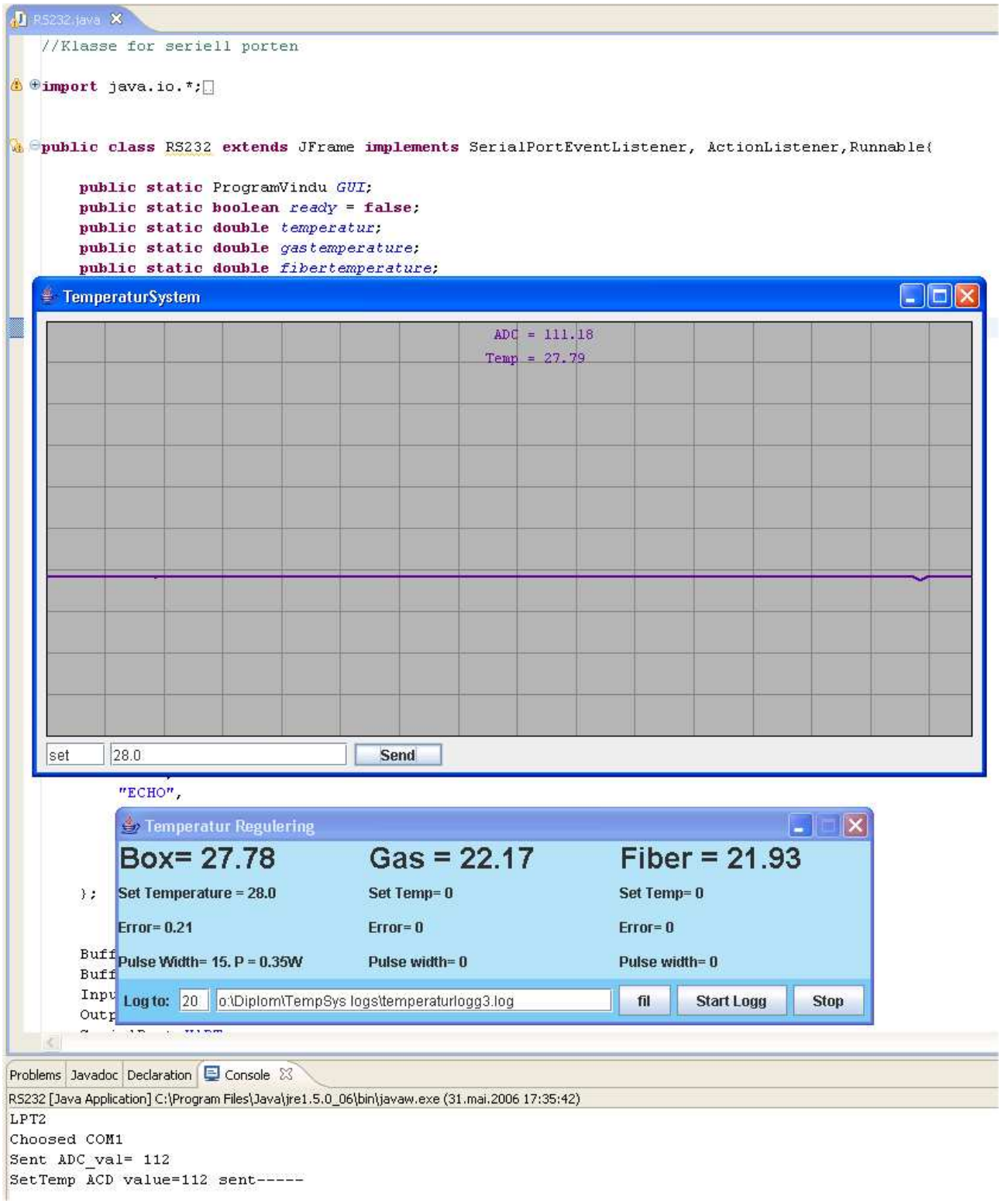

Figure B.2: Temperature Controller software. Java SDK5.0 virtual machine

C

Photographs form the lab

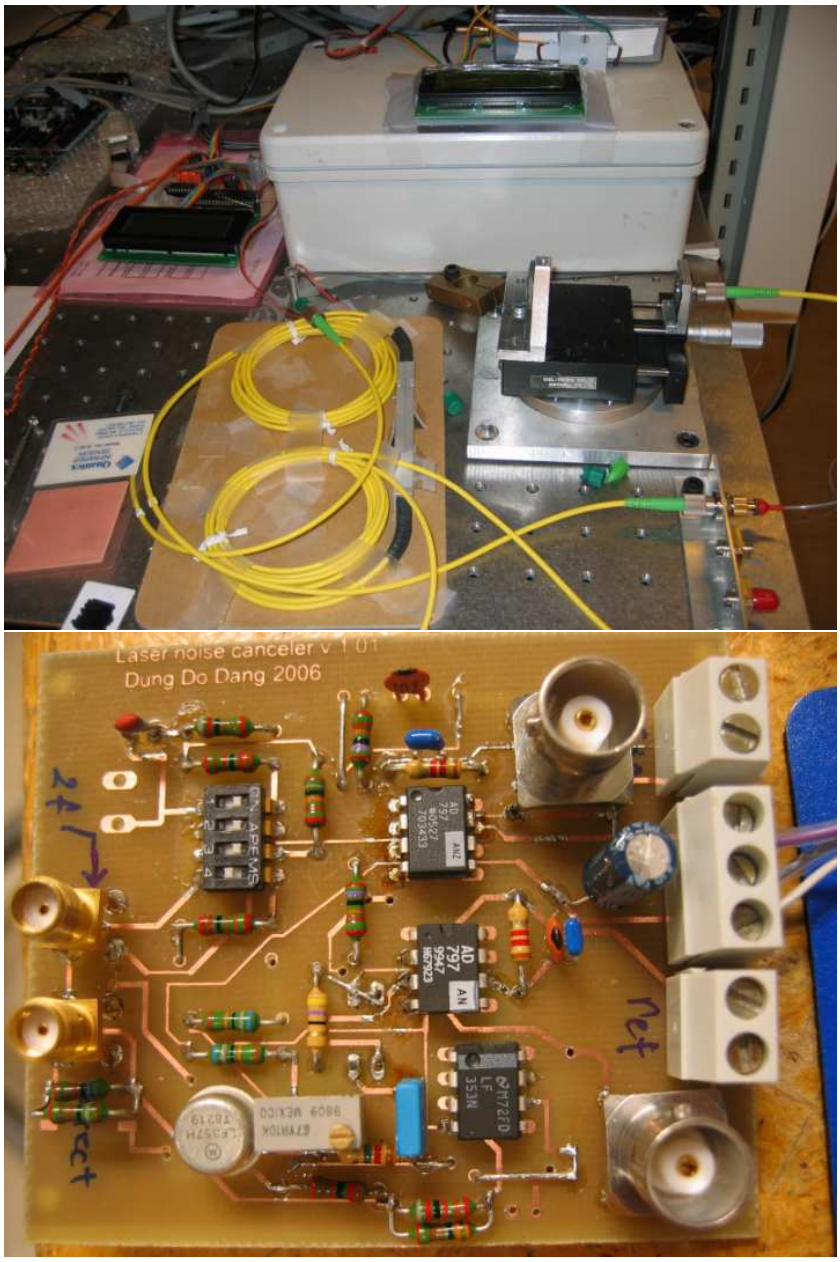

Figure C.3: Top: 2x2 fiber coupler, collimation lens, LaserGasII electronics inside a metal box. Bottom) Voltage domain noise subtracter.

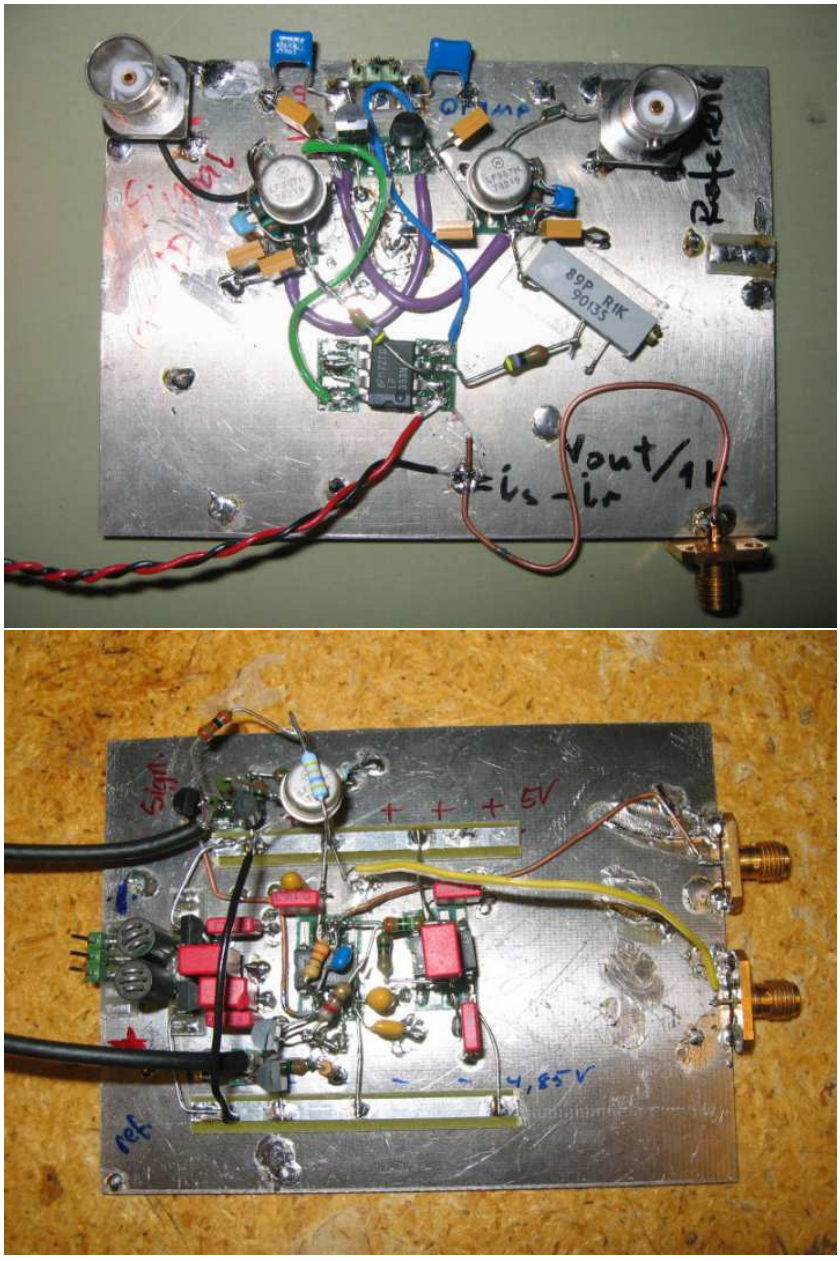

Figure C.4: Top: Voltage domain noise subtracter. Bottom: Current domain subtracter.

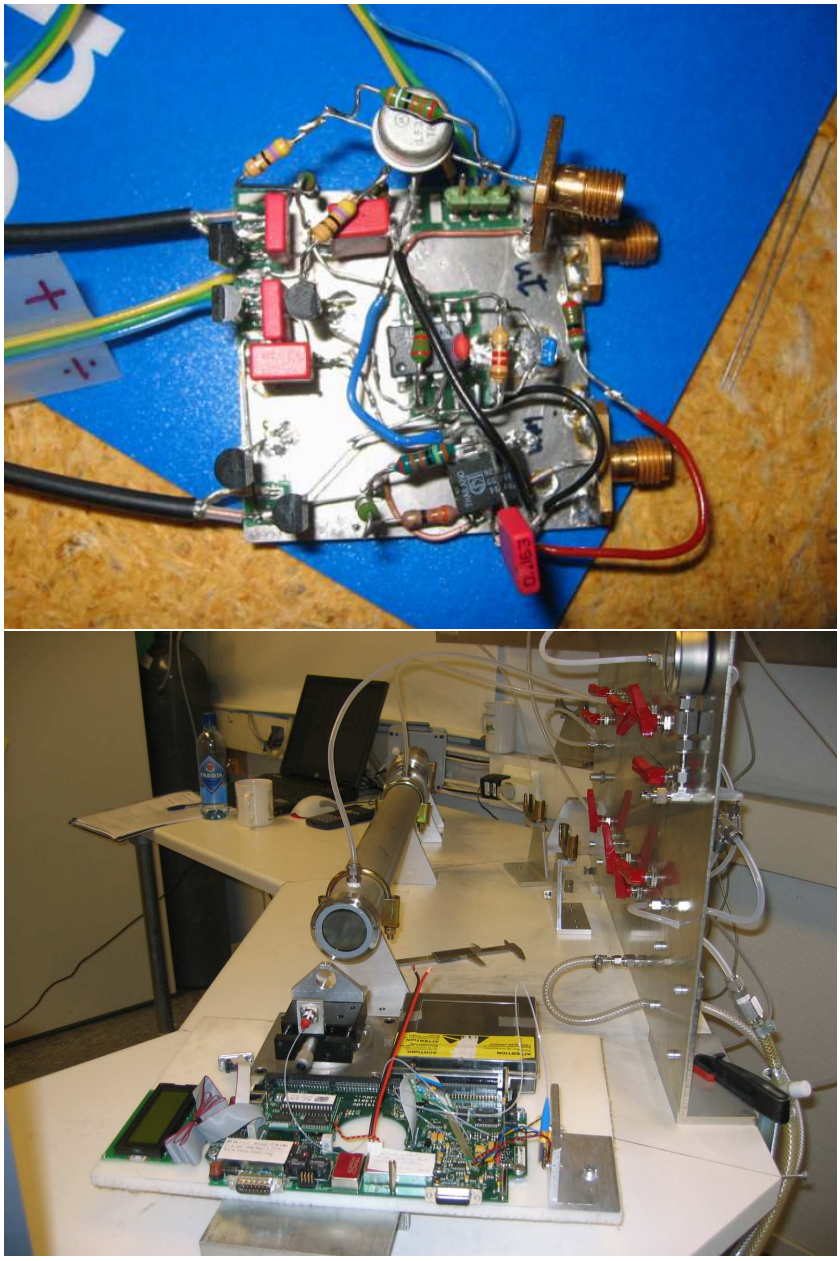

Figure C.5: Top: Current domain subtracter. Bottom: Calibration setup with the 0.712m optical path length gas cell.

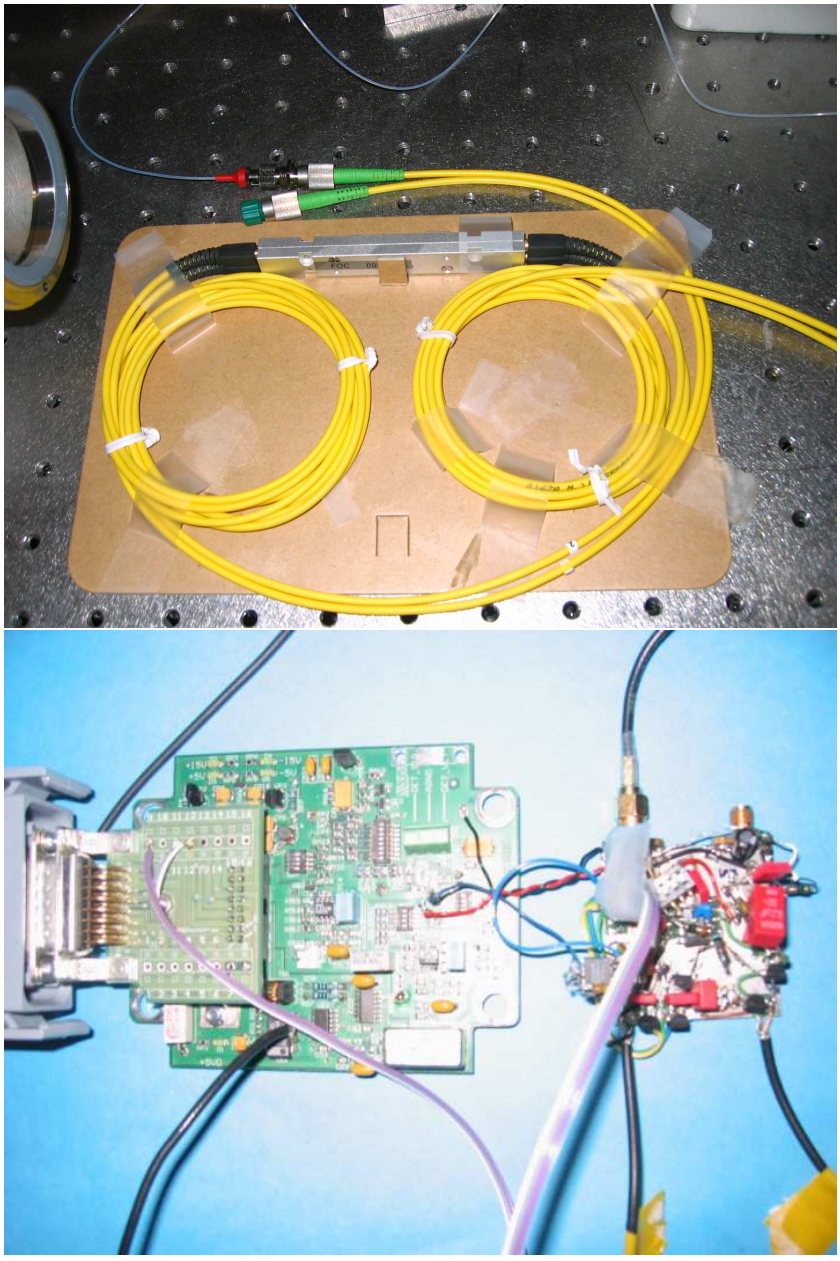

Figure C.6: Top: Fiber splitter. Bottom: Current domain subtracter and receiver board.

D

Voltage domain noise suppression circuit

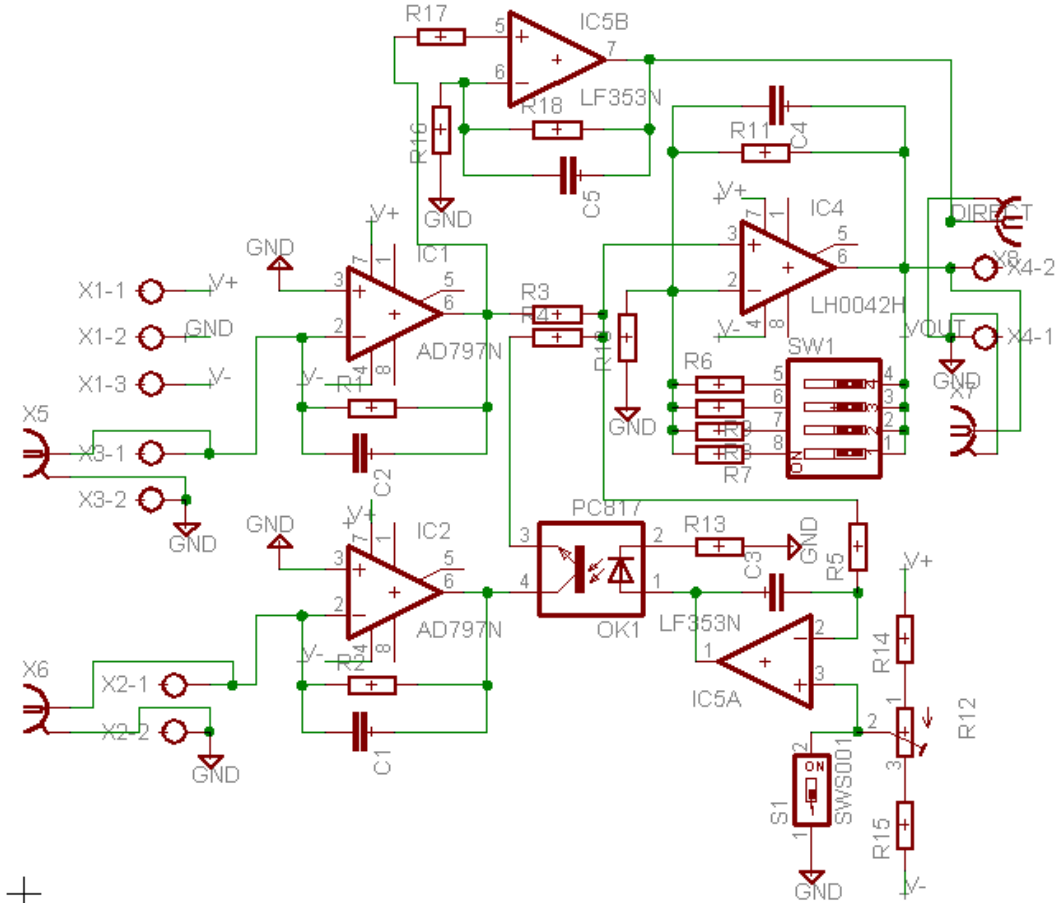

Figure D.7: Schematic diagram builded with Cadsoft Eagle version 4.15 Light edition.

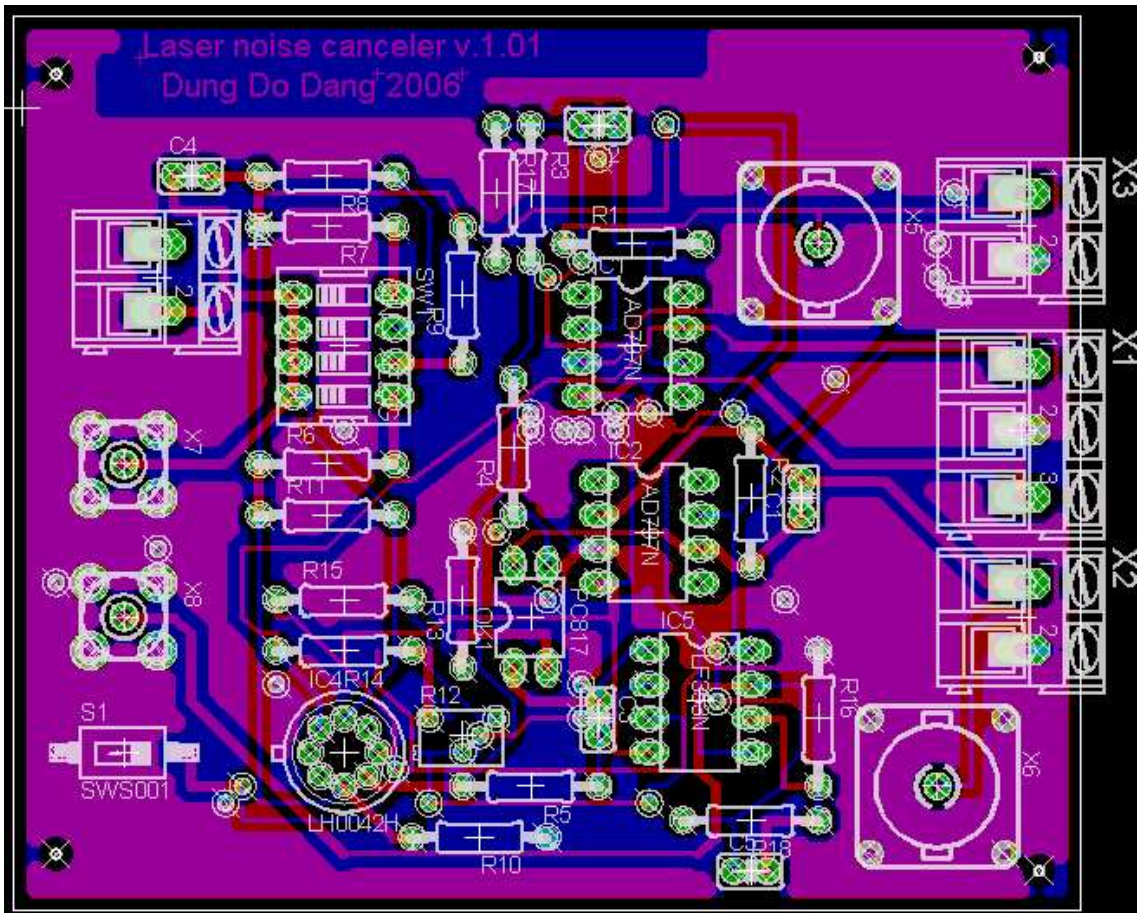

Figure D.8: Board layout and component placement. The bottom(blue) is the ground plane. Top plane is filled to save etching time

E

Temperature controller based on Atmel ATMega AVR

It turned out that we need precise controlled temperature to investigate the etalon effects of optical surfaces. The thermal expansion of the materials will affect the optical path length. When this optical path difference is comparable with one wavelength the second harmonic signal will change accordingly. To measure these effects we need to precise control the temperature of the optical materials of interest. In addition we need to log the temperatures and the time values simultaneously with the same format as the LaseGasII software in order to present the results in consistent graphical plots. Because of the difficulty to find commercially available equipments and the time limit in this thesis we decided to build an application specific temperature controller based on Atmel micro-controllers. The author is familiar with Atmel and programming tools like WinAVR. Atmel micro-controllers are small RISC micro-processors with input and output pins for external communication and a lot of useful internal functions. We also need a software to communicate with this micro-controller over the RS232 interface. The choice is simple since the author has JAVA experience. This software is written to communicate with the hardware and save the values in a text file for post-processing.

E.1 Hardware implementation

The hardware block diagram are shown in figure E.9.

E.2 Pulse width modulation to control the temperature

The temperature controller is a heater with a temperature sensor. In this way we can continuously measure the actual temperature and compare it with the reference temperature set in software. The regulator implemented for this purpose is a proportional regulator which takes the temperature difference and multiply this value with a constant. This new value is the control signal that determine the heating energy pumped into the object need to be heated. Figure E.10 shows the output waveform from the PWM pin (PIND7) on the ATMega16. This signal is connected to the gate of a N-channel power MOSFET to drive the resistors. The micro-controller is running at $4MHz$ and the PWM clock is running at 15.625kHz (a prescaling of 256). One period of the PWM wave is 255 clock cycles. The control signal of the regulator output (the regulator is implemented in software) determine the pulse width shown in figure E.10. The remaining clock cycles is set to zero if the pulse width is less than 255. Thus the time averaged energy pumped into the system is given by

$$P = \frac{w}{255} \cdot \frac{V^2}{R} \approx \frac{w}{255} \cdot 6 \tag{E.1}$$

where w is the pulse width, V is the power supply voltage and R is the total resistance. Figure E.10 shows the temperature inside the laser box as function of time. First the reference temperature is set to 30C and at t=36min a new reference value of 40C

is set. After some time dependent on the thermal time constant of the system the temperature reaches the reference value.

E.3 Logging routine of the measure values

Figure E.11 shows a plot of the temperature inside an aluminium box as function of time. The initial temperature of the box is 25C which is the ambient temperature in the lab. From the plot we can see that is takes around 6 minutes to raise the temperature inside the box to the input value from the JAVA program, 40C.

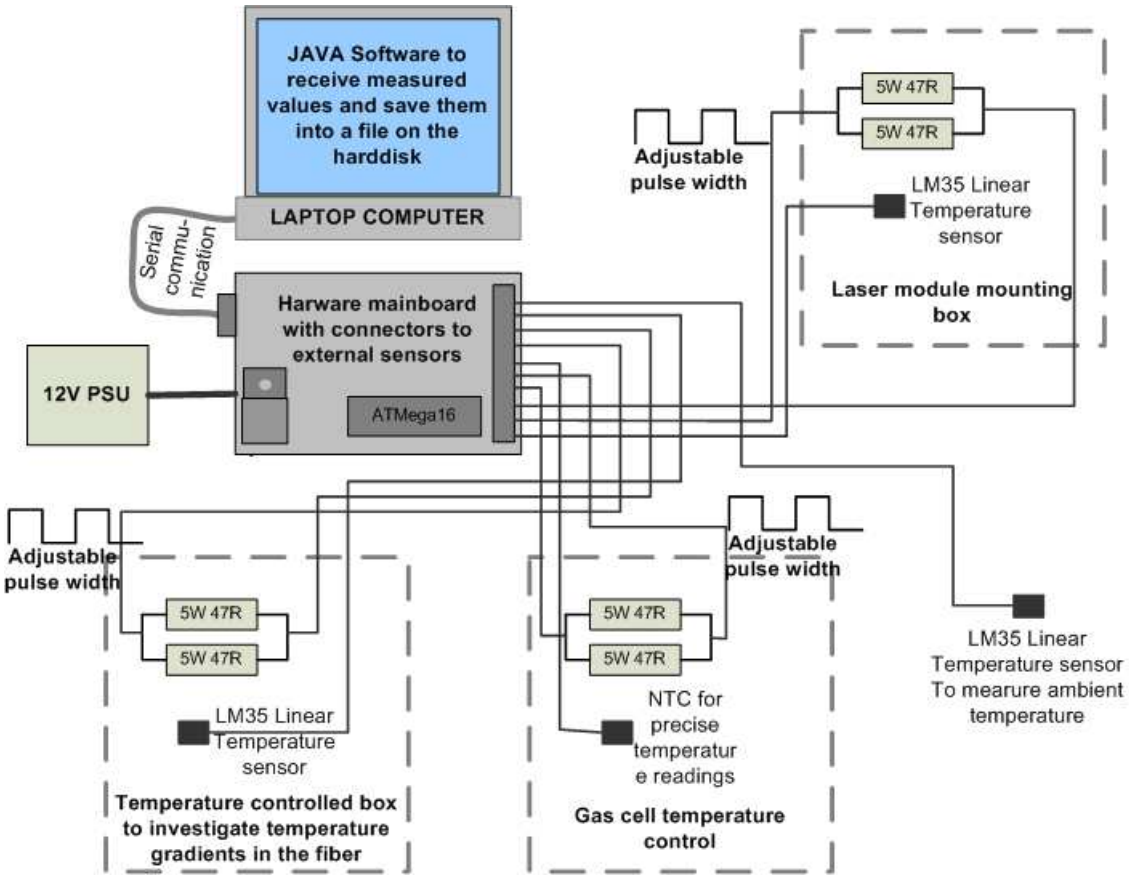

Figure E.9: The Atmel microcontroller reads the temperature from a linear temperature sensor that output a voltage proportional to the temperature, 100mV/K. Serial communication provides the Java software with temperature values. An algorithm calculate the pulse width from the temperature deviation from the wanted value. This pulse width is sent back to the microcontroller and is put to an output pin that is connected to the gate pin of the MOSFET transistor. The resulting voltage over the resistor is an time average of these pulses. This energy is concerted to heat.

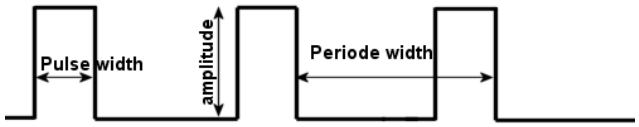

Figure E.10: The PWM (Pulse Width Modulation) pulse shape. The pulse width determine the heat power given off the resistor. One period is equal to 255 clock cycles of the 2kHz pulse generator clock. The power dissipated is equal to the time averaging of the pulses. Thus a pulse width of 25 is equal to 10% of the total power available, $V^2/R \approx 3W$

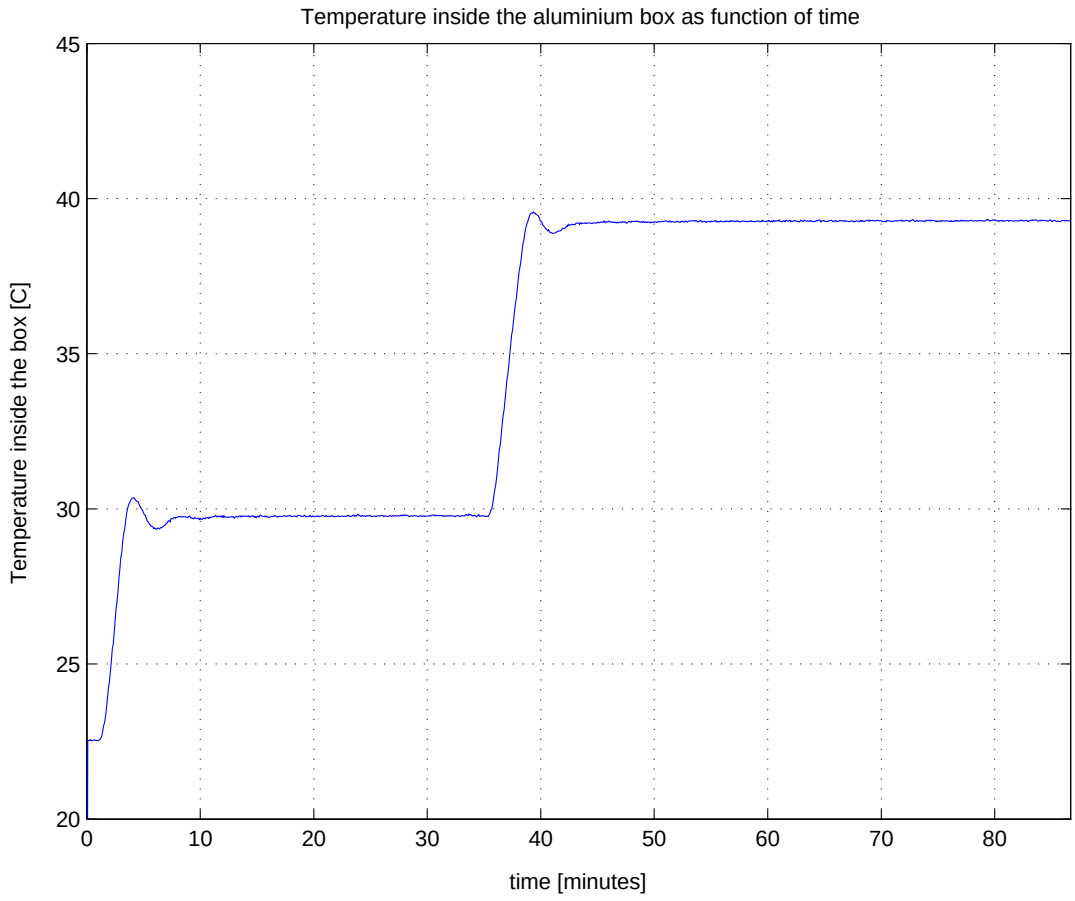

Figure E.11: The plot shows the temperature inside the box as function of time. First the micro-controller receives a reference temperature of 30C from the JAVA program and power up the resistors. After 10 minutes the temperature stabilizes at the reference temperature. It remains stable until a new reference temperature of 40C is sent to the micro-controller. Again, after a overshot the temperature remains stable at just below the set value of 40C. This small error is due to the nature of the proportional regulator.

F

Doppler shift measurement with wms

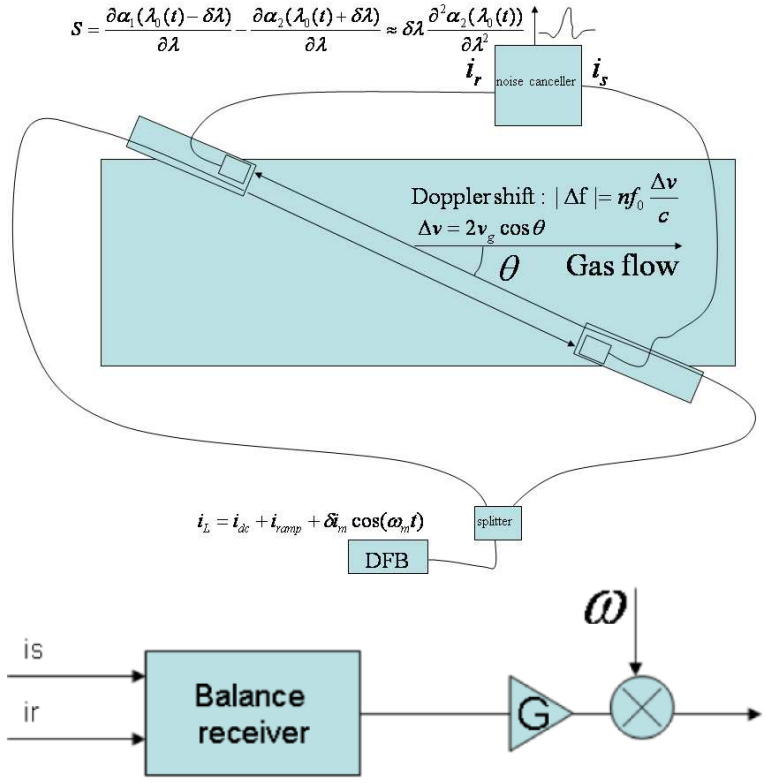

Figure F.12: Setup for measurement of the Doppler shift.

We present a new technique that can be used to measure the Doppler shift in frequency. This frequency shift can be used to calculate the gas flow in. Consider the instrument setup as shown in figure F.12. The Doppler shift in frequency is given by

$$|\Delta f| = f_0 \frac{\Delta v}{c} \tag{F.2}$$

where f_0 is the absorption line center, Δv is the gas velocity in parallel with the laser beam. 1m/s gas velocity gives approximately 0.66Mhz Doppler shift. Under low pressure the FWHM can be as little as several hundreds MHz. This measurements requires very narrow spectral width from the laser. Bragg fiber laser is well suited because of narrow linewidth. The gas flow has opposite velocity with respect to the laser beams. The absorption line is blue shifted in the reference beam and red shifted in the signal beam. If we assume same absorption and same optical path length for the two laser beams the noise canceller output is a difference of the reference and the signal photocurrent. The line position is shifted with respect to each other and the

mixer will pick out the difference in the first harmonic signal. This signal is given by

$$\frac{\partial \alpha_1(f_0 - \delta f)}{\partial f} - \frac{\partial \alpha_1(f_0 + \delta f)}{\partial f} \approx \delta f \frac{\partial^2 \alpha_1(f_0)}{\partial f^2} \tag{F.3}$$

where f_0 is the absorption line position when the gas flow velocity is zero and δf is the Doppler shift given by equation (F.2). This is true if the Doppler shift is small, $\delta f/\mathrm{FWHM} \ll 1$. This signal is proportional to the double derivative of the absorption line. The absorbtion is given by

$$\alpha(f) = Sg(f)NL \tag{F.4}$$

where S is the absorption line strength, g(f) is the absorption line profile, N is the concentration and L is the optical path length. This is a physical signal and δf can be calculated by measuring the 1f signal at the noise canceller output by the mixer. This signal amplitude is proportional to the Doppler shift, the line strength, the concentration and the optical path length. How far down we can measure the gas velocity is now only a signal to noise problem. To achieve high accuracy a strong absorption line should be used. In addition, higher concentration gives higher accuracy. The gas concentration can be measured by blocking the reference beam and used second harmonic detection. Figure F.13

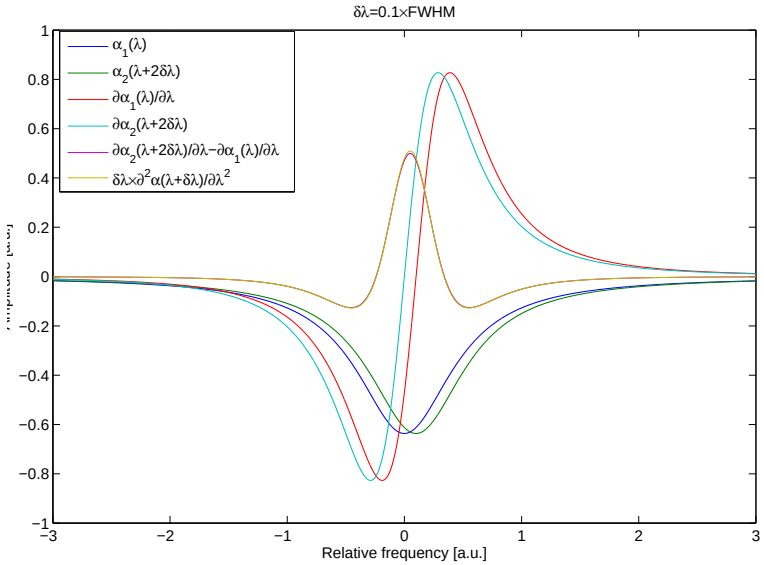

Figure F.13: The difference in the 1f signal can be used to calculate the gas velocity. Signal to noise ratio limits the accuracy.